INVERSION
OF POTENTIAL FIELD DATA

THEORY AND APPLICATIONS IN GRAVIMETRY AND MAGNETOMETRY

MAHMOUD MIRZAEI

GEOLOGICA ULTRAIECTINA

Mededelingen van de
Faculteit Aardwetenschappen
Universiteit Utrecht

No. 143

INVERSION
OF POTENTIAL FIELD DATA

THEORY AND APPLICATIONS IN GRAVIMETRY AND MAGNETOMETRY

MAHMOUD MIRZAEI

Promotor: Prof. Dr. R.K. Snieder,
Department of Geophysics,
Utrecht University.

Co-promotor: Dr. J.W. Bredewout,
Department of Geophysics,
Utrecht University.

Members of the dissertation committee:

Prof. Dr. J.C. Mondt,
Department of Geophysics, Utrecht University and
Shell Training Centre "Leeuwenhorst",
Noordwijkerhout, The Netherlands.

Prof. Dr. G. Nolet,
Department of Geological and Geophysical Sciences,
Princeton University, USA.

Prof. Dr. C.V. Reeves,
International Institute for Aerospace Survey and Earth Sciences,
Delft.

Prof. Dr. N.J. Vlaar,
Department of Geophysics,
Utrecht University.

INVERSION
OF POTENTIAL FIELD DATA

THEORY AND APPLICATIONS IN GRAVIMETRY AND MAGNETOMETRY

INVERSIE VAN POTENTIAALVELD GEGEVENS
THEORIE EN TOEPASSINGEN IN DE GRAVIMETRIE EN DE MAGNETOMETRIE

(met een samenvatting in het Nederlands en het Perzisch)

PROEFSCHRIFT

TER VERKRIJGING VAN DE GRAAD VAN DOCTOR
AAN DE UNIVERSITEIT VAN UTRECHT
OP GEZAG VAN DE RECTOR MAGNIFICUS PROF. DR. J.A. VAN GINKEL
INGEVOLGE HET BESLUIT VAN HET COLLEGE VAN DECANEN
IN HET OPENBAAR TE VERDEDIGEN
OP MAANDAG 30 SEPTEMBER 1996 DES NAMIDDAGS TE 12.45 UUR

DOOR

MAHMOUD MIRZAEI

GEBOREN OP 1 APRIL 1957 TE KOMEIN (IRAN)

PROMOTOR: PROF. DR. R.K. SNIEDER
CO-PROMOTOR: DR. J.W. BREDEWOUT

List of publications

- M. Mirzaei and J.W. Bredewout 1996. An iterative method for finding small magnetic objects in the subsurface by linear and nonlinear inversion. *Geophysical Prospecting,* **44,** 289-312.
- M. Mirzaei, J.W. Bredewout and R.K. Snieder 1996. Inversion of gravity data for interface geometry using subspace method (chapter 2). *In parameter identification and inverse problem in Hydrology, Geology and Ecology, J.Gottlib and P.Duchateau (Ed.),* Kluwer Academic Publishers, In press, 1996 (chapter 3).
- M. Mirzaei, J.W. Bredewout R.K. Snieder 1996. A subspace method inversion with application in gravity data interpretation. Submitted to *Applied Geophysics* (chapter 3).
- M. Mirzaei and J.W. Bredewout R.K. Snieder 1996. Subspace method for inversion of 3D gravity data with seismic constraints. Submitted to *Geophysical Prospecting,* (chapter 4).
- M. Mirzaei and J.W. Bredewout 1996. 3D microgravity inversion for detecting cavities. Submitted to *Environmental and engineering Geophysics* (chapter 5).

To my daughter, my wife and my parents

Contents

Chapter 1

General introduction

Inverse theory was developed by scientists and has been used in medical tomography, image enhancement, curve fitting, earthquake location, factor analysis, satellite navigation, mapping of celestial radio sources with interferometry, analysis of molecular structure by x-ray diffraction and determination of earth structure from geophysical data. Inverse theory provides mathematical techniques to obtain useful information about the physical world based on measurements (data). The resultant information from the inversion usually are some specific properties of the world. These properties are called "model parameters" and there is some specific method, usually a mathematical theory or model, which relates the model parameters to the data. Inverse theory in contrast to forward calculation, which predict the results of measurements on the basis of a model relevant to the problem, estimates model parameters using the data and a general principle or model. It should be noted that inverse theory provides information about unknown numerical parameters that go into the model, not to provide the model itself. Nevertheless, inversion can often provide a means for discriminating between several possible models. The model parameters involved in the inverse problem are in the form of discrete numerical quantities or of continuous functions of one or more variables. The first question that arises in the inverse problem is to determine whether the proposed model is an unique model or not. If it is not, then it is one of the infinite models that satisfy the observed data. This is known as the nonuniqueness of a solution of the inverse problem.

1.1 Nonuniqueness

Nonuniqueness of the inverse problem can occur because of:
- Inherent nonuniqueness.
- Uncertainty in the data and insufficient parameterization.

- Combination of both inherent nonuniqueness and uncertainty in data and insufficient parameterization.

1.1.1 Inherent nonuniqueness

There is an infinite number of models which can satisfy the observed data. For instance, potential field data are inherently nonunique. The nonuniqueness of potential data has been proven by the equivalent layer theorem which states that the gravity potential at any point outside a surface which is due to the matter inside the surface is the same as would be produced by a layer of matter distributed on the surface. This theorem points out that an infinite range of distributions of matter are possible which could fit the observed data. However, the nonuniqueness can be reduced if some constraints or *a priori* information on the parameters are imposed. For example, if the shape of the body causing the gravity anomaly is assumed to be a sphere or a cylinder, a simple expression can be obtained that leads to the unique solution. This means that initial constraints have to be imposed upon the distribution of matter inside the surface. However, even the assumption that the structures are two-dimensional does not give a unique solution to the gravity problem (Skeels 1947). The question of nonuniqueness can be investigated by examining the global properties of the misfit function. If the surface of the misfit function has a single minimum then the solution is unique and if it has more than one minimum with the same value then the solution is nonunique . Some interesting publications for further reading are Roy (1962), Backus and Gilbert (1970), Al-Chalabi (1971-a), Negi *et al*. (1973), Parker (1977), Menke (1989), Tarantola (1987).

1.1.2 Uncertainty in the data and insufficient parameterization

The uncertainty in the data can be caused by an experimental error and the insufficient parameterization by insufficient model specification. The inverse problem becomes ill-conditioned due to these effects. The inversion schemes with noise are dependent on the covariance of the noise and one has to design a criterion to discard this dependency of noise at a certain level. There are some criteria to cut-off the noise by filtering small eigenvalues (known as regularization which suppress unwanted oscillations in the model), e.g. Wiggins (1972), Jackson (1972), Koch (1985) in which a well known damped least-squares inversion scheme is utilized with singular value decomposition of the matrix to be inverted. Other regularization techniques have been set up to handle the ill-conditionality of the inverse problem, e.g. Tikhonov *et al*. (1977). Regularization techniques increase the accuracy of the estimated solution but degrade the spatial resolution. The trade off between accuracy and the resolution of the estimated model parameters are well discussed by Backus and Gilbert (1970).

1.1.3 Combination of both inherent nonuniqueness, uncertainty in data and parameterization.

When both the effect of inherent nonuniqueness and of the uncertainty in the data and insufficient parameterization are present in the inversion, even more difficulties occur in finding a reliable solution. A special strategy should be chosen to handle this problem, e.g. constraining some of the model parameters and employing regularization techniques.

1.2 Classification of the inverse problem

Inverse schemes are classified depending upon the relation between the changes in the model parameters and their effects on the observations. These relationships can be linear, weakly nonlinear and highly nonlinear.

1.2.1 Linear inverse problem

Linear dependency between data and model parameters, such as occurs for gravity and magnetic data which have a linear dependency with respect to density and magnetization respectively, leads to a system of linear equations. This system may be overdetermined (number of equations or data is more than number of model parameters) or underdetermined (number of equations is less than number of model parameters) or evendetermined (number of data is equal to number of model parameters). Since usually there is no exact solution for the resultant linear system of equations (even in cases where the problem is evendetermined), the system is usually solved in the least-squares sense which will lead to a matrix inversion.

Due to singularity or near singularity the inverse of the matrix does not exist or is computed inaccurately. The remedy to overcome such a situation has been proposed in the damped least-squares inversion (Marquardt 1963) and in the singular value decomposition technique (Penrose 1955).

1.2.2 Weakly nonlinear inverse problem

As long as the perturbation of the model from the initial model is small, we expect that the relationship between the change in model parameters and its effects on the observations is linear. Such problems are known as weakly nonlinear, and can be linearized. The linearization will results in a system of linear equations which can be solved, for the model perturbation, in the least squares sense by one of the available and stable

algorithms.

After estimating the model perturbation the current model is updated and the updated model should be used for further iterations. The iterations are continued until convergence is achieved, i.e. the model perturbation or the data misfit lies below a pre-assigned threshold. This type of inverse problem usually is solved by one of the gradient methods (Dennis *et al.* 1983).

1.2.3 Highly nonlinear inverse problem

The relationship is highly nonlinear and can not be linearized. Nonlinear inversion can be solved by the Simplex method (Polytope algorithm) or trial and error methods such as Simulated Annealing, Monte Carlo and Genetic Algorithm which are quite time consuming.

1.3 Solution of potential field data inversion

A solution of the inverse problem is often available by optimizing (minimizing or maximizing) a function of the model parameters. As mentioned before there may be a linear or a nonlinear dependence of the function on the parameters. The interpretation of potential field data (gravity and magnetic) in terms of the physical parameters (density or magnetization) is linear and in terms of shape parameters is nonlinear. Most optimization methods require the provision of an initial estimate. This initial estimate usually is acquired from information about the anomalous body or from the anomaly profile (Smith 1960). The position of initial search points generally determines the minimum or maximum to which the search will converge. By proper choice of the initial point therefore, a certain aspect of the anomalous body can be emphasised so that the optimum solution would be biased towards that aspect. The move from one point to another point in the model parameters space usually involves optimization of an objective function which is carried out by one of the optimization techniques. The process is repeated until some convergence criterion is satisfied (Al-Chalabi 1971-a).

Optimization methods may be classified as gradient methods and direct search methods. The gradient methods involves the calculation of partial derivatives of the objective function with respect to the variable parameters. Direct search methods do not usually employ partial derivatives of the object function. They are slower than the gradient methods, but more useful when the current search point is far from the optimum (such as the simplex or polytope algorithm). Owing to the complexity of the objective function, direct search methods should be employed at the early stages of the search where gradient methods tend to converge to an ill-defined local minimum.

In certain cases of inversions of gravity or magnetic data, parameters are simultaneously and iteratively adjusted and it is tried to find a minimum point in parameters space. By trial and error one or several optimum points may be found. These local minima with low function values may occur in geologically unfeasible regions. It is, therefore, important to confine such minima by using appropriate constraints.

A geometric representation may also be useful. In this manner (adjusting simultaneously parameters) a contour map of the objective function is plotted. The behavior of the objective function may then be studied visually by means of two-dimensional cross-sections. In feasible region, contours of a magnitude equal to the tolerance of the problem delimit domains in which each point provides a possible solution (possible amplitude of observational errors).

1.4 Nonuniqueness of gravity and magnetic data inversion

The most important factors responsible for a nonunique solution in the inversion of gravity and magnetic data are:
- Intrinsic ambiguity in potential fields.
- Incomplete knowledge of the full length of the anomaly which is a direct result of practical limitations.
- The anomalous feature is usually represented by models which are substantially simpler than the feature. This factor results in the existence of many models all satisfying the data equally well.
- Observational errors resulting from measurement, reduction, etc.
- The widths of individual parts of the model are small compared with the depth (causing a large number of highly oscillating models may then produce anomalies which closely agree with the observed anomaly).
- The decrease of resolving power of gravity and magnetic data with depth.
By improving these factors the solution becomes more unique (Al- Chalabi 1971-a).

1.5 History of gravity and magnetic data inversion

Gravity and magnetic surveys have been used widely over the years, resulting in a great amount of data with enormous areal coverage. Gravity and magnetic data have been used for mapping geological structures, especially in the reconnaissance stage of exploration. In recent years also robust and efficient inversion algorithms have been developed for detailed prospecting. The work done so far in gravity and magnetic data inversion can be classified into two domains: spatial domain and wavenumber or frequency domain.

Inversion of the data in the space or wave number domain can be implemented in one of the following ways:
- Inversion for solving shape and physical parameters simultaneously.
- Inversion for solving physical parameters (density, magnetization) while shape parameters are kept fixed.
- Inversion for solving shape parameters (depth, thickness, etc) fixing physical parameters (density or magnetization).

1.5.1 Spatial domain

In the three past decades considerable effort has been devoted to the explanation of gravity and magnetic anomalies by geometrical shapes whose parameters are estimated from data inversion in the spatial domain. From the many examples in the literature only some typical ones are given in the following.

1.5.1.1 Inverting data for solving both physical and shape parameters

In this case the inverse problem is completely nonunique which can be overcome by some special strategy. The behavior of the misfit function (discrepancy between the observed and predicted gravity data) was studied in the hyperspace of the model parameters (density and shape parameters) by Al-Chalabi (1971-b). The nonuniqueness of the problem is visible in the two-dimensional sections as a large number of well-defined local minima some of them being distinguished as unfeasible, others as possible solutions. He showed that unacceptable solutions can be confined by specifying some of the model parameters (reducing the nonuniqueness of the problem). In this work the nonuniqueness of the inverse problem of gravity and magnetic data is well shown and discussed. An iterative method based on trial and error was constructed by Bhattacharyya (1980) for evaluating the strike and magnetization vector and top and bottom of the blocks, constructing the model, with fixing the horizontal dimension of the block from the magnetic data. As he mentioned the drawback of this approach is that a unique solution can not be found.

A 3-D algorithm for joint inversion of magnetic and gravimetric data was introduced by Zeyen H. (1993) based on the use of *a priori* information. This information is used in the inversion in order to obtain a solution compatible with the given *a priori* information. The data is inverted for susceptibilities, remanent or total magnetizations, density and upper and lower bounds of a source whose form is restricted to a set of vertical rectangular prisms with fixed lateral bounds. This restriction hardly affects the ability to adjust the anomaly data but simplifies the model input and helps to keep the inversion process stable and fast. It is observed that the inversion process is more stable and straightforward for gravimetric than for magnetic data due to the higher second derivatives and therefore strong non-linearity of the magnetic depth parameters,

especially for near-surface sources, which introduce a tendency of these parameters to overshoot.

A 3D inversion of high precision gravity data was introduced by Camacho *et al.* (1994) for detection of cavities and galleries. The method of least-squares prediction is applied to separate the different wavelengths of the field by interpolating the correlated signals and filtering the random errors. The final residual values were used for 3-D global least-squares inversion to determine the densities, the origins and the radii of the spheres constituting the model. After inversion the spheres which show the highest adjusted density contrast are assumed to correspond to major cavities.

1.5.1.2 Inverting data for solving physical parameters

In this class of data inversion, the earth is divided into a limited number of cells of fixed size but of unknown physical parameters such as density or magnetization. Nonuniqueness of the solution is evident and algorithms have been developed to produce a single model by minimizing an objective function.

A generalized linear inverse (eigenvalue decomposition) approach was employed by Braile *et al.* (1975) to solve the density distribution for a two-dimensional body modeled by many horizontal rectangular prisms. Decreasing resolution of densities of individual prisms with increasing depth, as is expected for gravity problems, is shown by the analysis of the model resolution matrix. This method can not yield a compact or localized solution for the anomaly.

A single density contrast of a two-dimensional model was obtained with weighted-distance minimization of density contrast by the Backus-Gilbert approach by Green (1975). In this approach the model is made of rectangular prisms with initial density and fixed coordinates. The gravity data is inverted by successive applications of the method until a simple model of one density obtained. During the iterations, a weight is given to every prism to keep certain blocks at a known density, and the number of iterations is judged by an acceptable fit between profiles of model and data. In all cases, application is directed toward finding a compact body (during the iterations some blocks get zero density) with single density.

Linear programming was used by Safon (1977) in an underdetermined inverse gravity problem to give bounds on some physical parameters such as partial and total mass or position of the center of mass. The set of all solutions of this underdetermined problem is described by various convex diagrams of moments (a moment is defined as a linear functional of density); plots of these moments gives the bounds. Some constraints are used to reduce the underdeterminancy of the problem.

A constrained inverse gravity problem was posed as a linear least-squares problem with the variables being densities of two-dimensional prisms by Fisher (1980). Upper and lower bounds on the densities are prescribed so that the problem becomes a linearly constrained least-squares problem, which is solved using a quadratic

programming algorithm designed for upper and lower bound-type constraints. The solution is smoothed by damping, using singular value decomposition. If the solution is required to be monotonically increasing with depth, then this feature can be incorporated. He pointed out the only inflexibility in the method is the geometry, which should be changed in the light of an unsuccessful run.

The anomalous density distribution of a body was obtained by Last and Kubik (1983) by minimizing the volume or equivalently maximizing the compactness of the body with an iterative technique. The objective function was defined as a summation of the weighted squares of the model parameters and the misfit. Using an iterative method the objective function was minimized by adjusting the model parameters and the weights. The method was illustrated by the inversion of synthetic and real gravity data assuming a two-dimensional model consisting of a regular array of identical rectangular blocks whose densities were individually specified. The method was expanded for single density models. The advantage of this approach is that desirable geologic characteristics can be incorporated into the model.

The density distribution for a two-dimensional model was determined by minimizing the moment of inertia (criteria for homogeneous and more compactness of structures) with respect to the center of gravity or with respect to a given dip line passing through the body by Guillen et al. (1984). In this method the effect of noise and geologic constraints on the density contrast is also considered. In general the procedure which minimizes the volume will be appropriate in the case of a sedimentary basin, while the minimization of the moment of inertia with respect to the center of mass will be more suitable in the search for massive ore deposits, and the minimization of the inertia with respect to an axis will be more appropriate for dike-like structures.

A 3D gravity inversion was performed for modeling discrete bodies with nonuniform density distributions employing seminorm minimization by Hammer (1991). The seminorm minimization inversion chooses the simplest or most nearly uniform structure which fits the data within a specified misfit and provides a useful bound upon the density structure. In this method it is assumed that the density function comprises two-components: a uniform and a nonuniform component. If the uniform component is known exactly, then the minimization problem is to find a density function such that the absolute norm of the difference between the density function and an uniform component or absolute norm of the nonunform component is minimum (seminorm) and the data still fit. The inputs required by the inversion are the gravity anomaly field and the body shape. Tests using synthetic bodies show that the inversion reconstructs density trends but does not define sharp density boundaries. The inversion models lateral density variation more accurately than vertical inhomogeneities. The method was applied to model the density structure of seamounts.

A method was developed by Murata (1992) to estimate the Bouguer density from observed gravity data. The method assumes that a suitable density will lead to a smooth surface function fitted to the gravity anomalies calculated from the observations. With this assumption, the method fits a two-dimensional cubic B spline function to the

gravity data by finding a suitable density that gives the optimum trade-off between smoothness and goodness of fit to the gravity anomalies. This trade-off is interpreted by an objective Bayesian procedure and determined by minimization of Akaike's Bayesian information criterion (ABIC). When the anomalies correlate with topography, this method can effectively estimate the Bouguer density, because the Bouguer anomalies are estimated by the fitted curved function. This method can also be used to get information about the shallow rock type, where results of mapping and/or exposures are missing.

A compact 2D gravity inversion technique was extended by Barbosa *et al.* (1994) to allow compactness along several axes using Tikhonov's regularization method (1963). A regularizing operator is constructed by minimizing a smoothing functional that allows the incorporation of *a priori* information about maximum compactness of anomalous sources along several axes. This method is a generalization of the methodology developed by Guillen and Menichetti (1984). Relative weights can be assigned to each axis, leading to different mass concentrations around different axes. This method is particularly applicable to constant, linear density sources such as mineralizations along faults and intruded sills, dikes, and laccoliths in a sedimentary basin. The correct source density must be known with a maximum uncertainty of 40 percent; otherwise, the inversion produces thicker bodies for densities smaller than the true value and vice-versa. If information about the direction of the compactness axes is unsufficient the inversion can not represent the shape of the anomalous sources.

1.5.1.3 Inverting data for solving shape parameters

In this class the physical parameters are assumed to be known and nonlinear operators should be designed to determine the geometry of the source. However, geophysical inversion methods are most effective when a linear operator is applied, thus the problem is usually linearized about some initial model and then the inverse problem solved iteratively.

Two-dimensional gravity anomalies were interpreted by Corbato (1965) in order to determine the shape of a disturbing mass with known density contrast using a least-squares technique. The procedure starts with an initial model and the gravity anomalies are evaluated and compared with observed values. Adjustments are then made to the model by a least-squares approximation which uses the partial derivatives of the anomalies so that the residuals are reduced to a minimum. This method without any regularization was used for the case when the number of data and of model parameters was quite small.

Gravity and magnetic data were interpreted assuming a two-dimensional model by Pedersen (1977). The data are inverted for solving depth of the basin using a combination of singular value decomposition technique and the Marquardt method iteratively. The model is comprised of a limited number of rectangular prisms extending infinitely in one direction. During the iterations the densities or susceptibilities and the depth to

the top are kept fixed. After final solution, the resolution and information density matrices were analized. This method is used for a small number of data and of model parameters.

Stabilized linear inverse theory was applied to the problem of determining the topography of a subsurface density contrast from Bouguer gravity observations when the density contrast was kept fixed (Burkhard 1976). In this problem a linear combination of the Euclidean square norm of the errors and model parameters is minimized with considering a linear constraint about the model parameters. The concept of resolving power is extended to the problem with fixed linear constraints. The error of removal of the regional trend is also considered.

The generalized linear inverse method in the two and half dimensional case was used to invert simultaneously magnetic and gravity profiles by Menichetti *et al.* (1983). The joint inversion was used to reduced the ambiguity of the problem.

Gravity and magnetic data was inverted to obtain the continuous lower surface of a 2.5 dimensional sedimentary basin by Mickus *et al.* (1991). The problem is solved with linearized inversion employing the Backus and Gilbert technique (1967,1968,1970) using spectral expansion (Parker 1977). In this work an average model is calculated. A resolution analysis for synthetic and real data shows the high frequency oscillations can not be resolved and even though the final solution varies, the average models are very similar, except along the basin margins. Apart from this the final solution is initial model dependent, but the average models are independent of the initial model except at the margins.

1.5.2 Wave number domain

During the last three decades, spectral analysis of gravity and magnetic anomalies has been used in a variety of geological applications, such as the estimation of the depth, width, thickness, and physical parameters (density and magnetization) of a source responsible for an anomaly on the base of statistical assumptions. Inversion of the data in the wavenumber domain has some advantages (e.g. calculations are faster than the spatial domain) and disadvantages (e.g. transformation of an irregular data set to a regular one by which some information is lost). In the following some typical examples are given.

1.5.2.1 Wave number domain inversion for solving both physical and shape parameters

A method was developed for modeling and inversion of gravity anomalies by prismatic bodies by Garcia-Abdeslem (1995). The forward problem is solved in the wavenumber domain, while the power spectrum of the gravity anomaly is given by the product of

independent functions that describe depth, thickness, horizontal dimensions, and the density of the source body. The inverse problem is iteratively solved by a ridge-regression algorithm, starting from an initial trial of the geometry and density of the source body. A restriction for this method is imposed by the geometry of the prism as a representation of the source body. Nevertheless it can provide a first-order insight into the geology. Besides in mining geophysics, this method can be useful in archaeology for the search of buried artifacts.

1.5.2.2 Wave number domain inversion for solving physical parameters

Formulas for the calculation of the physical model parameters (density or magnetization distribution) both for gravity and magnetics from a generalized linear inversion scheme employing two-dimensional Fourier transformation were developed by Cribb (1976). It was also pointed out that the process of finding a distribution in the wavenumber domain leads to the familiar upward continuation and to a reduction is the amount of computations.

1.5.2.3 Wave number domain inversion for solving shape parameters

The formula used for the rapid calculation of the gravitational anomaly caused by a two-dimensional uneven layer of material (Parker, 1973) was rearranged to an iterative pro-cedure for calculating the shape of the perturbing body given the anomaly (Oldenburg, 1974). The advantage of this method is the possibility to handle a large number of model points. The convergence of the iteration can be assured by the application of a low-pass filter. The nonuniqueness of the inversion is due to two free parameters: the assumed density contrast between the two media, and the level at which the inverted topography is calculated. To reduce this ambiguity additional geophysical knowledge is required. Without additional information constraining these two parameters, the ambi-guity can not be reduced. The shortcoming of the method can be due to the fact that if the assumed density is too small or the reference level is too deep, no topography can be found which give rise to the given anomaly and also the convergence of the iteration is very sensitive to the bandwidth of the filtering. These limitations are shown both by syn-thetic and real data.

The Schmidt-Lichtenstein theory of nonlinear integral equations was applied to develop a noniterative inversion scheme of gravity data in terms of a single density con-trast by Granser (1987). The nonlinear method is based on the formula for the rapid cal-culation of the gravitational anomaly caused by a two-dimensional uneven layer of Parker (1973). The stability of the inversion scheme is restricted to a low-frequency domain with a theoretically derived cut off frequency which is dependent upon the amplitude of the gravity anomaly, the magnitude of the density contrast, and the mean depth of the interface. The method was tested by a synthetic profile-like and a 3-D field

example. Shortcoming of the method is a loss of high-frequency information due to the low-pass filtering which ensures the convergence of the inverse expansion series. However, sometimes this limitation may reflect the fact that sufficiently small-wavelength disturbances in the shape of the density interface have a vanishingly small effect on the gravity anomaly and this can be considered as an ill-posed problem.

A particular inversion was conducted by Chenot (1990) to take into account inhomogeneous density or magnetization distributions reflecting sediment compaction and basement heterogeneities: above the interface, the density can be approximated by an exponential function, and below it, an intrabasement contrast map can be used. The starting model was characterized mainly by the interface mean depth and the mean parameter contrast between the two media, which can be obtained from spectral analysis of the transformed data (wavenumber domain) and from constraints. The depth adjustment is completed iteratively under constraints using a space-domain formulation derived from the Bouguer-slab formula. The interface model effect is computed in the wavenumber domain. This technique can only be used in conditions where enough information is available about the parameters which define the model.

1.6 The aim of this work

The aim of this work is to develop inversion methods for determining the position and physical parameters of a body responsible for an anomaly, from potential field data. The methods that have been developed have the following advantages : reducing inherent nonuniqueness; handling strong nonlinearity; handling ill-conditionality due to the large number of data and of model parameters; fast convergence; robustness against noise and reducing nonuniqueness due to underdeterminancy.

In *chapter* 2 a robust method is developed that can handle the effect of inherent nonuniqueness of a highly nonlinear inverse problem when both physical and shape parameters are supposed to be estimated from the inversion and when the data represents more than one anomaly and contains some inaccurate or out-of range points (outliers). This method was successfully employed to detect unexploded bombs, left from second world at Schiphol airport in The Netherlands, from magnetic data obtained in boreholes.

In *chapter* 3 a subspace method is introduced to handle the ill-conditionality of an inverse problem due to the large number of data and of model parameters and when the objective function can be approximated by a quadratic surface. In this case the Hessian matrix (matrix of the second partial derivatives) should be calculated. This method is sufficient for the case when the assumed model is two dimensional since for the three dimensional case the calculation of the Hessian is rather cumbersome when the number of data and of model parameters is rather large. This method finds a solution with minimum variance very quickly. The method was applied to gravity data from the Roervalley graben in the southern part of The Netherlands to determine the shape of interfaces

separating layers (assuming a two and three- layer model).

In *chapter* 4 another subspace method is developed in which the calculation of the Hessian is avoided and the inversion converges fast to a solution with minimum variance. This method is sufficient for the case when the assumed model is three dimensional and when the objective function can be approximated only by the linear terms. Since the calculation of the Hessian matrix is avoided, the number of data and of model parameters can not be problematic. This method was successfully applied to gravity data for an area in The Netherlands where seismic results did not give a decisive answer about the continuation of a potential hydrocarbon reservoir.

In *chapter* 5 an inversion strategy is introduced which can combat with the problem of nonuniqueness due to underdeterminancy and is able to handle a large number of model parameters. It finds a solution which is localized and reliable. This method was used to detect man-made cavities near Maastricht in the south of The Netherlands from microgravity data.

Although the numerical methods introduced here are used for gravity and magnetic data interpretation, they can also be employed for other geophysical data interpretation. The work concentrates only on the spatial domain to overcome the difficulties of the wavenumber domain transformation. For instance an irregular data set should be transformed into a regular form before it can be used in the wavenumber domain, by which some information will be lost. Despite the drawbacks, in some cases inversion in the wavenumber domain has some advantages, e.g. it is faster.

1.7 References

Al-Chalabi M. 1971 a. Some studies relating to nonuniqueness in gravity and magnetic inverse problems. *Geophysics* **36**, 835-855

Al-Chalabi M. 1971 b. Interpretation of gravity anomalies by non-linear optimization. *Geophysical Prospecting* **20**, 1-16

Backus G. E. and Gilbert F. J. 1967. Numerical applications of a formalism for geophysical inverse problems. *Geophy. J. R. Ast. Soc.* **13**, 274-276.

Backus G. and Gilbert F. 1968. The resolving power of gross earth data. *Geophy. J. R. Ast. Soc.* **16**, 169-205.

Backus G. E. and Gilbert J. F. 1970. Frequency domain uniqueness in the inversion of inaccurate gross earth data. *Phill. Trans.Roy.Soc, London,* **206A**, 123-192.

Backus G. and Gilbert F. 1970. Uniqueness in the inversion of inaccurate gross earth data. *Philosophical Transactions of the Royal of London* **A226**, 123-192.

Barbosa V. C. F. and Silva B. C. 1994. Generalized compact gravity inversion. *Geophysics* **59**, 57-68.

Bhattacharyya B. K. 1980. A generalized multibody model for inversion of magnetic anomalies. *Geophysics* **45**, 255-270.

Braile L. W. Keller G. R. and Peeples W. J. 1975. Inversion of gravity data for two-

2017-2021.

Burkhard N. and Jackson D. D. 1976. Application of stabilized linear Inverse theory to gravity data. *Journal of Geophysical Research* **81**, 1513-1518.

Camacho A. G. , Vierira R., Montesinos F. G. and Cuellar V. 1994. A gravimetric 3D Global inversion for cavity detection. *Geophysical Prospecting* **42**, 113-130.

Chenot D. and Debeglia N. 1990. Three-dimensional gravity or magnetic constrained depth inversion with lateral and vertical variation of contrast. *Geophysics* **55**, 327-335.

Corbato C. E. 1965. A least-squares procedure for gravity interpretation. *Geophysics* **30**, 228-233.

Cribb J. 1976. Application of the generalized linear inverse to the inversion of static potential data. *Geophysics* **41**, 1365-1369.

Dennis J. E. and Schnabel R.B. 1983. *Numerical method for unconstrained optimization and nonlinear equations.* Englewood Cliffs, NJ: Prentice-Hall.

Fisher N. J. and Howard L. E. 1980. Gravity interpretation with the aid of quadratic programming. *Geophysics* **45**, 403-419.

Garcia-Abdeslem J. 1995. Inversion of the power spectrum from gravity anomalies of prismatic bodies. *Geophysics* **60**, 1698-1703.

Granser H. 1987. Nonlinear inversion of gravity data using the Schmidt- Lichtenstein approach. *Geophysics* **52**, 88-93.

Green W. R. 1975. Inversion of gravity profiles by use of a Backus- Gilbert approach. *Geophysics* **40**, 763-772

Guillen A. and Menichetti V. 1984. Gravity and magnetic inversion with minimization of a specific functional. *Geophysics* **49** 1354-1360.

Hammer P. T. C., Hildebrand J. A. and Parker R. L. 1991. Gravity inversion using semi-norm minimization: Density modeling or Jasper Seamount. *Geophysics* **56**, 68-79

Jackson D. D. 1972. Interpretation of inaccurate insufficient and inconsistent data. *Geophy. J. Roy. Astr. Soc.* **28**, 97-109.

Koch M. 1985. Non-linear inversion of local seismic travel times for the simultaneous determination of the 3-dimensional velocity structure and hypocentres-application to seismic zone Vrancea. *J. Geophy.* **56**, 160-173.

Kunaratnam K. 1972. An iterative method for the solution of a non-linear inverse problem in magnetic interpretation. *Geophysical Prospecting* **20**, 439-447.

Lakshmanan J. 1988. Generalized gravity anomaly: Endoscopic Micro Gravity (EMG). *Compagnie de Prospection Giophsique Francaise (CPGF) France* **ENG 3.1,** 331-334

Last B. J. and Kubik K. 1983. Compact gravity inversion. *Geophysics* **48**, 713-721.

Marquardt D. W. 1963. An algorithm for least-squares estimation of non- linear parameters. *Journal of the Society of Industrial and Applied Mathematics* **11**, 431-441.

Menichetti V. and Guillen A. 1983. Simultaneous interactive magnetic and gravity inversion *Geophysical Prospecting* **31**, 929-944.

Menke W. 1989. Geophysical data analysis. *discrete inverse theory.* Academic press Inc.

Mickus K. L. and Peeples W. J. 1992. Inversion of gravity and magnetic data for the lower surface of a 2.5 dimensional sedimentary basin. *Geophysical Prospecting* **40**, 171-193.

Negi J. G. Dimri V. P. and Garde S. C. 1973. Ambiguity Assessment of gravity interpretation for inhomogeneous multilayer sedimentary basin. *J.Geophy.Res* **78**, 3281-3286.

Oldenburg D. W. 1974. The inversion and interpretation of gravity anomalies. *Geophysic* **39**, 526-536.

Parker R. L. 1973. The rapid calculation of potential anomalies. *Geophysics. J. R. Astr. Soc* **31**, 447-455.

Parker R. L. 1977. Linear inference and underparameterized models. *Rev. Geophys.* **15**, 446-456.

Pedersen L. B. 1977. Interpretation of potential field data, a generalized inverse approach. *Geophysical Prospecting* **25**, 199-230.

Penrose R. 1955. A generalized inverse for matrices. *Proc. Camb. Phil. Soc* **51**, 406-413.

Roy A. 1962. Ambiguity in geophysical interpretation. *Geophysics* **27**, 90-97.

Safon C., Vasseur G. and Cuer M. 1977. Some applications of linear programming to the inverse gravity problem. *Geophysics* **42**, 1215-1229

Skeels D.C. 1947. Ambiguity in gravity interpretation. *Geophysics* **12**, 43-56.

Smith R. A. 1960. Some formulae for interpreting local gravity anomalies. *Geophysical prospecting* **7**, 607-613.

Tarantola A. 1987. Inverse problem theory. *Elsevier, Amsterdam.*

Tikhonov A. N. 1963. Solution of incorrectly formulated problems and the regularizations method. *Soviet Math. Doklady* **4**, 1035-1038.

Tikhonov A. and Arsenin V. 1977. *Solution of ill-posed problems.* Wiley and Sons, Washington D.C.

Murata Y. 1992. Estimate of upper crustal rock densities from gravity data based on an objective Bayesian procedure. *Geology survey of Japan, Higashi 1-1-3, Tsukuba, Ibaraki 305, Japan.*

Zeyen H. and Pous J. 1993. 3-D joint inversion of magnetic and gravimetric data with *apriori* information. *Geophys. J. int.* **112**, 244-256.

Wiggins R. A. 1972. The general linear inverse problem: Implications of surface waves and free oscillations for earth structure. *Rev Geophysics and space physics* **10**, 251-258.

Chapter 2

An iterative method for finding small magnetic objects in the subsurface by linear and nonlinear inversion

Abstract

A method to determine the position and magnetization vector of buried objects produc-
ing a magnetic anomaly is described. The data used were collected in boreholes. Since
the anomaly is due to a number of objects a "stripping" procedure is employed for find-
ing them. Therefore the process of inversion for finding all objects causing the anomaly
consists of a few inversion steps. In each inversion step, two dipoles are considered as a
model which approximates an object. The position and magnetic moment of each dipole
is the unknown parameters. Initial parameters are optimized by minimization of an
objective function. The optimization procedure consists of a combination of linear and
nonlinear inversion. The solution of the linear inversion is obtained by singular value
decomposition and of the nonlinear one by a six-dimensional simplex method (Polytope
Algorithm). After finding one object its effect is subtracted ("stripped") from the data
and with this reduced data set a new inversion step is started with new initial models.
The inversion steps for finding different objects are continued until the absolute norm of
the data becomes less than some adjustable value. The data will also be inverted assum-
ing a three-dipole model to find the effect of using a more complex model in the inver-
sion. The efficiency of the method is demonstrated using synthetic and real borehole
data.

2.1 Introduction

It is well-known that an infinite number of differing models can provide possible alternative interpretations for observed potential field data. The solutions of inversion of magnetic anomalies usually involves nonuniform magnetization distributions and no particular restrictions regarding the shape of the anomalous body. Under certain constraints, this ambiguity can be reduced, so that a given anomaly may be interpreted in terms of a reliable solution.

Inversion of potential field data in terms of the shape of the anomalous body is a non-linear and with respect to physical parameters a linear problem. In some cases the extent of ambiguity can be reduced by specifying one or more parameters:
(a) With a fixed susceptibility or density, magnetic or gravity data can be inverted to determine the shape parameters of the body. Shown e.g. by Corbato (1965) ; Al-Chalabi (1971a) ; Kunaratnam (1972) ; Pedersen (1977) ; Menichetti and Guillen (1983) ; Mickus and Peeples (1992).
(b) Keeping shape parameters fixed, the physical parameters can be calculated for a body consisting of many blocks or prisms. This leads to finding approximately the distribution of the physical parameters. Shown e.g. by Green (1975) ; Braile, Keller, and Peeples (1975) ; Safon, Vasseur, and Cuer, (1977) ; Bhattacharyya, (1980) ; Last and Kubik (1983) ; Guillen and Menichetti (1984).

In some cases both physical parameters and shape parameters can be considered as unknown parameters. Then linear and nonlinear inversion can be employed for solving physical and shape parameters. This method was used by Bredewout *et al.* (1993) for finding unexploded bombs at Schiphol airport. They used a one-dipole model for each magnetic object which can only be justified if the distance between the bomb and measurement point is large compared to the size of the bomb. In the present paper models consisting of two or three dipoles will be considered. The reason for this is that a bomb, due to differences in thickness and geometry of the different parts, can not be considered as a homogeneously magnetized spherical object. Demagnetization effect are more important for the middel part of the bomb, where the shell is relatively thin, than for the thicker top and bottom.

The magnetic data inversion aims at calculating the physical parameters (the vectors of the magnetic moments) and the position parameters (the position of the object) without specifying any of these parameters. In this case the inverse problem will be ambiguous. The ambiguity can be reduced by selecting two strategies:

1. An appropriate model; one of the factors causing ambiguity is representing the anomalous feature by a model which is substantially simpler than the feature (Al-Chalabi 1971b) . Therefore, choosing a model which is compatible with the object causing the anomaly can reduce the degree of ambiguity.

2. Employing a combination of linear and nonlinear inversion offers the possibility of keeping fixed position parameters while inverting the data for physical parameters

and vice versa.

Moreover, the borehole data provide information about a good starting position, close to the object, for the linear and nonlinear inversion. This advantage and employing the two above strategies yields a solution which is acceptable.

2.2 Calculation of the model response

Following Panofsky and Phillips (1962) the anomalous magnetic field at the position $\mathbf{r}$ caused by a magnetized body is given by:

$$\Delta\mathbf{B}(\mathbf{r}) = \int_v \mathbf{G_B}(\mathbf{r},\mathbf{s}) \cdot \mathbf{M}(\mathbf{s})d^3\mathbf{s} \tag{1}$$

Where $\mathbf{M}(\mathbf{s})$ is the magnetization vector at $\mathbf{s}$ and $\mathbf{G_B}(\mathbf{r},\mathbf{s})$ is Green's function (actually a matrix) which can be written as (Panofsky and phillips 1962; Parker, Shure and Hildebrand 1987)

$$\mathbf{G_B}(\mathbf{r},\mathbf{s}) = \frac{\mu_0}{4\pi}\nabla_r\nabla_r\frac{1}{|\mathbf{r}-\mathbf{s}|} = \frac{\mu_0}{4\pi}\left[\frac{3(\mathbf{r}-\mathbf{s})(\mathbf{r}-\mathbf{s})^T}{|\mathbf{r}-\mathbf{s}|^5} - \frac{\mathbf{I}}{|\mathbf{r}-\mathbf{s}|^3}\right] \tag{2}$$

where μ_0 is permeability of free space with value $4\pi\times10^{-7}\ VsA^{-1}m^{-1}$, superscript " T " indicates matrix transpose and $\mathbf{I}$ is an identity matrix.
The vertical component of the anomalous field has to be calculated using:

$$\Delta B_z(\mathbf{r}) = \hat{\mathbf{e}}_\mathbf{z}^T \cdot \Delta\mathbf{B}(\mathbf{r}) = \int_v \hat{\mathbf{e}}_z^T \cdot \mathbf{G_B}(\mathbf{r},\mathbf{s}) \cdot \mathbf{M}(\mathbf{s})d^3\mathbf{s} \tag{3}$$

Where $\hat{\mathbf{e}}_z$ is a unit vector in the vertical direction.
The predicted data d_i^{pre} at the position $\mathbf{r}_i$ is the difference of the vertical component of the magnetic field at two positions $\mathbf{r}_i^u$ and $\mathbf{r}_i^l$ vertically above and blow the position $\mathbf{r}_i$ (middel of positions $\mathbf{r}_i^u$ and $\mathbf{r}_i^l$). This can be calculated as follows

$$d^{pre}(\mathbf{r}_i) = \int_v \hat{\mathbf{e}}_z^T \cdot (\mathbf{G_B}(\mathbf{r}_i^u,\mathbf{s}) - \mathbf{G_B}(\mathbf{r}_i^l,\mathbf{s})) \cdot \mathbf{M}(\mathbf{s})d^3\mathbf{s} \tag{4}$$

where superscript " pre " indicates predicted for the data.
With $\mathbf{G}(\mathbf{r}_i,\mathbf{s}) = \hat{\mathbf{e}}_z^T \cdot (\mathbf{G_B}(\mathbf{r}_i^u,\mathbf{s}) - \mathbf{G_B}(\mathbf{r}_i^l,\mathbf{s}))$ equation (4) becomes

$$d^{pre}(\mathbf{r}_i) = \int_v \mathbf{G}(\mathbf{r}_i,\mathbf{s}) \cdot \mathbf{M}(\mathbf{s})d^3\mathbf{s} \cdot \tag{5}$$

Replacing the continuous magnetization, $\mathbf{M}(\mathbf{s})$, by p magnetic dipoles with magnetic moments $\mathbf{m}_j$ at positions $\mathbf{s}_j$ ($j=1,\cdots,p$) the integral in equation (5) is replaced by a summation:

$$d^{pre}(\mathbf{r}_i) = \sum_{j=1}^{p} \mathbf{G}(\mathbf{r}_i, \mathbf{s}_j)\mathbf{m}_j \cdot \qquad \qquad (6)$$

Each of the vectors $\mathbf{r}_i$, $\mathbf{r}_i^u$, $\mathbf{r}_i^l$, $\mathbf{s}_j$ and $\mathbf{m}_j$ is three dimensional.

2.3 Methods for solving linear and nonlinear inversion

We aim to determine the positions and magnetic moments of the dipoles which approximate small objects causing the anomalies. A nonlinear inversion is used to find the best positions of the dipoles to fit the data.

In each step of this nonlinear inversion method an objective function must be calculated at a number of fixed positions. For each of these fixed positions the best fitting values for the magnetic moments of the dipoles are determined by linear inversion. These best values are used for the calculation of the objective function of the non-linear inversion (see figure 2.1)

2.3.1 Linear inverse problem

In the linear inversion n observations (difference of the vertical component of the anomalous magnetic field) $\mathbf{d}_o = (d_{o1}, d_{o2}, \cdots, d_{on})^T$, with standard deviations σ_i, are inverted to find the magnetic moments of the p dipoles, $\mathbf{m}_j$, using the following weighted least squares criterion (Menke 1989) :

$$\sum_{i=0}^{n} |w_i(d_{oi} - \sum_{j=1}^{p} \mathbf{G}(\mathbf{r}_i, \mathbf{s}_j)\mathbf{m}_j)|^2 = Min \qquad \qquad (7)$$

where w_i is a weighting factor which will be specified latter.
The above criterion is used to give an approximate solution to the following linear set of equations

$$\mathbf{W}\tilde{\mathbf{G}}\tilde{\mathbf{M}} = \mathbf{W}\mathbf{d}_o \cdot \qquad \qquad (8)$$

In this equation $\mathbf{d}_o$ is the data vector with dimension n, $\tilde{\mathbf{G}}$ is a matrix with dimension $n \times 3p$ whose elements are the components of the Green function (in the x,y and z direction) used in equation (6), $\tilde{\mathbf{M}}$ is the vector of the magnetic moment components with dimension $3p \times 1$ and $\mathbf{W}$ is a $n \times n$ diagonal weighting matrix.
The generic form of the above equation is

$$\mathbf{A}\mathbf{x} = \mathbf{b} \qquad \qquad (9)$$

where $\mathbf{A}$, $\mathbf{x}$ and $\mathbf{b}$ stand for $\mathbf{W}\tilde{\mathbf{G}}$, $\tilde{\mathbf{M}}$ and $\mathbf{W}\mathbf{d}_o$ respectively. There are some algorithms for solving the above linear sets of equations such as Gauss Jordan Elimination, LU
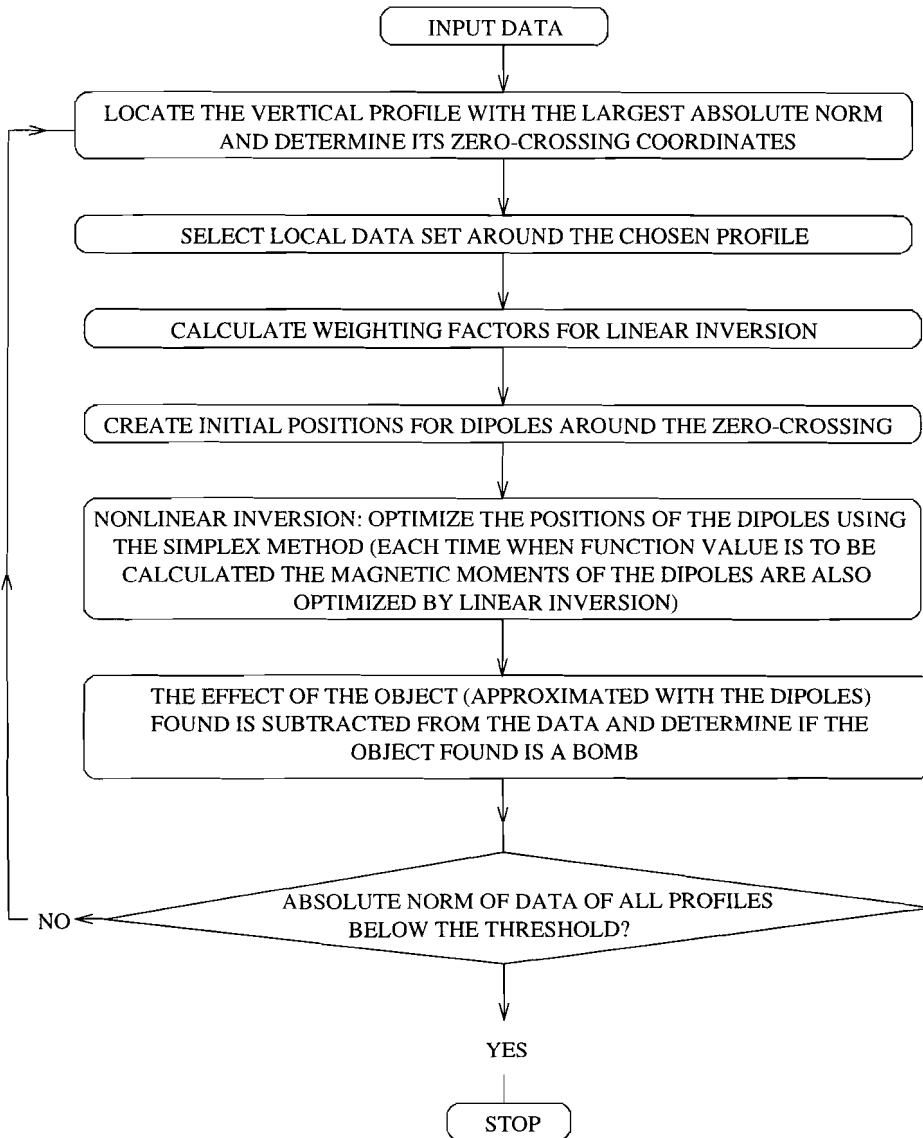
Figure 2.1: Block diagram showing the inversion scheme of magnetic vertical profiles.

decomposition, and singular value decomposition.

In some cases the normal equations in the least squares method are singular or very close to being singular. In the former case there is no solution at all and in the latter

case LU decomposition or Gaussian elimination may give a solution vector, $\mathbf{x}$, whose components are large and when multiplying by the matrix $\mathbf{A}$, may give a very poor prediction to $\mathbf{b}$.

To overcome this deficiency we use the singular value decomposition technique. This method determines the solution in such a way that the euclidean norms of both prediction error $|\mathbf{Ax} - \mathbf{b}|^2$ and model parameters $|\mathbf{x}|^2$ are minimized by zeroing the small eigenvalues of the square matrix $\mathbf{A}^T\mathbf{A}$ (see e.g. Store and Bulirsch 1980; Press et al 1986). Singular value decomposition techniques truncating small eigenvalues have been used for inversion of different geophysical data by Jupp and Vozoff (1974) ; Braile, Keller and Peeples (1975) ; Pedersen (1977) ; Menichetti and Guillen (1983) ; Ward and Young (1980) ; Narasimha Rao *etal.* (1994). In our case the machine precision was 10^{-6} and single precision variables mode was used for all calculations, thus eigenvalues less than *largest eigenvalue* $\times 10^{-6}$ were truncated.

2.3.2 Nonlinear inverse problem

To find the position and the approximate size of the buried small objects it can be assumed that the effect of the anomalous object is the same as the effect of one dipole or a limited number of dipoles when the size of the object causing the anomaly is small compared with the distance to the measurement points.

As mentioned before, the objective function is nonlinear with respect to the position parameters (the positions of the dipoles). The solution $\mathbf{s}$ is to be found by minimization of the following objective function:

$$F(\mathbf{s}) = \sum_{i=0}^{n} |w_i(d_{oi} - \sum_{j=1}^{p} \mathbf{G}(\mathbf{r}_i, \mathbf{s}_j)\mathbf{m}_j)| \cdot \tag{10}$$

The objective function, $F(\mathbf{s})$, is the absolute norm of the data misfit (l_1 norm).
It has already been discussed in the literature that using l_1 norm criterion has superiority to l_2 norm or least-squares criterion when the data represent more than one anomaly and contain some inaccurate or out-of-range points (outlier). Generally speaking the l_1 norm is more robust against the noise than l_2 norm criterion. Shown e.g. by Menke (1989) ; Vigneresse (1977) ; Clarebout and Muir (1973) ; Barrodale and Young (1966).

In order to obtain a reliable solution, a nonlinear optimization procedure is used to find $\mathbf{s}$ but for every position where $F(\mathbf{s})$ is to be computed, the components of the magnetic moments $\mathbf{m}_j$ are optimized by solving the weighted linear inversion with fixed $\mathbf{s}$. This will reduce the nonuniqueness of the problem.

To solve the nonlinear part of the problem the simplex method or Polytope Algorithm is used which is suitable for l_1 norm minimization since it only uses function calculation and not partial derivatives for the minimization.

Direction set methods such as a combination of the steepest descent method and inverse Hessian matrix and the variable metric method were also tested. Both methods need calculation of first partial derivatives and use the l_2 norm criterion for the minimization of the objective function. None of these methods could converge to a reliable solution.

The following (mentioned by Nelder and Mead, 1965) is an additional justification for the simplex method:
- " When the curvature of the landscape, measured by the Hessian matrix of second order derivatives, is changing rapidly, the simplex method is more efficient than other methods which depend on arguments applicable to quadratic form". When the sources responsible for the anomalies are close to the measurement points and the model contains high spatial frequencies the curvature of the objective function will change very rapidly with position. The present inverse problem satisfies this condition thus the simplex method is an efficient method for the minimization of the objective function.

The simplex method used here is described e.g. by Nelder and Mead (1965). This method is sufficient where the number of the model parameters is moderate and is suitable for the present problem with the number of the model parameters being six or nine. It optimizes the initial position of the dipoles iteratively. The iterations are terminated when the fractional range from the highest to lowest value of the objective function and also the vector distance moved are less than 0.05 and 0.01 m. The maximum number of iterations for optimization is set to 200.

2.4 Efficiency of the method

2.4.1 Synthetic data

The efficiency and the limitations of the method will be shown using some synthetic borehole data.

Here, the conditions under which the real data were acquired, are simulated. In the real data a borehole is drilled from the surface to a certain depth and a PVC pipe is fixed in it. The boreholes (pipes) are arranged in equidistant parallel rows.

We assume a cartesian coordinate system which x and y directions show rownumber and pipenumber respectively. The position of the pipes is shown in figure 2.2. The depth of the boreholes, the distance between rows, and between pipes in a row is assumed to be 7, 2.8 and 1.4 m respectively.

The difference between the vertical components of the magnetic field at two positions 0.4 m above each other is calculated (using equation 4) and considered as one measurement at the point half way between these two positions. The distance between measurement points in each pipe is 0.25 m. The total number of measurements is 348.
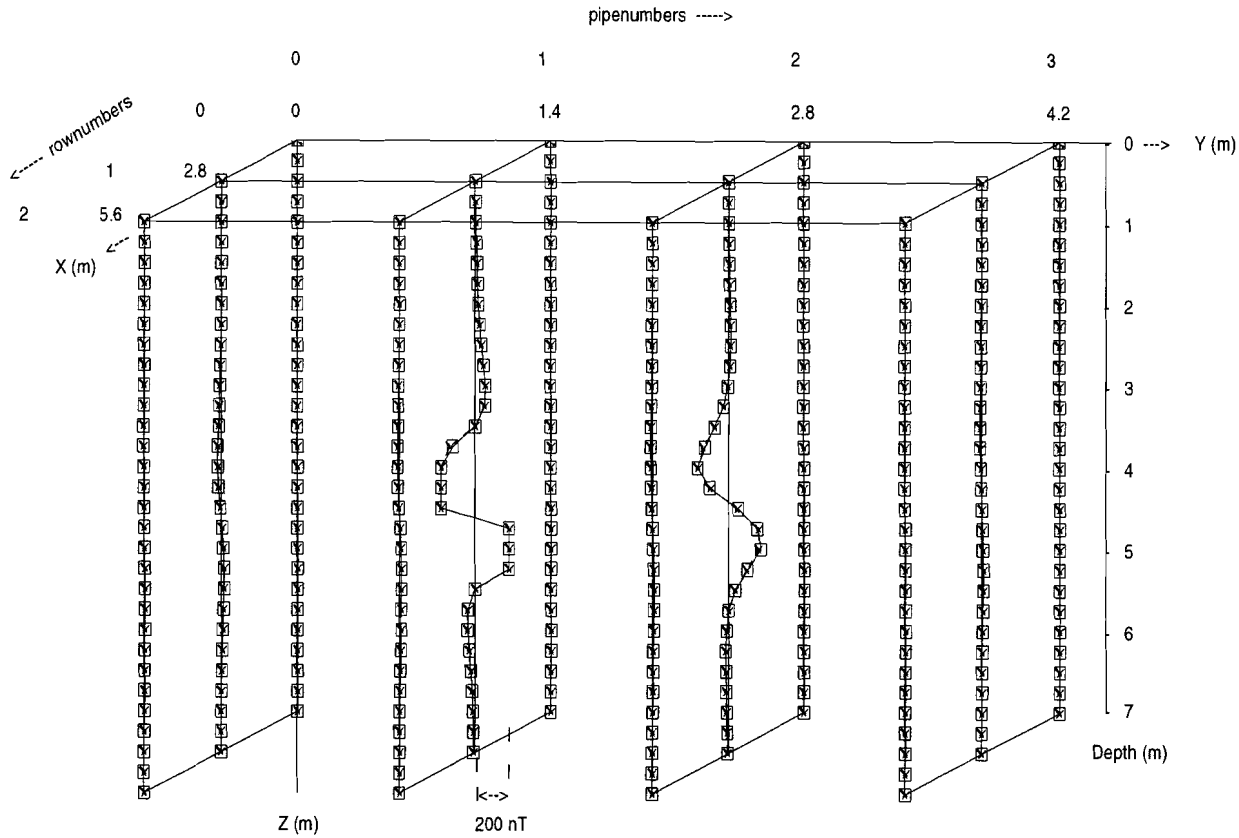
Figure 2.2: Synthetic observations (squares) and predicted data due to the inverted model (crosses). Larger amplitudes are clipped at -200 and +200 nT. The largest amplitudes in row: 1 pipe: 1 (the closest to the object) from the true model and inversion were 685 nT, -713 nT and 671 nT, -749 nT, respectively.

With the above explanations we can now define the weighting factors w_i which are used in the linear and nonlinear inversion. They are the same for all data corresponding to one pipe (vertical profile) and only change from pipe to pipe. This factor is defined for each pipe as follows

$$w_i = \left(\frac{\sum\limits_{i=1}^{ndp} |d_i|}{ndp} + \beta \right)^{-\alpha} .$$ (11)

β is a constant and prevents the factor from becoming large when the absolute norm of the data of pipes (vertical profiles) are very small. α is also a constant and d_i are the data (synthetic or real) and ndp is the number of the data in each pipe. After some tests the best value found for α was 0.6 and for β was 60 nT. If the anomalies are smaller and the noise level is lower β can be smaller.

In this way more weight is given to data from a pipe far from the object, where the anomaly is small (e.g. 50 nT), while the weight for the data from the pipe close to the object (anomaly e.g. 5000 nT) is less (this is true for the cases when looking for small magnetic objects in the subsurface).

In all tests (also for real data) the fit in the tables is defined as follows:

$$Fit = \frac{\sum\limits_{i=1}^{n} |d_i| - \sum\limits_{i=1}^{n} |r_i|}{\sum\limits_{i=1}^{n} |d_i|} \times 100$$ (12)

where n is the number of the local data set and d_i are data and r_i are residuals (differences between original and predicted data).

In all synthetic examples, 5% Gaussian noise (N) was added to the signal (S). The signal to noise ratio is defined as (Ward and Young 1980)

$$\frac{S}{N} = \left(\frac{\sum\limits_{i=1}^{n} (d_i^{pre})^2}{n\sigma^2} \right)^{\frac{1}{2}}$$ (13)

where n is the number of data, d_i^{pre} are synthetic noise-free data, and σ^2 is the variance of the data error.

In the following four trials with synthetic data will be explained:
Trial 1. In the first example the anomalous field is assumed to be due to a narrow long object which can be approximated by a two-dipole model. This object is positioned between rows 1,2 and pipes 1,2. The coordinates of the two dipoles and the components

of the magnetic moments of the two dipoles (true model) are presented in table 2.1 (trial 1). The effect of this object is calculated for all observation points. In the first example the standard deviation (σ) of the noise was 3.9 nT. The data was inverted by assuming a two-dipole model.

For a two-dipole model there are six parameters; three coordinates (x_1, y_1, z_1) of the first dipole and three coordinates (x_2, y_2, z_2) of the second dipole. Therefore, for the nonlinear minimization a six dimensional simplex method has to be used, with seven initial points which will be constructed at about zero-crossing depth around the pipe containing the data with the maximum absolute norm. This is done because the object will be the closest to the pipe with the maximum absolute norm of the data and because for a vertically magnetized object (which is most likely in The Netherlands where the earth magnetic field is nearly vertical) the zero-crossing of the anomalous field is at the

Six dimensional simplex method (synthetic data)									
Trial	Dipole	TM/IM	x	y	z	m_x	m_y	m_z	m_t	Fit
1	1	TM	3.30	1.80	4.10	-0.69	0.99	1.92	2.26	95%
		IM	3.30	1.81	4.10	-0.55	0.91	1.94	2.21	
	2	TM	3.60	1.90	3.75	1.24	-0.57	2.12	2.52	
		IM	3.59	1.89	3.74	1.14	-0.52	2.05	2.40	
2	1	TM	3.40	4.60	3.75	0.49	0.59	2.23	2.35	97.3%
		IM	3.32	4.72	3.63	0.53	0.54	1.56	1.73	
	2	TM	3.20	4.50	4.10	-0.74	0.57	1.92	2.13	
		IM	3.25	4.45	4.06	-0.09	-0.05	2.40	2.40	
3	1	TM	2.30	1.10	3.70	0.49	0.39	1.03	1.20	95.0%
		IM	2.22	1.08	3.74	0.11	0.68	1.36	1.52	
	2	TM	2.40	1.20	4.00	-0.54	-0.27	0.82	1.01	
		IM	2.42	1.27	4.02	-0.20	-0.60	0.47	0.97	
	3	TM	3.10	3.20	4.10	0.89	0.59	1.43	1.78	
		IM	3.17	3.13	4.10	0.85	0.77	1.50	1.89	
	4	TM	3.20	3.30	3.75	-0.54	-0.97	1.22	1.65	
		IM	3.21	3.29	3.78	-0.77	-1.11	1.40	1.95	
4	1	TM	4.15	2.10	4.05	-1.00	1.50	2.10	2.76	95.7%
		IM	4.15	2.13	3.98	-0.77	1.38	3.05	3.43	
	2	TM	4.30	2.10	3.80	0.50	-0.10	1.50	1.58	
		IM	4.43	2.08	3.68	0.24	0.04	0.51	0.56	

Table 2.1: The results of the synthetic data inversion. **TM** and **IM** stand for true model and inverted model. **x, y, z** and **m_x, m_y, m_z** show the position coordinates (in m) and magnetic moment components (in Am^2) of the dipoles respectively. The **m_t** indicates the total magnetic moment of one dipole in Am^2.
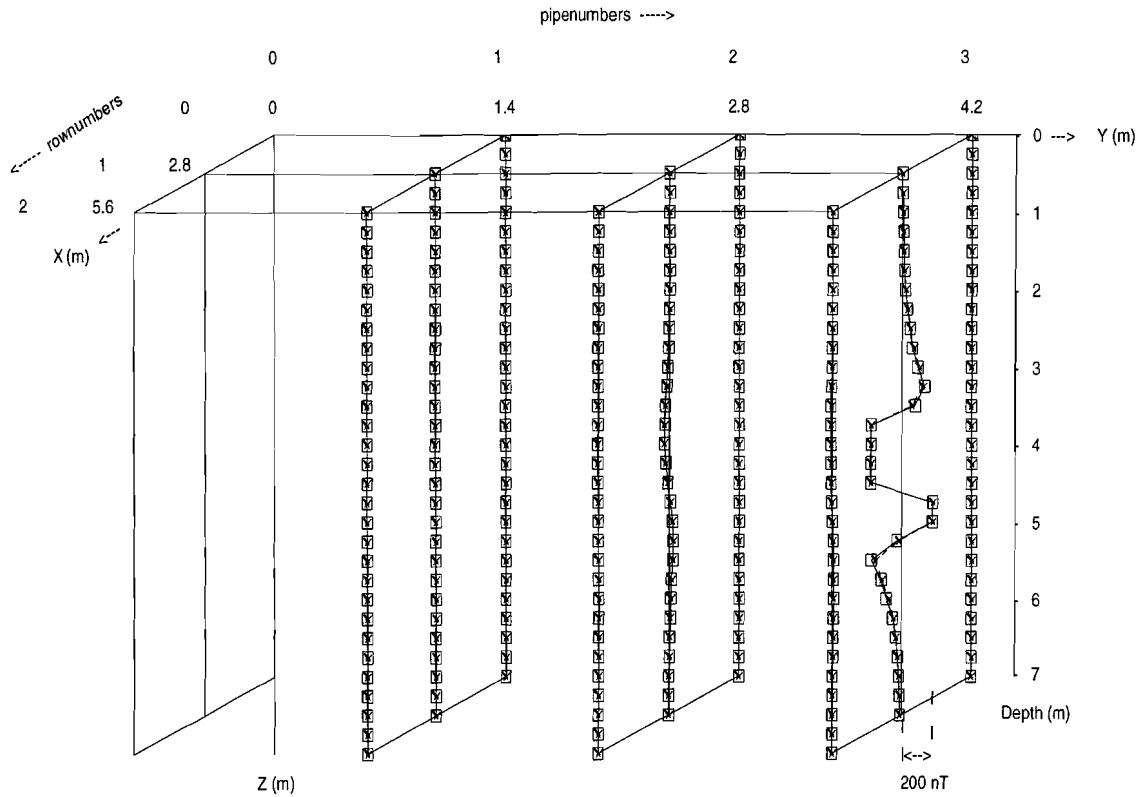
pipenumbers ----->

Figure 2.3: Synthetic observations (squares) and predicted data due to the inverted model (crosses). The object is to the right of the row: 1 pipe: 3. The largest amplitudes before and after inversion were 2103 nT, -1751 nT and 2117 nT, -1745 nT, respectively.

depth of the object. It should be mentioned that measurements on excavated bombs showed that the induced magnetization is always much stronger than the remanent magnetization (Bredewout, 1989).

After fixing the positions of the dipoles, the weighted linear inversion is started for each initial point. By linear inversion the best magnetic moments for each couple of dipoles and the data misfit can be found (for each initial point). These data misfits are the first calculated objective functions for the simplex routine. The routine returns seven optimized locations of the dipoles with their data misfit. The best point with the minimum value is the final position of the dipoles. The results are arranged in table 2.1 (trial 1).

As can be seen, the position of the dipoles are better resolved than the components of the magnetic moments since the least squares criterion was used in the linear inversion to solve the magnetic moments of the dipoles and the absolute norm criterion for the nonlinear one to solve for the position of the dipoles.

The original and predicted data are plotted in figure 2.2. Because the amplitudes of the anomalies have a wide range, we cut them off at ± 200 nT, in order to show the small amplitudes better.

Trial 2. In the second trial the object is placed outside the space where the rows and pipes are positioned. In this case the position of the object is near row 1, pipe 3. Only the data of nine pipes (figure 2.3) were used for the inversion since the effect of the data of other pipes was negligible. The original model and the results of the inversion after adding noise to the data ($\sigma = 8.2\ nT$) can be seen in table 2.1 (trial 2).

The positions of the dipoles are better resolved than the components of the magnetic moments of the dipoles by the data. This effect can be explained by the small number of data used in the inversion. When the number of data becomes less, it has less influence on the inverted model and causes the condition number to become larger and in turn the model to be more affected by noise. The fit between the original and inverted data is shown in figure 2.3. This example indicates that this method can also be used for the the case where the data is only measured on a plane at the surface (the measurement points will be on a horizontal plane instead of a vertical plane) .

Trial 3. In the third trial the anomalous field is assumed to be due to the existence of two small objects while each object is approximated by a two-dipole model. The first object is positioned between rows 0, 1 and pipes 0, 1 and the second one between rows 1, 2 and pipes 2, 3. The standard deviation of the data is 5.9 nT. The first object was found in the first inversion step, and after subtracting the effect of this object from the data, the second inversion step found the second object. The results of this example are shown in table 2.1 (trial 3).

Again the position of the dipoles was better resolved by the data than the magnetic moment components. The error of about ± 0.05 m in finding the position and about $\pm 20\%$ for the total magnetic moments of the dipoles seems to be reasonable when searching for small iron objects that must be dug out.
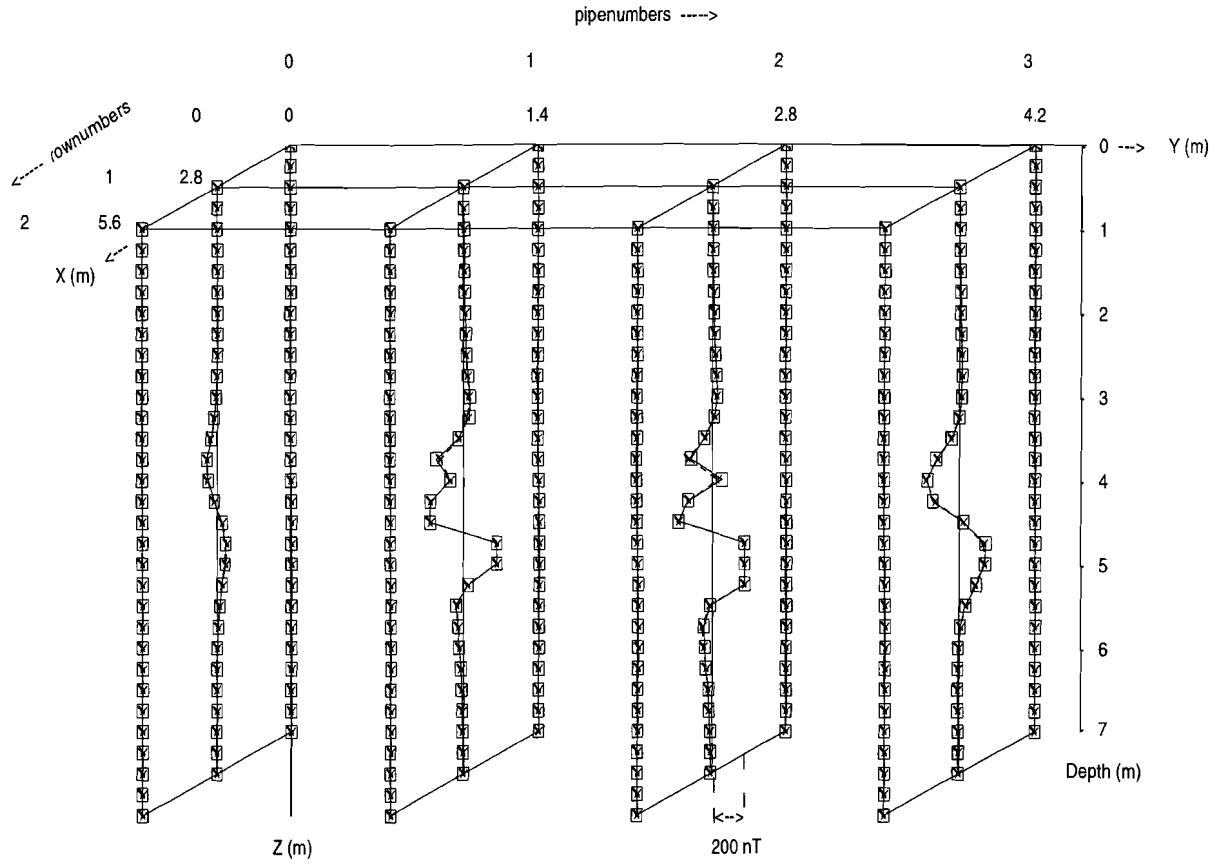
Figure 2.4: Synthetic observations (squares) calculated for a model consisting of two objects and predicted data due to the inverted model (crosses).

The distance of the dipoles for the first and the second object before and after inversion were 0.33 m, 0.39 m and 0.37 m, 0.36 m respectively. The fit between original and inverted data is plotted in figure 2.4.

Trial 4. If the source responsible for an anomaly is close to the measurement points (the distance being smaller than two times the size of the object), the data not only has large amplitudes, but also can not be explained by a one-dipole model. For this situation choosing a more complex model will better explain the data since the data contains more information about the source (size or shape). This will be quantified latter during inversion of real data. On the contrary if the source is not close to the measurement points the data will contain less information about the source. Then inversion of the data can only give rough information about the source.

Now the effect of using a two-dipole model for the case when the data has small amplitude (due to the object being not close to the measurement points compared with the size of the object) will be investigated.

Consider an object between rows 1, 2 and between pipes 1, 2 which is rather far from most of the pipes. The effect of the object is calculated using a two-dipole model. The data were inverted assuming a two-dipole model. The results are shown in table 2.1 (trial 4). The magnitude of the magnetic moment of the first dipole is large compared with the second one thus the effect of the object is almost explained by one dipole since the components of the magnetic moment of the second dipole are small. In this case the distance between measurements and the object was more than two times the size of the object. The original and inverted data are plotted in figure 2.5. The fit of this trial was 96 percent.

We have found empirically that if the distance of the measurements (pipes) from the object are more than two times the size of the object, then the data will not contain much information about the size of the object since most of the effect of the object can be explained by a one-dipole model. Using a model with more than one dipole can only slightly improve the fit. However, using a two-dipole model (six dimensional simplex method) for this case instead of a one-dipole model (three dimensional simplex method) makes the results of the inversion more reliable due to acquiring more initial models for the inversion (there is more chance that the minimum found is a global one when more initial models are used for the inversion).

2.4.2 Real data

The borehole data used (measured with a differential vertical flux gate magnetometer) were collected at Schiphol airport in the Netherlands where many unexploded bombs had been left from the second world war, down to depths of 10 m. The three dimensional simplex method, approximating the magnetic object by one dipole, was employed earlier by Bredewout, Nolet and Nijdeken (1993) for detecting bombs at Schiphol airport. In the present paper the data were inverted by assuming three different models:
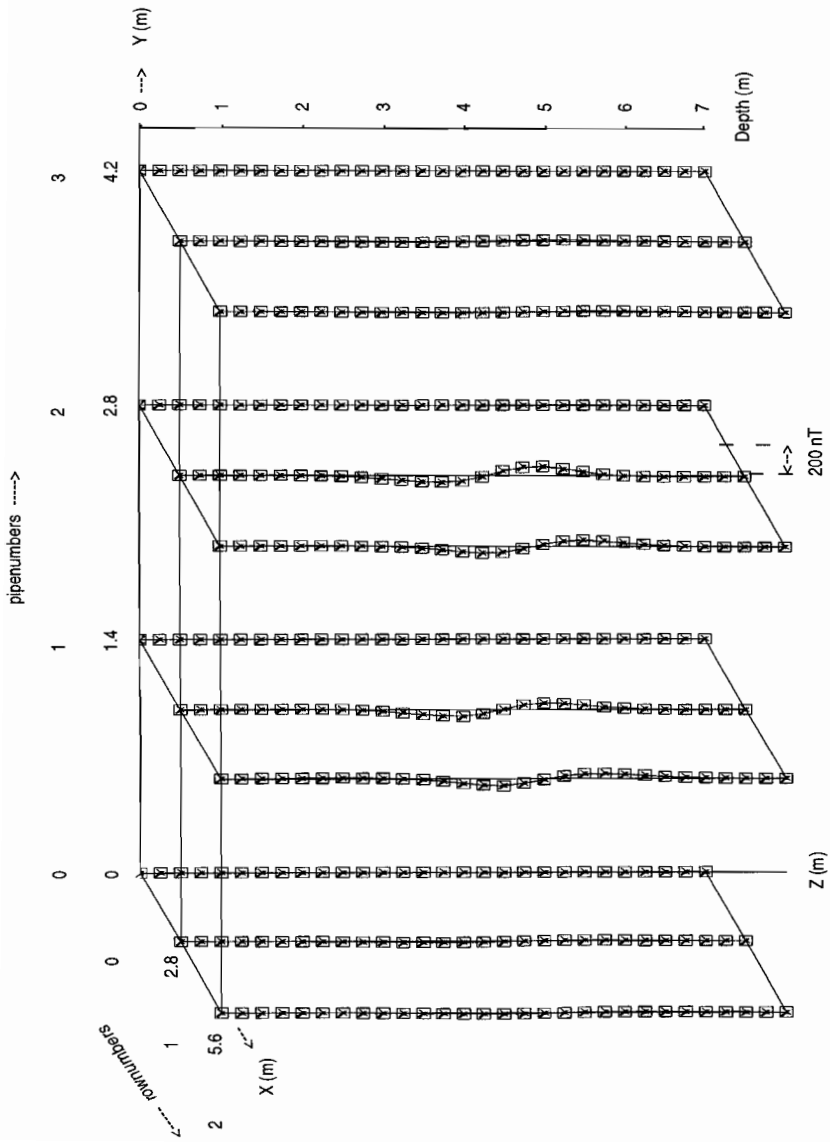
Figure 2.5: Synthetic observations (squares) calculated for a model consisting of one dipole far from most of the pipes and predicted data (crosses) due to the inverted model consisting of two dipoles.

The first was a two-dipole model with six unknown magnetic moment components for the linear inversion and six unknown parameters which define the position of the two dipoles for the nonlinear inversion. The simplex method in six dimensions is used to improve the initial position of the dipoles.

The second was a three dipole-model. The nine dimensional simplex method was employed for the inversion.

For comparison, inversion with a one-dipole model (three dimensional simplex method) was also performed.

2.4.2.1 Two-dipole model, six dimensional simplex

To test the method a few data set were chosen which had been collected in boreholes (pipes) in the vicinity of a buried bomb. The locations of rows and pipes are indicated in figure 2.6. The distance between pipes and rows is 1.4 m and all distances are measured with respect to the origin (row: 0 pipe: 0).

The starting positions are chosen around the pipe containing the data with maximum absolute norm and at a depth where the observed anomaly shows its zero-crossing. In each inversion step the data are taken from the pipes (maximum 25) around the pipe with maximum absolute norm of the data. After finding an object its effect is subtracted from the data and a new inversion step is started around a new pipe contains the data with the highest absolute norm. These steps are repeated until the absolute norm of the data of all pipes is below 75 nT, which is the minimum effect to be expected from a small bomb at a distance of 1.6 meter from the pipe. The magnetic moment of each object found can be compared with that to be expected from a real bomb (Bredewout *et al.* 1993), and it can be decided if the object found is a bomb.
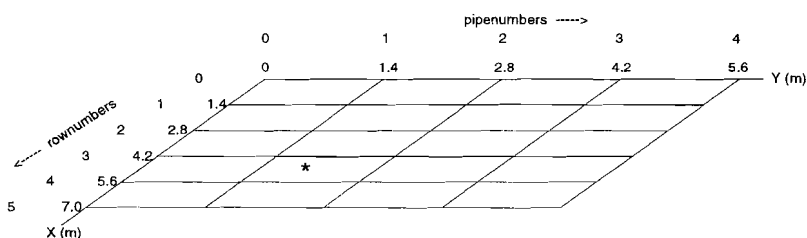

*Figure 2.6: The position of the rows and pipes for real data in the x-y plane. The " * " shows the position of the bomb, projected on the x-y plane.*
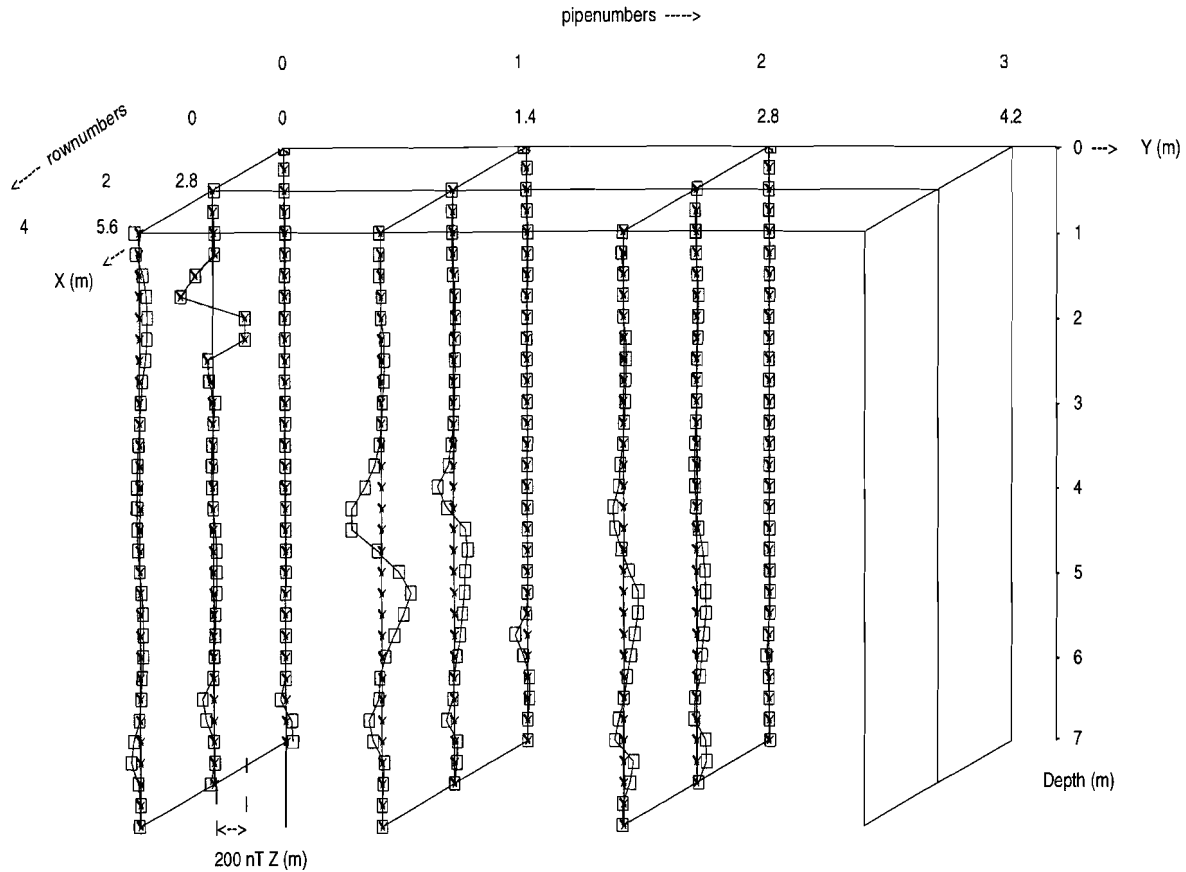
Figure 2.7: Observed (data set 1) and predicted data using the six dimensional simplex method for the first step of the inversion. Not the bomb but another object near row: 2 pipe: 0 was found.
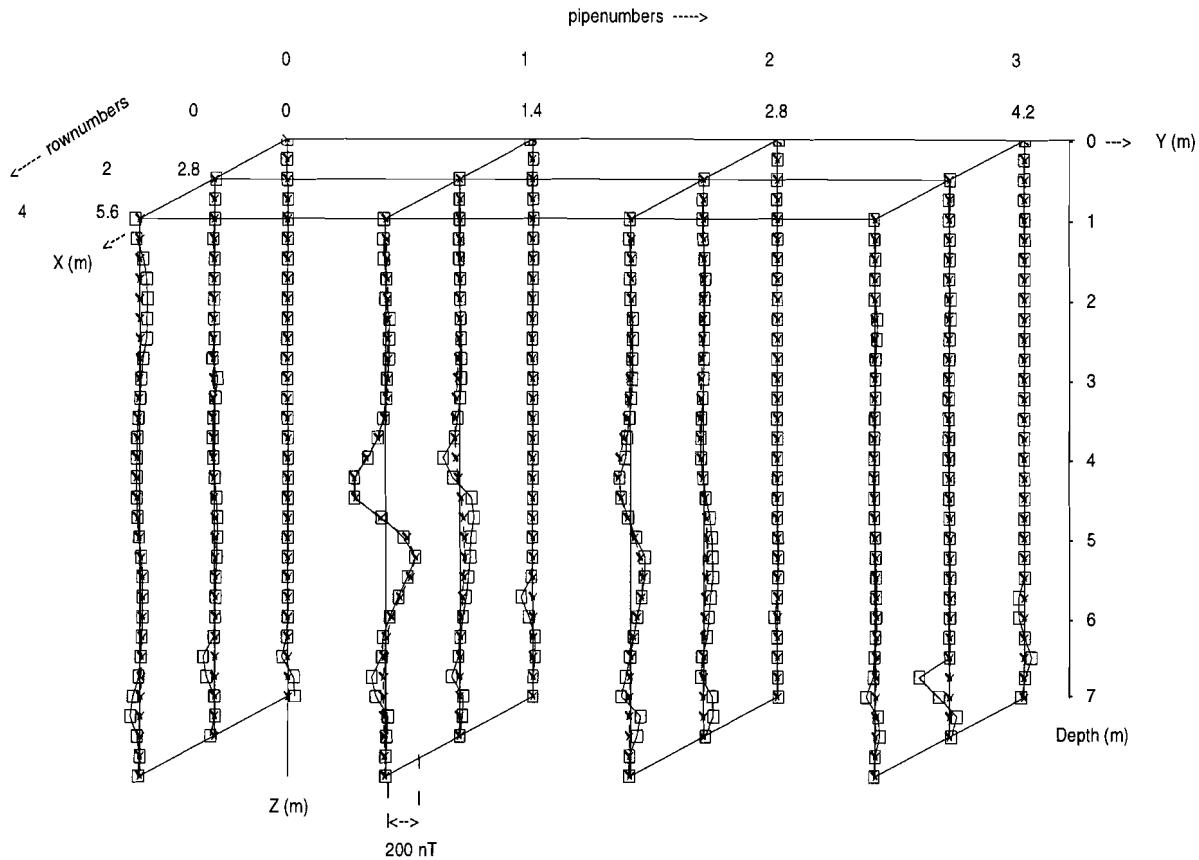
Figure 2.8: Observed (data set 1) and predicted data using six dimensional simplex method for the second step of the inversion, in which the bomb was found.

Three data sets were used for testing the method:

1. The first data set contains the data from rows 0, 2 and 4. The first inversion step was started around the pipe with the maximum absolute value of the data (row: 2 pipe: 0). For this inversion step only the data of 9 pipes were used for the inversion since the effect of the data of other pipes was negligible (figure 2.7). The first object found, at depth 1.41 m, was very close to pipe: 0 row: 2 (figure 2.7). This object was explained by a two-dipole model was not interpreted as a bomb. Latter digging showed it to be a steel rod.

After subtracting the effect of this object the reduced data set is shown in figure 2.8. The starting positions for the second inversion step was around row :4 pipe: 1. In this step the data of 12 pipes was used for the inversion and the object found was a bomb (also proved by latter digging). The results of the three and six dimensional simplex method of this step are presented in table 2.2 (data set 1).

Comparison of the results shows that choosing a two-dipole model does not improve the fit very much (only about 5%) compared with the one-dipole model. In this model the first dipole has small magnetic moment compared with the second one and the coordinates of the position of the second dipole are roughly the same as those of the one-dipole model(with accuracy of ± 0.05 m). The fit between measured and predicted data for the six dimensional simplex method is plotted in figure 2.8 . From these it is concluded that there is no advantage in assuming a two-dipole model for this data set, since the pipes containing the data with large absolute value are absent and the data contains no information about the size of the body.

The unfitted data is due to two sources:

(a) an unsatisfactory model for the bomb; this misfit is very small since the effect of the bomb is sufficiently explained by the dipoles found;

(b) a thin layer enriched in magnetic minerals (almost in all pipes between 5 and 7 m depth).

After subtracting the effect of the bomb from the data the inversion program continues and finds other dipoles, close to the pipes, to explain the effect of the thin magnetic layer (see figure 2.1).

2. The second data set contains the data from row 1,3 and 5.

In this data set the pipe with the highest absolute norm of the data is pipe 1 in row 3 which is close to the bomb.

Now the first object found by the inversion was the bomb. The results of this step are arranged in table 2.2 (data set 2). The fit between measured and predicted data is shown in figure 2.9-a.

3. The third data set (figure 2.9-b) consists of the rows 2, 3 and 4. Pipe 1 in row 3 contains the data with the largest absolute norm and the data of other pipes also have large amplitudes. The results of this step are arranged in table 2.2 (data set 3). The fit is plotted in figure 2.9-b.

From the results it can be seen that inversion of the second and third data set assuming a two-dipole model improves the data misfit about two times compared with

| Three, six and nine dimensional simplex method (real data)										
Data set	3D/6D/9D	Dipole	x	y	z	m_x	m_y	m_z	m_t	M_t	Fit
1	3D	1	4.55	1.79	3.83	0.15	-0.05	4.37	4.37	4.37	27.3%
	6D	1	5.19	1.54	3.90	0.23	0.62	-0.03	0.66	4.28	32.2%
		2	4.58	1.81	3.87	-0.10	-1.00	4.30	4.41		
2	3D	1	4.74	1.81	4.27	-3.91	0.48	4.78	6.20	6.20	26.7%
	6D	1	4.44	1.79	4.26	-1.35	1.26	2.27	2.93	4.65	54%
		2	4.59	1.60	3.76	1.68	-2.64	2.21	3.71		
	9D	1	4.42	1.50	4.28	0.40	-1.57	-0.36	1.66	6.55	59.2%
		2	4.49	1.64	4.21	-0.72	4.65	3.58	5.91		
		3	4.54	1.59	3.92	-2.00	-1.14	2.59	3.47		
3	3D	1	4.57	1.89	3.96	1.72	-0.11	3.73	4.10	4.10	25.3%
	6D	1	4.58	1.67	3.81	0.55	-0.86	2.85	3.03	5.28	53.2%
		2	4.33	1.83	4.22	0.25	0.87	2.37	2.54		
	9D	1	4.31	1.83	4.39	-2.46	0.66	1.13	2.79	5.58	56.7%
		2	4.56	1.64	3.91	0.44	-1.85	4.10	4.52		
		3	4.24	1.61	4.07	0.08	0.36	-.07	0.37		

Table 2.2 :The results of the real data inversion. **3D, 6D** and **9D** *stand for three, six and nine dimensional simplex method and* M_t *shows the total magnetic moment of one object in* Am^2.

the one-dipole model: from 26.7% to 53.9% and from 25.3% to 53.2% respectively. This is due to the fact that the measurement points were rather close to the bomb (since the data plots show large amplitudes) , thus the data was more affected by the size of the bomb. The fact that the method has not been able to explain hundred percent of the local data set in this step proves that there are either still effects of other sources or the model should be even more complex to explain the unfitted data (three-dipole model will be tested later).

The distance between the two dipoles (indicative for the length of the bomb) in both cases is about 0.5 m. The position of the dipoles in the six dimensions shows the bomb stands up about in a vertical position.

If the effect of the bomb is subtracted from the data, in the next inversion steps the inversion program can find other dipoles to explain the residual data set.

From the tests it is seen that if the measurement points are close to the anomalous body (within two times the size of the object) a simple model (one-dipole model) is not sufficient to explain the data and a more complex model (for example a two-dipole model) can better explain them.
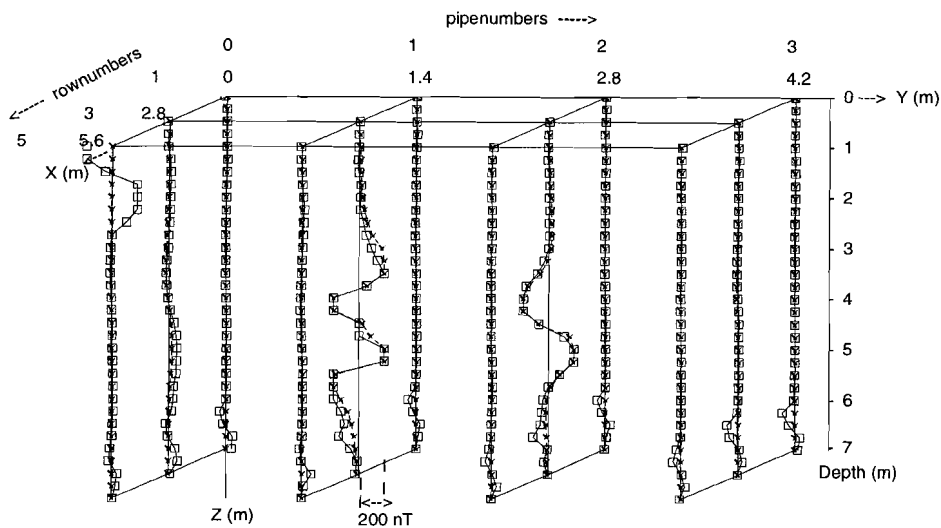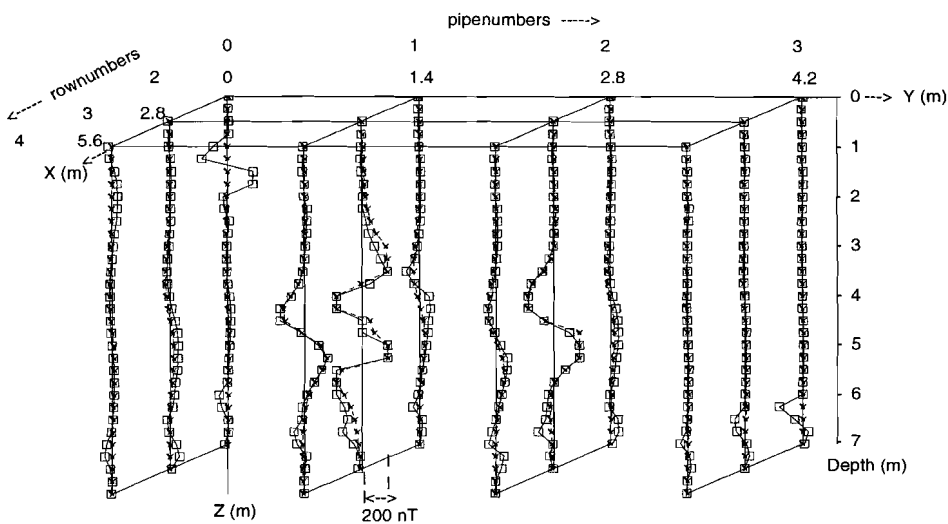
Figure 2.9: Observed and predicted data. The largest amplitude of the observations and of the predictions from the inversion in row: 3 pipe: 1 were: a. 2448 nT, -2520 nT, and 2530 nT, -2438 nT (data set 2) b. 2448 nT, -2550 nT, and 2518 nT, -2433 nT (data set 3). These were again cut off at -200 and +200 nT.

The most important point in employing a simplex method is acquiring more different initial models (for three dimensional simplex method 4 and for six dimensional 7) than in most gradient methods (only 1) for the inversion. This brings more confidence that the minimum found is a global one or very close to it. The only deficiency in employing the simplex method with more dimensions seems to be spending more time on the calculations in one step but this is compensated by a more reliable solution and by a smaller number of steps required.

2.4.2.2 Nine dimensional simplex method

As seen in the six dimensional case, selecting a sufficient model for the problem in hand, leads to a better explanation of the data.

It is therefore worth while to test the algorithm assuming a three -dipole model.

The inversion method is analogous to the two-dipole case, but now the simplex method will be employed in nine dimensions.

The results of this case for the second and third data set is also presented in table 2.2. From the results it can be seen that the fit is slightly improved compared with the six dimensional cases: from 53.9% to 59.2% and from 53.2% to 56.7% respectively. The magnetic moment of the third dipole is much smaller than that of the two other ones (0.37 nT against 2.79 nT and 4.52 nT); this means the third dipole has had little effect on the predicted data. The distance between two dipoles (dipole 1 and 2) is 0.57 m while the real length of the bomb found at Schiphol airport was about 0.7 m.

From the results it is inferred that assuming a three-dipole model for the inversion will only slightly improve the fit and thus it is not economic to consider models with more than two dipoles for all inversion steps. If we are interested in details of a certain object found by the six dimensional simplex method then other inversion strategies should be considered. For instance knowing the position of the objects found by the six dimensional simplex method some cells can be constructed around this position and a linear inversion can be performed.

2.5 Conclusions

Although there are many solutions for a magnetic anomaly, this nonuniqueness can be reduced to some extent by taking advantage of the problem in hand. In our problem we have a lot of borehole data and the information from these data indicate the starting positions close to the source, in each inversion step, for the linear and nonlinear inversion. This, and alternative optimization of the position and magnetic moments during the process of the inversion, leads to finding a solution which is reliable.

Choosing a sufficient model for a problem in hand can improve the fit and yield a reliable solution. Selecting two-dipole and three-dipole models in the cases where the data were collected close to the object (close compared with the size of the object) improves the fit and the solution, but not the calculation time (compared with that for the one-dipole model).

The results of the six or nine dimensional simplex method are more reliable than those of the three dimensional one since the former starts inversion with more different initial models, around the pipe with maximum absolute norm, than the latter and this gives more chance for the inversion to end up in a global minimum or very close to it.

The results of the tests of synthetic noisy data show that the method can resolve the position of an object better than its magnetic moment components due to using l_1 and l_2 norm criteria in the nonlinear and linear inversion which solve the position and magnetic moment components of an object.

The results for the magnetic moments and the positions of the dipoles are not exactly the same for different data sets and different models due to the following reasons:
a. The different data sets used and observational errors with different magnitude.
b. The existence of the inherent nonuniqueness in potential field data which could not be damped perfectly for this special problem.
c. The different number of initial models used for three, six and nine dimensional simplex method.

This routine can also be adapted for the case where the data has been measured in one plane, for example the earth's surface.

2.6 References

Al-Chalabi M. 1971-a. Interpretation of gravity anomalies by non-linear optimization. *Geophysical Prospecting* **20**, 1-16.
Al-Chalabi M. 1971-b. Some studies relating to nonuniqueness in gravity and magnetic inverse problems. *Geophysics* **36**, 835-855.
Barrodale I., Young A. 1966. Algorithms for best l_1 and l_∞ linear approximations on a discrete set. *Num.Math* **8**, 295-306.
Bhattacharyya B.K. 1980. A generalized multibody model for inversion of magnetic anomalies. *Geophysics* **45**, 255-270.
Braile L.W., Keller G.R. and Peeples W.J. 1975. Inversion of gravity data for two-dimensional density distribution. *Journal of Geophysical Research* **79**, 2017-2021.
Bredewout J.W. 1989. Optimalisatie van bomdetectie of Schiphol. *Rapport AEG-89-07*.
Bredewout J.W., G. Nolet and G. Nijdeken 1993. The inverse problem for local magnetizations, applied to bomb detection at Schiphol Airport. *Extended Abstracts*,

55-*th EAEG-congres, Stavanger*, PO43 (2 pages).

Claerbout J.F., Muir F. 1973. Robust modeling with erratic data. *Geophysics* **38**, 828-844.

Corbato C.E. 1965. A least-squares procedure for gravity interpretation. *Geophysics* **30**, 228-233.

Green W.R. 1975. Inversion of gravity profiles by use of a Backus- Gilbert approach. *Geophysics* **40**, 763-772.

Guillen A. and Menichetti V. 1984. Gravity and magnetic inversion with minimization of a specific functional. *Geophysics* **49**, 1354-1360.

Jupp D.L.B. and Vozoff K. 1975. Stable iterative methods for the inversion of geophysical data. *Geophys. J. R. astr. Soc.* **42**, 957-975

Kunaratnam K. 1972. An iterative method for the solution of a non-linear inverse problem in magnetic interpretation. *Geophysical Prospecting* **20**, 439-447

Last B.J. and Kubik K. 1983. Compact gravity inversion. *Geophysics* **48**, 713-721.

Menichetti V. and Guilen A. 1983. Simultaneous interactive magnetic and gravity inversion. *Geophysical Prospecting* **31**, 929-944.

Menke W. 1989. Geophysical data analysis: *discrete inverse theory*. Academic press Inc.

Mickus K.L. and Peeples W.J. 1992. Inversion of gravity and magnetic data for the lower surface of a 2.5 dimensional sedimentary basin. *Geophysical Prospecting* **40**, 171-193.

Narasimha Rao B., Ramakrishna P. and Markandeyulu A. 1994. Some aspects in inversion of potential field data: a damped approximate inverse approach. *Journal of Applied Geophysics* **32**, 219-233.

Nelder J.A. and Mead R. 1965. A simplex method for function minimization. *Computer Journal* **7**, 308.

Panofsky W.K.H. and Phillips M. 1962. Classical Electricity and Magnetism, Addison-Wesley, Reading P.143.

Parker R.L., Shure L. and Hildebrand J.A. 1987. The application of inverse theory to seamount magnetism. *Reviews of Geophysics* **25**, 17-40.

Pedersen L.B. 1977. Interpretation of potential field data a generalized inverse approach. *Geophysical Prospecting* **25**, 199-230.

Press W.H., Flannery B.P., Teukolsky S.A. and Vetterling W.T. 1986. *Numerical Recipes, the art of scientific computing*. The press Syndicate of the university of Cambridge.

Safon C., Vasseur G. and Cuer M. 1977. Some applications of linear programming to the inverse gravity problem. *Geophysics*. **42**, 1215-1229.

Store J. and Bulirsch R. 1980. *Introduction to numerical analysis*. New York: Springer-Verlag.

Vigneresse J.L. 1977. Linear inverse problem in gravity profile interpretation. *J.Geophys* **43**, 193-213.

Ward R.W. and Young C.Y. 1980. Mapping seismic attenuation within geothermal systems using teleseisms with application to the Geysers-Clear lake region. *J. Geophys. Res.* **85**, 5227-5236.

Chapter 3

Inversion of 2D gravity data for interface geometry using the subspace method

Abstract

The subspace technique is employed for inversion of gravity data. The basis vectors chosen are the normalized eigenvectors of the second derivatives (the Hessian matrix) of the objective function calculated for an initial model. The matrix inversion in the subspace of the model parameters will be better conditioned due to the smaller dimensionality and the limited number of eigenvectors used in the inversion. Since the most significant eigenvectors corresponding to the largest eigenvalues are used in the inversion, those elements of the model which are likely to have less influence in fitting the data or lead to local minima are eliminated. The solution of the inversion, in the subspace of the model parameter, in this way has small variance. This method was tested by inverting gravity data assuming two-and three-layer model. The tests proved fast convergence and stability of the inversion against the noise.

3.1 Introduction

In most geophysical inverse problems there is a non-linear dependence of the observable quantities on the parameters describing the model. The most common way of solving a nonlinear inversion is to make a local linear expansion about current model and then to conduct a linear inversion for perturbation of the model required to match the observed data. The updated model should be used as the basis for a further linear inversion and the iterations are continued until convergence is achieved, i.e. the model perturbation or

the data misfit lies below a preassigned threshold. This type of inversion depends on the direct solution of a set of simultaneous linear equations which lead to a matrix inversion. This approach has been employed by many people to invert gravity or magnetic data for solving position parameters, e.g. by Corbato (1965) ; Kunaratnam (1972) ; Pedersen (1977) ; Menichetti (1983) ; Mickus (1992).

The solution of a set of simultaneous linear equations is computationally very intensive when the number of data points and of model parameters become large. Thus for large scale problems, linearized techniques involving inversion of a Hessian matrix rapidly become difficult to handle. It can therefore be computationally advantageous to use techniques which can achieve convergence without the inversion of large matrices. To handle this problem, subspace techniques can be applied. Subspace techniques use a local minimization of an objective function in a subspace spanned by a limited number of vectors in the model space. The spanning vectors are called basis vectors. It is well known that the success or failure of a subspace technique depends upon the selection and the number of basis vectors chosen for the subspace.

The subspace technique and its application to large-scale inverse problems are discussed by Kennett and Williamson (1988), Oldenburg et al (1993) and Sambridge (1990).

In contrast to other authors we use as basis vectors the eigenvectors of the Hessian (second derivative of the objective function) matrix calculated for an initial model. Since the variance of the solution is related to the curvature and this in turn to the Hessian of the objective function, the variance of the solution can be controlled by selecting those eigenvectors which correspond to the largest eigenvalues. Because the inverse problem is non-linear, we consider an iterative procedure for this case in which no large matrices need to be inverted since only a limited number of eigenvectors are taken into the inversion. This makes inversion fast and stable against the noise. It should also be stressed that the basis vectors will be calculated only once for the initial model (reference model).

3.2 Methodology

A solution of most nonlinear inverse problems can be approached by minimization of an objective function and the minimization may be stated in terms of an optimization problem. The choice of the objective function depends on the nature of the problem and the error statistics of the data. If it is reasonable to assume Gaussian statistics then we can choose to minimize the sum of squares of differences between observed and predicted data

$$F(\mathbf{x}) = \frac{1}{2} (\mathbf{d_0} - \mathbf{d(x)})^{\mathrm{T}} \mathbf{C_d}^{-1} (\mathbf{d_0} - \mathbf{d(x)}), \tag{1}$$

where $\mathbf{x}$, $\mathbf{d(x)}$ and $\mathbf{d_0}$ are model parameters, predicted data and observed data vectors

respectively and $\mathbf{C_d}$ is the data covariance matrix, incorporating errors in the data. If it is necessary a, regularization term can be added to the above objective function. The aim is to find $\mathbf{x}$ in such a way that F ($\mathbf{x}$) is minimum.

Any solution of the above problem may be expanded in the following form

$$\mathbf{x}_i = \mathbf{x}_i^{ref} + \sum_{j=1}^{P} V_{ij}\alpha_j \qquad i = 1,\cdots,M \tag{2}$$

where $\mathbf{x}_i^{ref}$ are M parameters describing the reference model, V_{ij} are the i-th component of the orthonormal basis vectors (j=1, ..., P), α_j are expansion coefficients which we seek to estimate. Usually P is less than M. Each set of expansion coefficients, α_j, defines a point in a P-dimensional model space. The vector form of (2) is

$$\mathbf{x} = \mathbf{x}^{ref} + \mathbf{V}\alpha. \tag{3}$$

Since we will fix the reference model and basis vectors during the process of inversion only the expansion coefficient vector α should be estimated. Due to the nonlinearity of the inverse problem this can only be achieved after some iterations.

In each iteration model perturbations are given by

$$\delta\mathbf{x} = \mathbf{V}\delta\alpha \tag{4}$$

If $F(\mathbf{x})$ is a smooth function of $\mathbf{x}$ we can make a locally quadratic approximation about some current model $\mathbf{x}$ by truncating the Taylor series for $F(\mathbf{x})$:

$$F(\mathbf{x} + \delta\mathbf{x}) = F(\mathbf{x}) + \gamma^T\delta\mathbf{x} + \frac{1}{2}\delta\mathbf{x}^T \mathbf{H} \ \delta\mathbf{x} \tag{5}$$

in terms of the gradient vector γ and the Hessian matrix $\mathbf{H}$. The gradient and the Hessian matrix of the objective function, equation (1), can be calculated from:

$$\gamma = -\mathbf{G}^T\mathbf{C}_d^{-1}(\mathbf{d}_o - \mathbf{d}(\mathbf{x})), \tag{6}$$

$$\mathbf{H} = \mathbf{G}^T\mathbf{C}_d^{-1}\mathbf{G} - \nabla_\mathbf{x}\mathbf{G}^T\mathbf{C}_d^{-1}(\mathbf{d}_o - \mathbf{d}(\mathbf{x})) \tag{7}$$

where $G_{ij} = \dfrac{\partial d_i(\mathbf{x})}{\partial x_j}$. The Frechet derivatives G_{ij} can often be found analytically. In equation (7) the term $\nabla_\mathbf{x}\mathbf{G} = \nabla_\mathbf{x}\nabla_\mathbf{x}\mathbf{d}(\mathbf{x})$ appears with the data misfit, which describes the nonlinear dependency of the data on the model parameters. Since the nonlinearity is usually weak, the term is neglected in the computation of the Hessian.

If we replace $\delta\mathbf{x}$ (in equation 5) by its equivalence from equation (4) we have a new objective function in terms of $\delta\alpha$. Now minimization of the new objective function $F(\delta\alpha)$ with respect to new model parameters can be approached in the subspace of the original model parameters. The new model perturbations ($\delta\alpha$) can be determined by minimizing the objective function setting $\dfrac{\partial F(\delta\alpha)}{\partial(\delta\alpha_j)} = 0$, for $j = 1,\cdots,P$. This will result in the following relationship:

$$\delta\alpha = -(\mathbf{V}^T\mathbf{HV})^{-1}\mathbf{V}^T\gamma. \tag{8}$$

The model perturbation for each iteration can be approached by back projecting through equation (4)

$$\delta\mathbf{x} = -\mathbf{V}(\mathbf{V}^T\mathbf{HV})^{-1}\mathbf{V}^T\gamma. \tag{9}$$

If the number of selected basis vectors is P (P < M) matrix inversion of the projected Hessian is executed in the subspace of the original model parameters space. The small $P \times P$ projected Hessian matrix $\mathbf{V}^T\mathbf{HV}$ is usually well conditioned with reasonable choices for the basis vectors $\mathbf{V}$. The above equation (9) represents the generalized linear inversion formula for the subspace method.

For constructing the projected Hessian matrix we need to evaluate terms like

$$H_p^{(ij)} = \mathbf{v}^{(i)T}[\mathbf{G}^T\mathbf{C_d}^{-1}\mathbf{G}]\mathbf{v}^{(j)} \qquad i,j = 1,\cdots P \tag{10}$$

where $\mathbf{v}^{(i)}$ are column vectors of the matrix $\mathbf{V}$. It is not necessary to construct the matrix $\mathbf{G}^T\mathbf{C_d}^{-1}\mathbf{G}$ since only the following terms are needed for evaluating $\mathbf{H_p}$

$$H_p^{(ij)} = \mathbf{b}^{(i)T}\mathbf{C_d}^{-1}\mathbf{b}^{(j)}, \tag{11}$$

where $\mathbf{b}^{(i)} = \mathbf{G}\,\mathbf{v}^{(i)}$, so only a single vector multiplication is required for each element of the Hessian.

When the model perturbation, $\delta\mathbf{x}$, is estimated the current model, $\mathbf{x}$ can be updated and the updated model can be used for further iterations. The iterations will be continued until significant reduction in the Root Mean Squared (RMS) error between data and model response is no larger observed.

3.3 Choice of Basis Vectors

Formula (9) gives the model perturbation in terms of the basis vectors $\mathbf{V}$. Now the question is, how should the basis vectors be chosen. If the objective function (original) has a very sharp minimum in the vicinity of the estimated solution we would expect that the solution is well determined in the sense that it has small variance. Conversely, if the objective function $F(\mathbf{x})$ has a broad minimum, the solution would have large variance. Since the curvature of a function is a measure of the sharpness of its minimum, we expect that the variance of the solution is related to the curvature of the objective function at its minimum. The curvature of a function can be measured by its second derivative (Menke, 1989). If we calculate the second derivative of the objective function in the vicinity of its minimum and decompose it into its eigenvalues and eigenvectors, the eigenvectors corresponding to large eigenvalues give the best directions of movement to a solution which has small variance.

From the above argument we choose the normalized eigenvectors of second derivatives of the objective function (the Hessian matrix) as basis functions. The

Hessian matrix is calculated for a reasonably close reference model, as obtained from a rough analysis of the data possibly supplemented with information from seismic data, and decomposed into eigenvalues and eigenvectors using the singular value decomposition algorithm. Normalized eigenvectors are the basis vectors of the expanded solution.

For homogeneous sampling each basis vector represents a different spatial frequency, or wavelength for the model perturbations. In our case the basis vectors are very similar to sine and cosine functions and only a relatively small number P is required to describe a model. This forces each model parameter α_j to be constrained by many data and results in an overdetermined problem. The redundancy in the data set may therefore be used to provide some statistical reliability in the estimated model parameters.

If eigenvectors corresponding to small eigenvalues are used in the inversion as part of the directions of the movement in the model space, they will make large perturbations in the model without having any significant effect on the predicted data. Since these directions of the movement (eigenvectors corresponding to small eigenvalues) are omitted by a cut-off in the number of the eigenvectors, matrix inversion executed in the subspace of the model parameters will be fast and stable.

The conjugate gradient or singular value decomposition method can be used for solving linear inversion. By iterating the procedure we can approach the optimum value of α. Back transformation into full model space will result in an optimum solution for **x**.

3.4 Uncertainty and Resolution of the Resulting Model

The uncertainty in the resulting model arises both from the finite number of data and the observational errors in the data. In practical situations the observed data are unavoidably contaminated by errors. The uncertainty of the estimated model due to the data error propagation and resolution has been discussed by many authors (e.g. Wiggins 1972, Jackson 1972, Burkhard 1976). If the objective function is a smooth function of the model parameters and can be linearized in the neighbourhood of some reference model, the relationships of the data error analysis and resolution of the linear inversion can approximately be used for the nonlinear one.

If the data are standardized to zero mean and unit variance we may write a covariance matrix **C** for propagated data error from linear inversion in the form

$$\mathbf{C} = \mathbf{H_{sb}}^+ = \mathbf{V}(\mathbf{V}^T\mathbf{H}\mathbf{V})^{-1}\mathbf{V}^T \tag{12}$$

where $\mathbf{H_{sb}}^+$ is the generalized inverse of the subspace method. The square roots of the diagonal elements of the matrix **C** give the uncertainty in each individual parameter estimate due to data error propagation.

Model perturbations in each iteration in the least squares sense, say $\delta\mathbf{x}$, are given by solving the following linear equations system

$$\mathbf{H}\ \delta\mathbf{x}^{true} = -\ \boldsymbol{\gamma} \cdot \tag{13}$$

Premultipling both sides of the above equation by $\mathbf{H_{sb}}^+$ results in

$$\mathbf{H_{sb}}^+\mathbf{H}\ \delta\mathbf{x}^{true} = -\ \mathbf{H_{sb}}^+\boldsymbol{\gamma} \cdot \tag{14}$$

Since the right hand side of the above equation is just the estimated model, $\delta\mathbf{x}$, the following equation gives the relation between estimated and true model perturbation for the linearized inversion

$$\delta\mathbf{x} = \mathbf{H_{sb}}^+\mathbf{H}\ \delta\mathbf{x}^{true} \cdot \tag{15}$$

The resolution matrix $\mathbf{R}$ can be defined as

$$\mathbf{R} = \mathbf{H_{sb}}^+\mathbf{H} \tag{16}$$

If $\mathbf{R}$ is the unitary matrix then all model perturbation parameters are resolved perfectly. If the ith row of the resolution matrix $\mathbf{R}$ is denoted by $\mathbf{r}_i(\xi)$ then the parameter x_i can be considered as the weighted average of the whole set of parameters with the averaging kernel $\mathbf{r}_i(\xi)$. The averaging kernels $\mathbf{r}_i(\xi)$ are typically maximum in a range about the position parameter ξ.

Using the equivalence of the generalized inverse, $\mathbf{H_{sb}}^+$, from equation (12) the resolution matrix can be written in the form

$$\mathbf{R} = \mathbf{V}(\mathbf{V}^T\mathbf{H}\mathbf{V})^{-1}\mathbf{V}^T\mathbf{H}. \tag{17}$$

The resolution matrix will be the unitary matrix if its rank is M. The more eigenvectors are used as basis vector in the inversion, the more the errors of the data will propagate into the estimated model parameters and the more the resolution will improve ($\mathbf{H_{sb}}^+\mathbf{H}$ will approach the unitary matrix). Thus there is a trade off between error propagation and model resolution.

3.5 Forward Calculation

For the sake of brevity, we restrict the methodology to the case of two-dimensional gravity sources. Extensions to three-dimensional modeling are straightforward.

A finite region in the vertical $x - z$ plane is divided into M rectangular prisms. Each prism is infinite in the y-direction. Upper and lower boundary of the prisms approximate interfaces between layers. Between two interfaces the density contrast is assumed to be constant.

The vertical component of the gravitational attraction g of one elementary prism at a measurement point (x_o, y_o) is given by

$$g(x_o, y_o) = K\rho \int_x \int_z \nabla_z \log \frac{1}{|\mathbf{r} - \mathbf{r_o}|} \, dx \, dz \qquad (18)$$

where K is the gravitational constant, ρ the density contrast and $\mathbf{r}$ and $\mathbf{r_0}$ are the vector distances from the origin to a point of the prism and the observation point respectively. For simplicity we assume the observation point is at the origin , $\mathbf{r_0} = \mathbf{0}$.

After integration and some manipulations the gravity effect of one elementary rectangular prism is given by:

$$g = K\rho \left\{ x_2 \log \frac{x_2^2 + z_2^2}{x_2^2 + z_1^2} + 2z_2 \left(\tan^{-1} \frac{x_2}{z_2} - \tan^{-1} \frac{x_1}{z_2} \right) \right.$$

$$\left. - x_1 \log \frac{x_1^2 + z_2^2}{x_1^2 + z_1^2} - 2z_1 \left(\tan^{-1} \frac{x_2}{z_1} - \tan^{-1} \frac{x_1}{z_1} \right) \right\} \qquad (19)$$

Where x_1, x_2, z_1 and z_2 are the boundaries of the elementary prism.

In general we assume a model consisting of n layers and n-1 interfaces which separate the layers. The nth layer is also assumed to be extended to infinity. Each layer consists of M elementary prisms whose lower boundaries approximate the interface between the layers. Each interface and each elementary prism within one layer is indexed by i and j respectively. From these conventions the effect of all M elementary prisms at one observation point can be calculated by summing up the effect of all elementary prisms, assuming the density contrast is the same for all prisms within each layer, as follows

$$g = K \left\{ \sum_{i=1}^{n} \sum_{j=1}^{m} (\rho_i - \rho_{i+1}) \left(x_{2_{ij}} \log \frac{x_{2_{ij}}^2 + z_{2_{ij}}^2}{x_{2_{ij}}^2 + z_{1_{ij}}^2} + 2z_{2_{ij}} \left(\tan^{-1} \frac{x_{2_{ij}}}{z_{2_{ij}}} - \tan^{-1} \frac{x_{1_{ij}}}{z_{2_{ij}}} \right) \right. \right.$$

$$\left. \left. - x_{1_{ij}} \log \frac{x_{1_{ij}}^2 + z_{2_{ij}}^2}{x_{1_{ij}}^2 + z_{1_{ij}}^2} - 2z_{1_{ij}} \left(\tan^{-1} \frac{x_{2_{ij}}}{z_{1_{ij}}} - \tan^{-1} \frac{x_{1_{ij}}}{z_{1_{ij}}} \right) \right) \right\}, \qquad (20)$$

where $\rho_{i+1} = 0$ if $i = n$.

The first partial derivatives of the predicted data with respect to the model parameters (lower boundary of each elementary prism) can be obtained from:

$$\frac{\partial g}{\partial z_{2_{ij}}} = 2K(\rho_i - \rho_{i+1}) \left(\tan^{-1} \frac{x_{2_{ij}}}{z_{2_{ij}}} - \tan^{-1} \frac{x_{1_{ij}}}{z_{2_{ij}}} \right) \quad j = 1, \ldots, m \quad i = 1, \ldots, n \qquad (21)$$

3.6 Efficiency of the Method

We tested the efficiency of the method with synthetic and real data to determine inherent limitations. The following examples assume a priori that the density contrast between layers are constant and known.

3.6.1 Example with synthetic data assuming a two-layer model

We consider an interface separating two layers with a density contrast of -0.5 g/cm^3. The interface is approximated by the lower boundaries of 40 rectangular prisms. The maximum depth of the interface is about 4.5 km. The width of the model and of the profile are 27 and 30 km respectively (figure 3.2-a lower part, dashed line). The effect of the model was calculated at 100 observation points. 5% Gaussian noise was added to the data. The standard deviation of the noise was 2.3 mGal.

Taking a horizontal flat interface at a depth of 2 km as reference model the Hessian was calculated and decomposed into its eigenvalues and eigenvectors. Figure 3.1-b shows plots of normalized eigenvectors or basis functions ordered from top to bottom in order of decreasing corresponding eigenvalues. These are very similar to Fourier series. Each eigenvector plot shows the relative weights that each of the model parameters receive in each eigenvector. Eigenvectors corresponding to large eigenvalues show a less oscillatory behavior. These eigenvectors give the best constrained search directions in model space and have the most significant effect on the predicted data. The more eigenvectors used in the inversion the more oscillatory will be the inverted model.

Now the question is how many eigenvectors should be used in the inversion. Therefore, the logarithm of the condition number (the ratio of the largest eigenvalue λ_1 to each eigenvalue λ_i) is calculated and plotted versus eigenvalue numbers (figure 3.1-a). This plot does not show any sharp cut-off number above which the eigenvalues start to decrease rapidly. Thus from this point we can not decide about the number of eigenvectors to be used in the inversion without causing instability. By doing some tests we have found empirically that if eigenvalues are chosen with a condition number less than one hundred then inversion is stable. This empirical upper limit for the number of eigenvectors has been used in the inversion. In this example it corresponds with an eigenvalue number 12.

First we will show the effect of the number of the eigenvectors used in the inversion on the final results. During the process of inversion the reference model is kept fixed and only the perturbations to the model are optimized.

The solid line in the bottom panel of figure 3.2-a shows the obtained model after 4 iterations, when 5 eigenvectors are used. The resultant model is a smooth model and the misfit is greater than the standard deviation (3.96 against 2.30 mGal). Vertical bars denoting an uncertainty less than 0.1 km on the estimated model which are quite small.
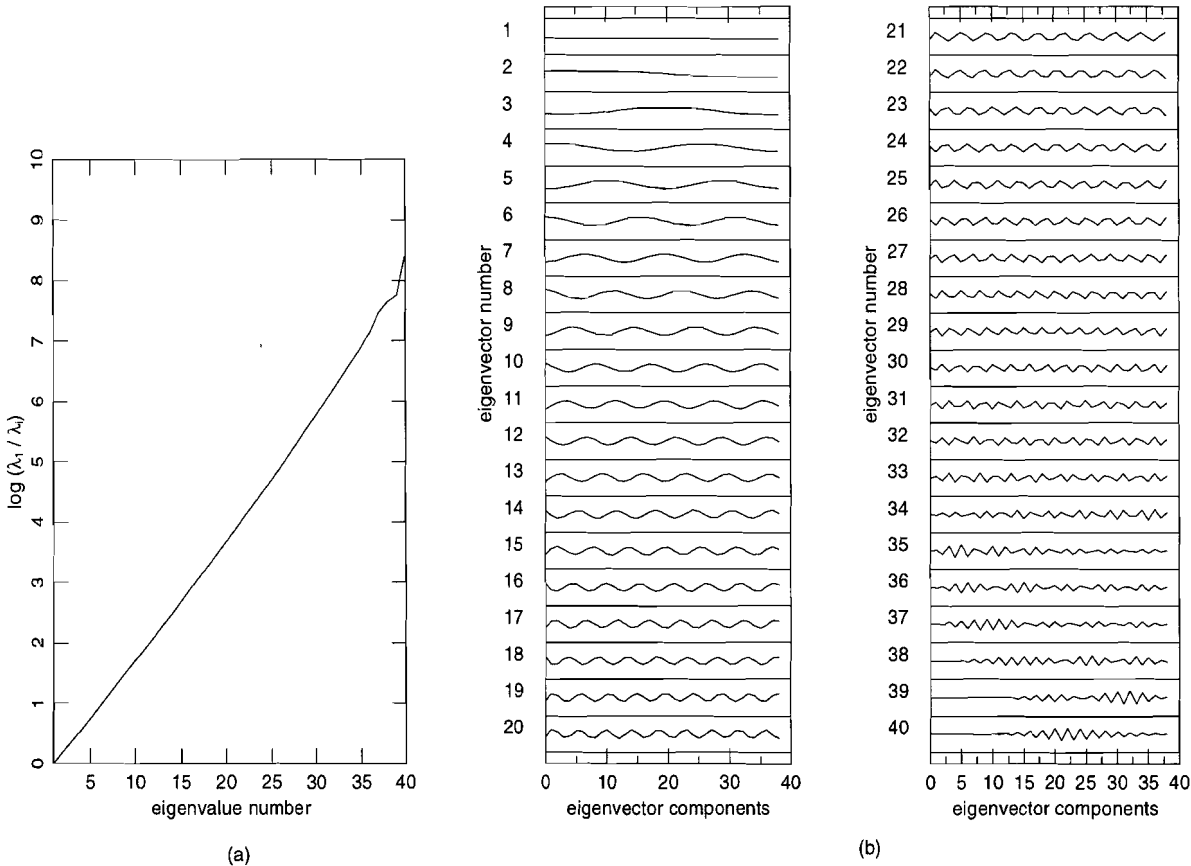
Figure 3.1: Eigenvalues and eigenvectors calculated for an initial model at depth 2 km and 100 observations. a) Largest eigenvalue divided by each eigenvalue plotted on a logarithmic scale with base 10. b) Normalized eigenvectors of the Hessian matrix (vertical scale of each eigenvector box is from -1 to +1).
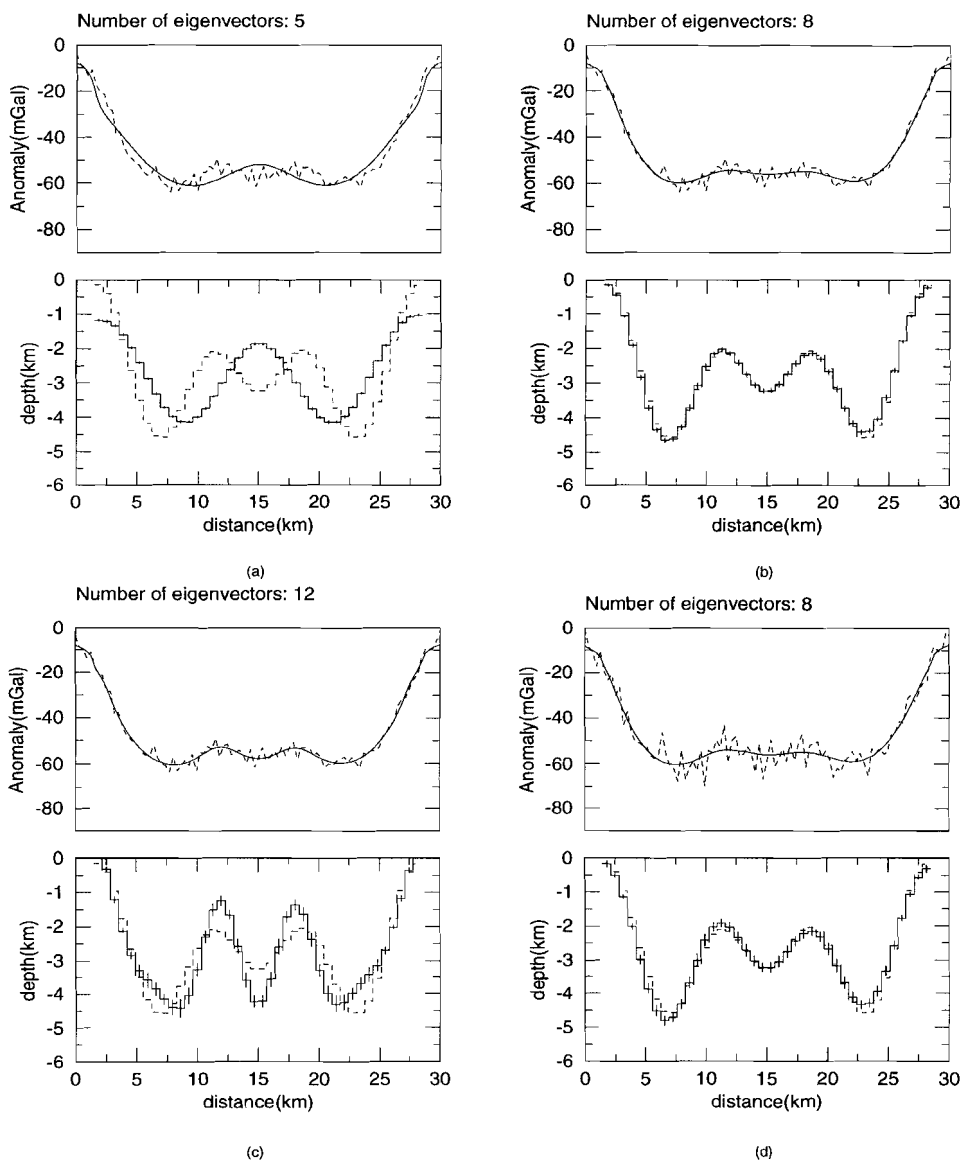
Figure 3.2: In each part the top panel shows the fit between the predicted (bold curve) and synthetic data (dashed curve) and the bottom panel shows the agreement between the inverted model (bold curve) and true model (dashed curve). The data was inverted using a) 5 b) 8 c) 12 d) 8 eigenvectors respectively. In (a), (b), (c) cases the level of noise was 5% and in (d) 10%.

Using 8 eigenvectors (figure 3.2-b) the misfit after four iterations is slightly less than the standard deviation (2.24 against 2.30 mGal). Figure 3.2-b shows that the true model is almost retrieved and noise is not minimized.

Figure 3.2-c shows large perturbations generated in the model which indicate instability in the inversion. For this case using 12 eigenvectors we obtained a misfit of 2.15 mGal, which is less than the standard deviation. This indicates that the data are being fit excessively, which is an additional indication that too many basis vectors have been used.

These plots show that only a limited number of eigenvectors (in this case 7 or 8) may be used in the inversion without degrading the data fit. The number of basis vectors to be used depends in general on the number of data, on the distance of measurements points from the sources responsible for the anomaly and on the reference model.

We also increased the level of the noise to ten percent and inverted the data using 8 eigenvectors. The results are shown in figure 3.2-d. The model is almost retrieved. The uncertainties of the model parameters are still small (vertical bars plotted on the inverted model). This test shows again stability of the inversion against the noise.

The results of the inversion for different reference models will be almost the same if they are not selected too far from the mean depth of the true interface. The maximum number of eigenvectors which can be used in the inversion depends on the selected depth for the reference model and the number and configuration of the data. By doing some tests we found that the best choice for a reference model is the mean depth. Information about the mean depth of single interface can be obtained from the data itself or from other sources.

3.6.2 Example with real data assuming a two-layer model

In order to test the algorithm with real data a set of gravity measurements taken across the Roervalley graben in The Netherlands has been used. The measurements are irregularly spaced and of varying precision. The profile is 70 km long and consists of 234 measurements. The unfiltered data without any smoothing or interpolation was used for the inversion. The density contrast between basement and sedimentary rock is -0.55 g/cm^3, which was obtained from well information. The model is assumed to be a 2D one.

In the first trial the interface was approximated by the lower boundary of 20 elementary prisms. We assumed a flat interface at a depth of 0.7 km as reference model and inverted these dense data using all 20 eigenvectors. Due to the large number of data points each part of the model will be well constrained and the matrix inversion well conditioned.

While inversion for a small number of model parameters and dense data is usually very stable, it can not represent a detailed model. Figure 3.3-a shows the results of the

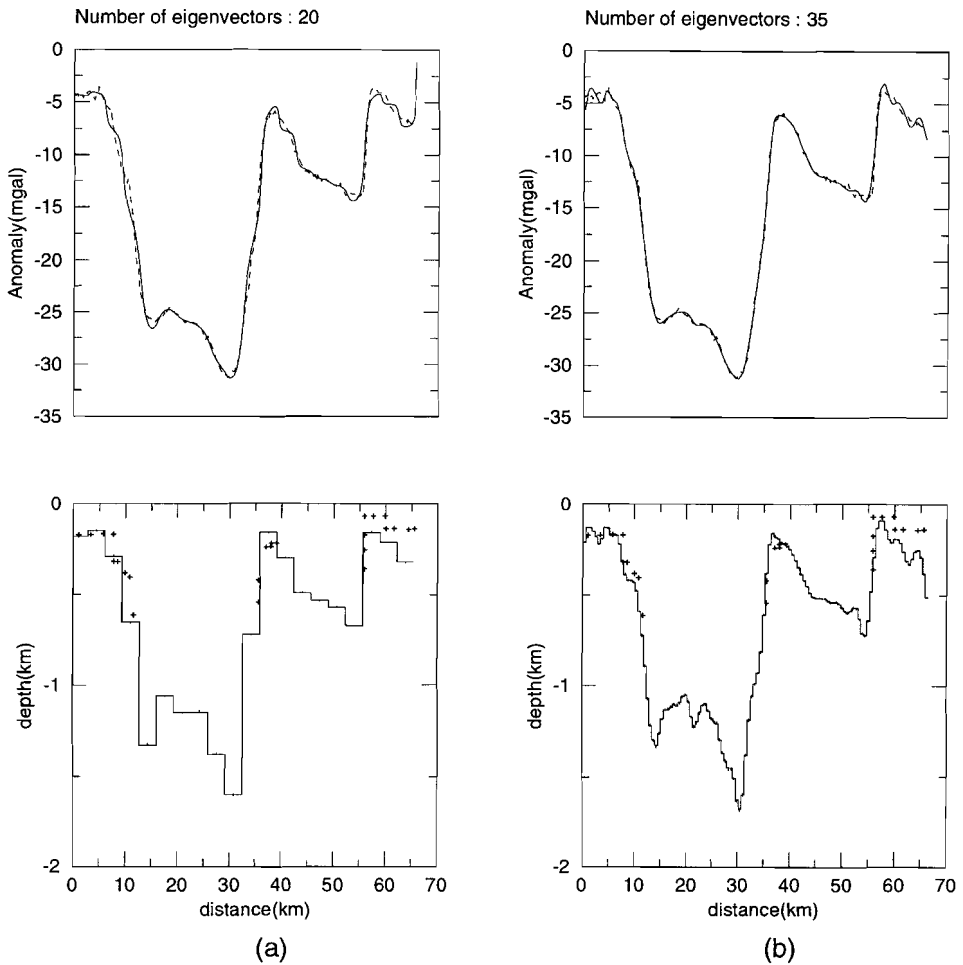Number of eigenvectors : 20   Number of eigenvectors : 35

Figure 3.3: In each part the top panel shows the fit between predicted data (bold curve) and observed data (dashed curve) and the bottom panel shows the inverted model. The results of the inversion were obtained with a) 20 b) 35 eigenvectors. The crosses show some information from bore holes and mining activities.

inversion after 4 iterations. The fit between predicted and observed data is not indeed very good because of the inadequate number of model parameters. The misfit for this trial was 0.92 mGal. The uncertainty of the model parameters was calculated by assuming a standard deviation (noise level) of 0.3 mGal for the observations. On the inverted model the uncertainties, shown by vertical bars, are smaller than 0.02 km and therefore hardly visible. The existence of the faults in the model is evident. The crosses in the figure are the depth information from bore holes and mining activities. Apart from the
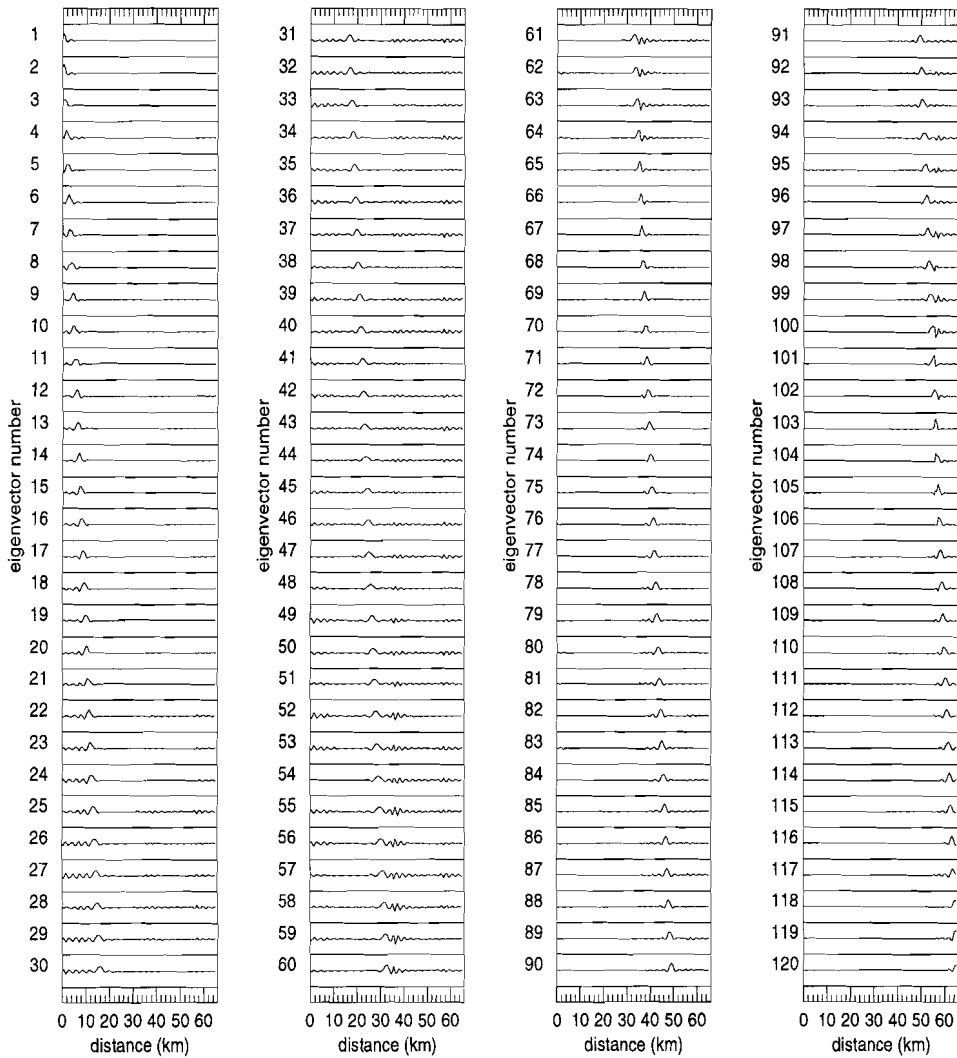
Figure 3.4: Resolution matrix plots when 35 eigenvectors are used in the inversion (vertical scale of each model parameter box is -1 to +1).

margins there is a good agreement with the inverted model.

In the second trial we modeled the data with 120 parameters. Then, the condition number becomes 100 for an eigenvalue number of 35, which therefore can be considered as the upper limit for the number of eigenvalues to be used. In figure 3.3-b we show the results when 35 eigenvectors are used in the inversion. After 4 iterations the

misfit was reduced to 0.45 mGal. On the plots a better fit is observable in the middle part than at the margins since the edges are less constrained by the data. It can be seen that a number of steep faults are detected by using a limited number of eigenvectors and in most parts there is agreement between the model and the crosses. Comparing these results with those from a model with 20 parameters shows great improvement in the data fit and in details of the obtained model.

The rows of the resolution matrix of the last example are plotted in figure 3.4. The plots show how well each model perturbation parameter is estimated independently. As can be seen, each model perturbation parameter is estimated as a local average of some neighbouring model parameters. The measure of dependency of each model perturbation parameter is proportional to the width of the corresponding peak. This width can be seen to be rather small. We can improve the resolution using more eigenvectors but it may minimize the noise and also introduce artifacts to the model.

We also did some tests with other reference models. If the reference model is chosen to be close to the mean depth the results are almost the same. The features which are close to the reference model will be better resolved .

3.6.3 Example with synthetic data assuming a three-layer model

Our model will be a 2-D stratified density structure consisting of variable-thickness homogeneous layers and it is well known that inversion for solving the interfaces from the gravity data is not unique, i.e, many models will fit the data. If some constraints are considered for the inversion the nonuniqueness will be reduced to some extent. For example, the solution to the inversion of the gravity data for the interface of a two-layer model, as used in the preceding paragraph, is almost unique provided that the density contrast and the average depth are known.

In the cases where the model consists of more than two layers the inversion for solving the interfaces from the data will be nonunique.

We consider a simple model with two interfaces separating three layers of constant density to find the limitations for the inversion of gravity data for more than one interface. We assume the first and second layer have density contrasts -0.60 and -0.40 g/cm^3 respectively with the third layer (the basement). Each interface is approximated by 40 model parameters (figure 3.6-a lower part, dashed line). The maximum depth is about 4.5 km. Observations (all have the same level) were generated and 5% Gaussian noise was added to these data. The length of the profile is 30 kilometer. We assumed a reference model with two horizontal interfaces at depths 1.5 and 3.5 km. We parameterized the model in such a way that the depth of the first interface and the thickness of the second layer were taken as unknown model parameters.

The eigenvector and eigenvalue plots are shown in figure 3.5. On the plot of eigenvalues (figure 3.5-a) a jump in the eigenvalue spectrum is visible around
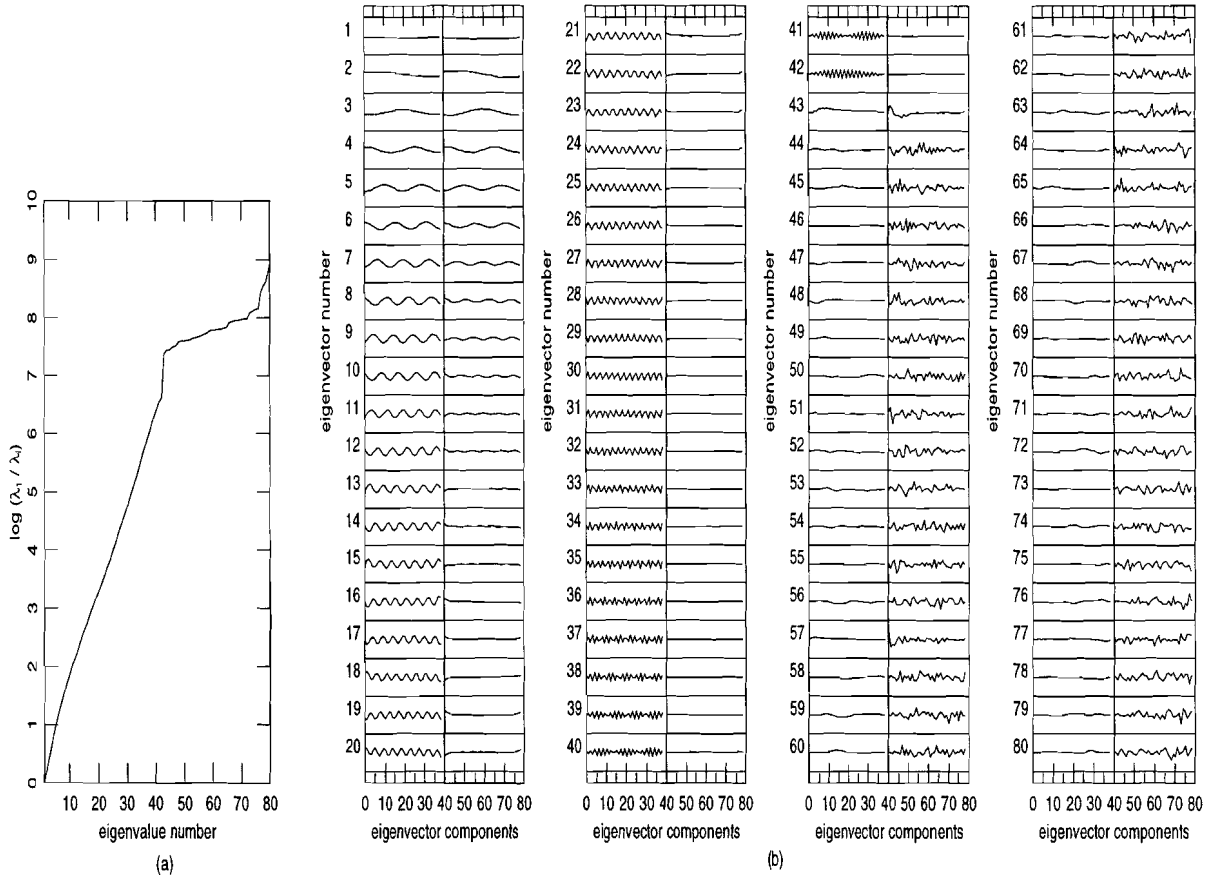
Figure 3.5: Eigenvalues and eigenvectors calculated for an initial interface at depth 1.5 and a thickness 2.0 km for 120 observations. a) Largest eigenvalue divided by each eigenvalue plotted on a logarithmic scale with base 10.

eigenvector 42. This jump can be seen to be associated with eigenvectors with very short wavelength perturbations of the second interface. The number of eigenvalue at this position can not be considered as an upper limit since the condition number for this position is too high (10^7).

The upper limit 100 for the condition number, as before, can be a criterion in selecting number of eigenvectors for the inversion. In figure 3.5-b from eigenvector 1 to about 40 the components of eigenvectors, corresponding to the first interface, have much larger amplitudes than those corresponding to the thickness of the second layer except from 1 to about 8 whose amplitudes are almost the same for both the interface of the first layer and the thickness of the second layer. These eigenvectors are corresponding to the first 8 largest eigenvalues. Each of these 8 eigenvectors gives almost the same weight to each model parameter corresponding to the interface and thickness which have the same position. These eigenvectors also have the largest effect on the predicted data. From about eigenvector number 41 to 80 the situation is quite opposite. The components of eigenvectors corresponding to the thickness of the second layer possess larger amplitudes but are more oscillatory than those of the first one. This effect is also observable in the eigenvalues plots by a sharp jump at eigenvalue number 40 (figure 3.5-a). The facts suggest that the first interface will be more constrained by the data than the second one and can better be resolved by the eigenvectors corresponding to the largest eigenvalues. Only the long wavelength perturbations of the second interface are constrained by the eigenvectors 1-8. If it is tried to use more eigenvectors in the inversion the second interface will be more oscillatory and less reliable than the first one and also cause more instability in the inversion.

To have a solution with positive depths and thicknesses from the inversion we use positivity constraints as follows: We introduce new model parameters by transformation $x_j^{new} = \sqrt{x_j}$. With this transformation each element of the new sensitivity matrix has the form $G_{ij}^{new} = 2\ G_{ij} x_j^{new}$.

In the first trial we inverted the data using 6 eigenvectors. The misfit after 4 iterations reduced to 3.50 mGal which is larger than the true one (2.89 mGal). This shows the poor convergence due to using less eigenvectors in the inversion. The results of this trial, depicted in figure 3.6-a, show that the estimated model is smooth.

In the second trial we increased the number of eigenvectors to 8. The inversion process (without positivity constraint) ended up to a poor convergence due to some negative results for the depths and thicknesses. This poor convergence is due to the fact that the initial model does not lie very close to the true solution. To improve the convergence we combine the Marquardt method in the inversion by adding a constant to each diagonal element of the Hessian matrix, calculated at each iteration for the current model. After this modification the diagonal elements of the Hessian will have the following form:

$$H_{jj} \Rightarrow H_{jj}(1 + \lambda) \cdot \qquad (22)$$

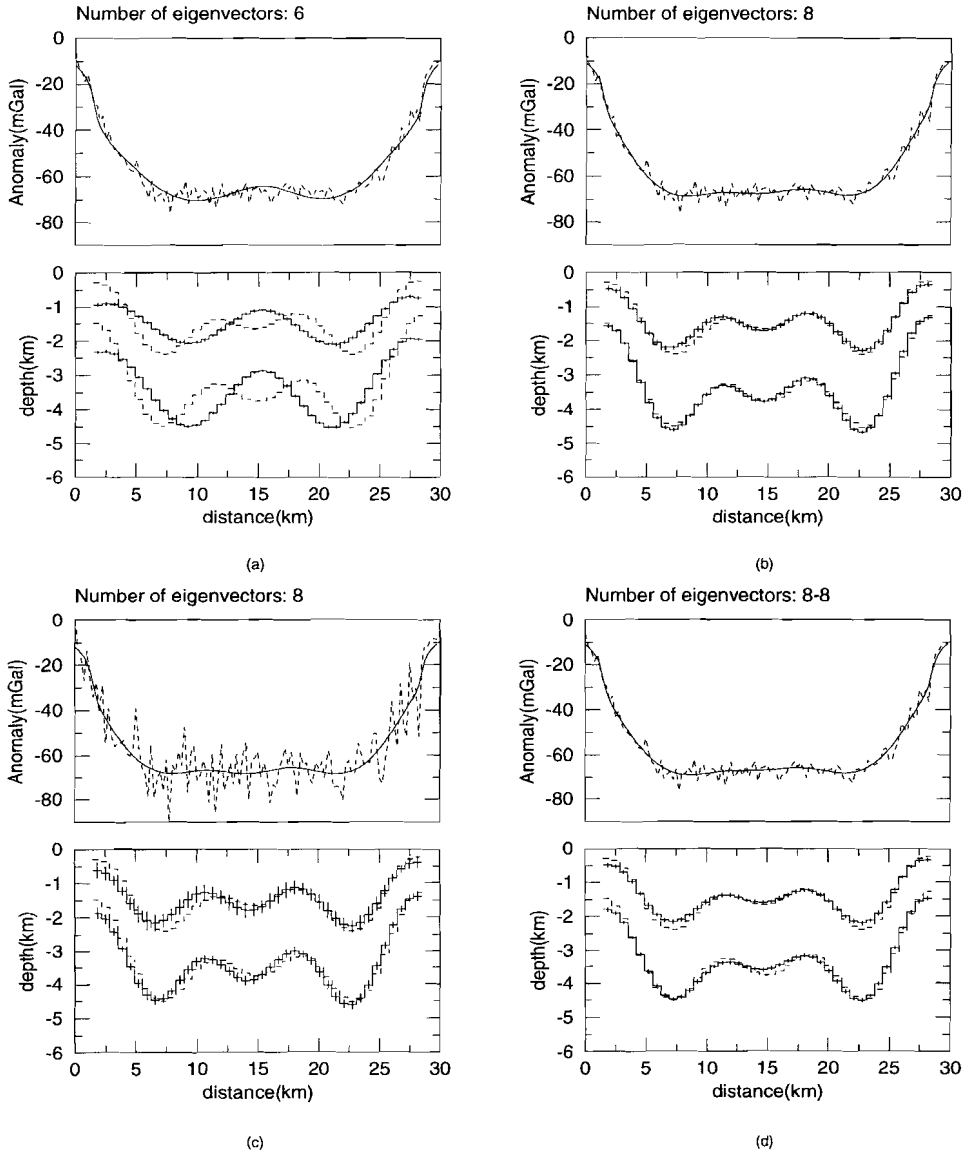As can be seen, some fractional of a diagonal element is added to the same diagonal

Figure 3.6: In each part the top panel shows the fit between the predicted (bold curve) and synthetic data (dashed curve) and the bottom panel shows the agreement between the inverted model (bold curve) and true model (dashed curve). The 120 observations were inverted using a) 6 eigenvectors, 5% noise) 8 eigenvectors 5% noise c) 8 eigenvectors 15% d) 8-8 eigenvectors.

element. The constant λ is initialized at the first iteration and when convergence makes progress it will be reduced. In the final iteration this parameter will be set to zero.

Tests showed that choosing different values for λ will not affect the final results of the inversion but may increase the number of iterations.

The inversion process of the above example converged to a solution using an initial $\lambda = 1$ and 8 eigenvectors after 6 iterations. The misfit for this case was 2.84 mgal. The results of this inversion (figure 3.6-b) shows the true model is almost retrieved. The inversion process also converged to the same solution using positivity constraints and without using the Marquardt method ($\lambda = 0$) after 7 iterations.

To test the stability of the inversion against noise we added 15% Gaussian noise to the data. The results of this inversion after 6 iterations using $\lambda = 1$ and 8 eigenvectors are shown in figure 3.6-c. The error bars for the estimated model are larger than when we added 5% noise to the data. The true and estimated standard deviation (misfit) were 8.67 and 8.53 mgal respectively.

3.6.4 Example with synthetic data assuming a three-layer model using different basis vectors for each set of model parameters

As mentioned in the literature when the inverse problem depends on multiparameter classes, simple gradient methods mix parameters of different character and physical dimensionality. This may lead to rather poor convergence. However, using the subspace method this problem can be overcome by choosing different basis vectors for different parameter types.

To show how the subspace method, using eigenvectors of the Hessian as basis vectors, can be adopted for the cases when parameters have different dimensionality we just use the above example although our model parameters have the same dimensionality.

For this case we consider two classes; model parameters corresponding to the first interface as class one and those corresponding to the thickness of the second layer as class two. The first and second class both consist of 40 model parameters. Each eigenvector associated with each eigenvalue consists of 80 components. The first 40 ones are corresponding to the first class and the rest to the second one. Also each basis vector corresponding to each class has 80 elements.

For the first class the first 40 elements of a basis vector are the first forty elements of an eigenvector and the rest is filled up by zeros.

For the second class the first 40 elements are filled up by zeros and the rest are elements of an eigenvectors from 41 to 80.

After constructing basis vectors they should be again normalized.
The matrix of the basis vectors has the following form

$$V = \begin{bmatrix} V^{(1)^T} & 0 \\ 0 & V^{(2)^T} \end{bmatrix} \tag{23}$$

The matrix V has dimension $M \times P$ and the matrices $V^{(1)}$ and $V^{(2)}$ have dimensions $M1 \times P1$ and $M2 \times P2$ respectively. Where M is the total number of model parameters and P1 and P2 are the number of basis vectors (corresponding to the largest eigenvalues) used for the first and second classes and M1 and M2 are the number of model parameters for the two classes.

To avoid linear dependency between different basis vectors it is helpful to orthonormalize the basis vector V_i using the following relationship

$$V_i = V_i - \frac{(V_i \cdot V_j)}{(V_j \cdot V_j)} V_j, \qquad \text{for } i = 1, \cdots, P; \quad j = 1, \cdots, i-1 \tag{24}$$

If the Hessian matrix H is partitioned as follow

$$H_\alpha = \begin{bmatrix} H_\alpha^{(1)^T} & 0 \\ 0 & H_\alpha^{(2)^T} \end{bmatrix} \tag{25}$$

for calculation of the projected Hessian matrix $V^T H V$ it is necessary to calculate only those elements of this matrix which correspond to the diagonal blocks H_{11} and H_{22} since the basis vector matrix V is block diagonal with some zero elements. This will reduce calculation time.

To test this idea we used the same synthetic data, with five percent noise. Model parameters are the depth of the first interface and thickness of the second layer (40 and 40). We chose the same number of basis vectors for both classes (8-8) and also for convergence we chose $\lambda = 1$. The results of the inversion after 7 iterations with misfit 2.88 (figure 3.6-d) are almost the same as when the same basis vectors were used for both classes.

If different number of eigenvectors (for instance 5-8 8-4,...) are used for each class the interface and thickness parameters have different resolution or smoothness as we saw in the two-layer case.

Since the resolving power of the potential field data reduce with the depth it is recommended to use less or an equal number of basis vectors for the model parameters corresponding to deeper features than the shallow ones since these parameters are less constrained by the data.

It should be mentioned that there is a trade off between the solutions of the two interfaces in all above examples due to the nonuniqueness. This trade off depends on the initial model chosen for the inversion.

By doing a number of the tests we have found that choosing different initial models for the inversion does not have much effect on the rate of convergence and convergence is always fast.

For the above examples when we took the depth of the first interface and the thickness of the second layer as model parameters it is assumed there is some *prior* information about these parameters; for instance the average depth of the interfaces or the thickness of the layer.

For real data inversion, assuming a three-layer model, the constraints should be used in the inversion or at least a good initial model should be selected for the inversion (from other sources) to reduce the degree of the nonuniqueness.

We showed how the eigenvectors of the Hessian can be partioned as basis vectors for the subspace method. This was done for the case when it was assumed that model parameters were of two classes. This partioning can be extended easily for the cases when model parameters are of more then two classes.

3.6.5 Example with real data assuming a three-layer model

We will interpret the results of the inversion of another data set from the province of Noord-Brabant in The Netherlands, by assuming a three-layer model. The data set consists of 313 measurements. The length of the SW-NE running profile is about 80 km. An interpreted seismic section is available. The section consists of a few layers. Within each layer the density is assumed to be constant and known. Our aim was to invert the data for solving the shape of two interfaces and in turn the thickness of the layer between these two interfaces which could not be well resolved by the seismic data. Density contrasts of -0.284 and -0.130 g/cm^3 were selected, with respect to the basement density (2.67 g/cm^3) , for the first and second layer respectively. The density information was obtained from a well in the area.

We chose the depths of the first interface and thicknesses of the second layer as model parameters. For the depths of the first interface a flat initial model at depth 2.0 km and for the thicknesses 0.5 km were considered. This information is from the seismic interpretation which indicated the depth of the first interface varies between 1 and 4 km and thickness between 0 and 1 km. For this case the first interface and thickness of the second layer are approximated each by 40 model parameters.

The eigenvalues and eigenvectors of the Hessian are plotted in figure 3.7-a and 3.7-b. The eigenvalue plot shows a jump at eigenvalue number 41 where the eigenvalues corresponding to the second layer start to build up. This position corresponds with condition number of 1000 which is rather large. Thus from this point we can not make a decision about the number of eigenvectors which should be taken for the inversion. Therefor as before, we chose the number of eigenvectors in a such way that the condition number is less than 100. For this case the upper limit could be 26 eigenvectors. Eigenvector plots again show different weights which each model parameter will get from each eigenvector. They also show the fact that eigenvectors corresponding to the largest eigenvalues can resolve   both model parameter sets, corresponding to the first

(a)

(b)
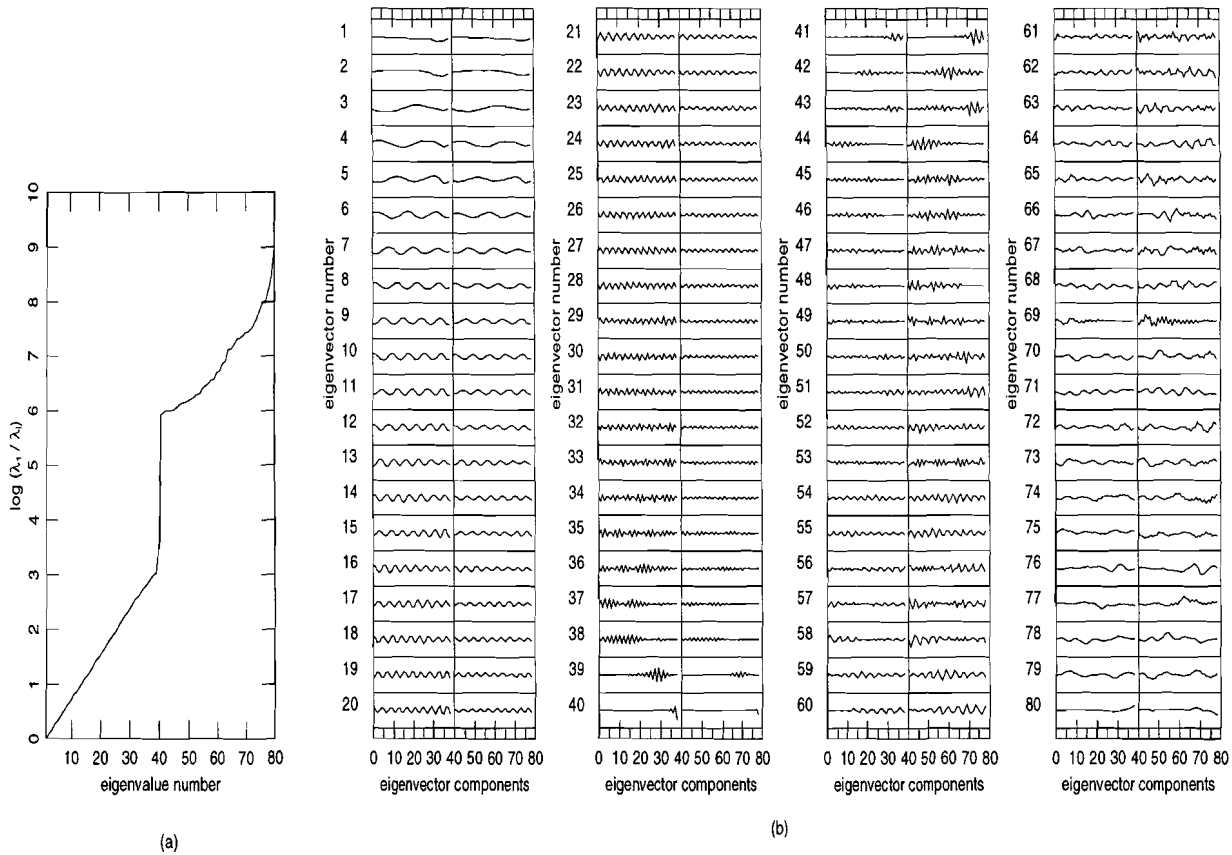
Figure 3.7: Eigenvalues and eigenvectors calculated for an initial interface at depth 2 km and thickness 0.5 km for 313 real observations. a) Largest eigenvalue divided by each eigenvalue plotted on a logarithmic scale with base 10. b) Normalized eigenvectors of the Hessian matrix (vertical scale of each eigenvector box is -1 to +1).
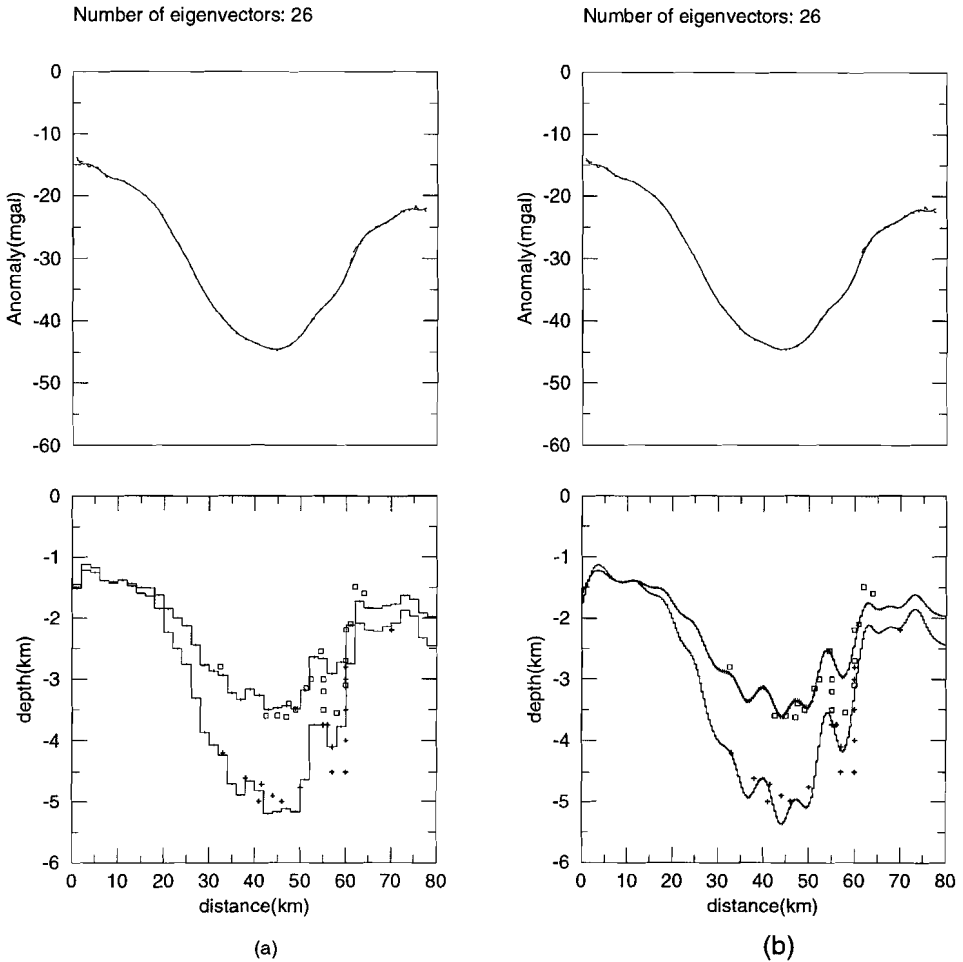
Figure 3.8: In each part the top panel shows the fit between predicted data (bold curve) and observed data (dashed curve) and the bottom panel shows inverted model. The results of the inversion were obtained with a) 26 eigenvectors, 80 model parameters b) 27 eigenvectors, 400 model parameters. The squares and crosses on the plots are some parts of the interfaces from the seismic interpretation.

interface and the thickness of the second layer, almost equally well. But, if more eigenvectors are taken into account, the resulting model will be more oscillatory and in turn less reliable. The results of the inversion using 26 eigenvectors and combining the Marquardt method with an initial $\lambda = 1$ after 7 iterations with misfit 0.15 mgal are plotted in figure 3.8-a. For calculation of uncertainties of the estimated model parameters (shown by vertical bar on the plots and hardly visible) a standard deviation of 0.2 mgal
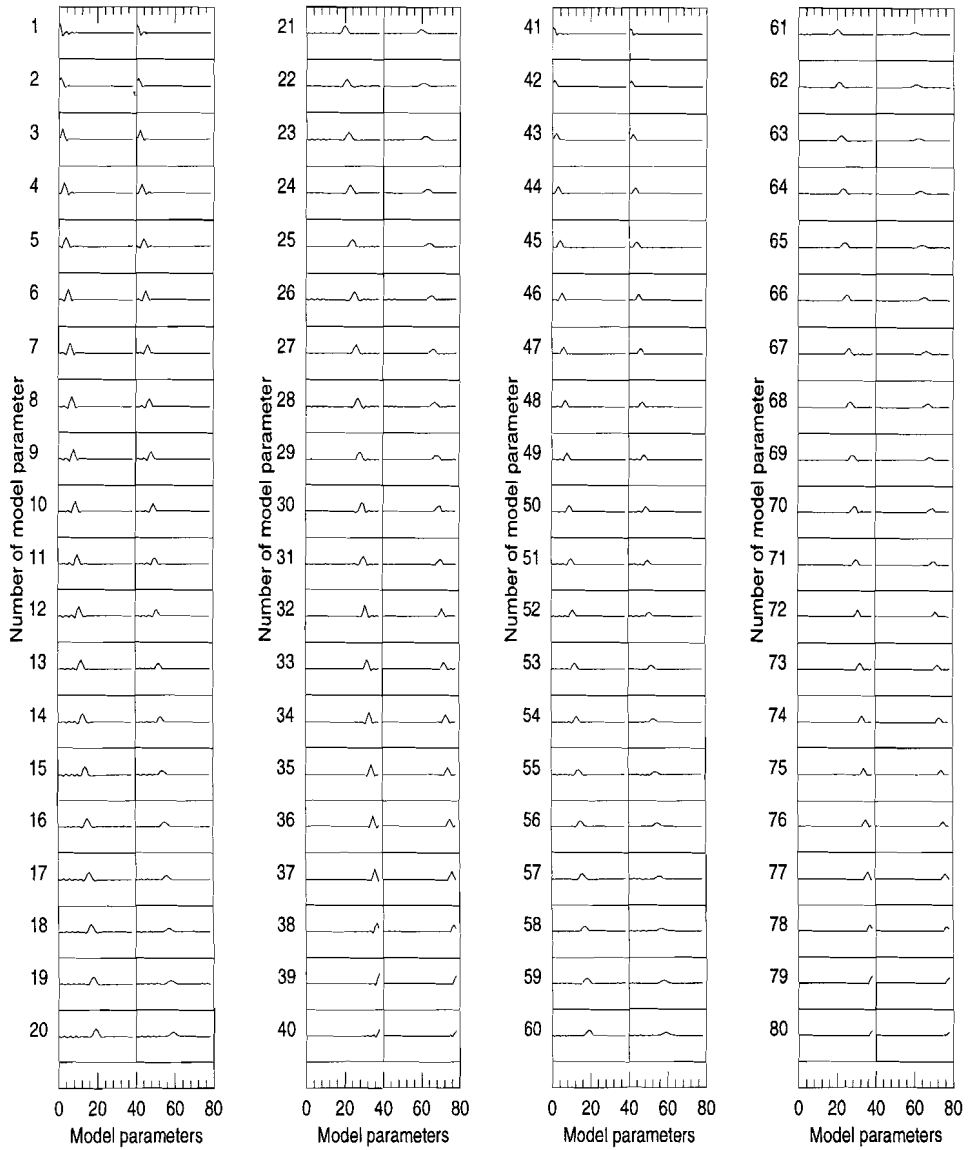
Figure 3.9: Resolution matrix plots when the model is parameterized by 80 model parameters and 26 eigenvectors are used in the inversion of 313 real data (vertical scale of each model parameter box is from -1 to +1).

was used. As can be seen on the plots, a number of faults are detected. The positions of the faults are the same as those from the seismic interpretation. The estimated depth of

the basement in most places agrees with the seismic results. The thickness of the second layer vanishes on the left and also decreases in the right margin which again shows agreement with the seismic results. The side effects in the margins are due to absence of data and this effect is quite normal for the inversion.

We also inverted the data without combining the Marqurd method. The number of iterations for this case increased to 9 and misfit again was 0.15 mgal. With a number of tests we have found that combining the Marquardt method sometimes speeds up the rate of the convergence especially when the initial model is too far from the true earth model. To investigate the effect of fine parametrization on the results of the inversion we approximate the first interface and thickness of the second layer each by 200 model parameters. The results of this trial for 400 model parameters using 27 eigenvectors, corresponding to condition number 100, and $\lambda = 1$ after 9 iterations are shown in figure 3.8-b. The faults are again detected (between 50 and 60 km) in spite of using a small number of eigenvectors.

Using this limited number of eigenvectors for the inversion will degrade the resolution of each model parameter since they will be estimated as an average of all model parameters although this averaging is very localized around each estimated model parameter.

We have plotted the resolution matrix for the first trial with the real data and when the model is parameterized by 80 model parameters (figure 3.9). It can be seen on the plots that each model perturbation parameter is estimated as a linear combination of all model perturbation parameters but this estimation is localized. The trade off between model parameters corresponding to the first and second interface can also be seen on the plots. The plots also indicate that model parameters associated with the first interface are better resolved than those of the thickness. In general most of the model parameters have small resolution width except those which correspond to the right margin, on the positions where the data are absent (the end of the data profile is at 76 km while the end of the model is at 80 km). If more eigenvectors are used in the inversion the resolution will be improved but the model will be more uncertain and less reliable due to construction of artifacts into the model.

3.7 Conclusion

We minimized an objective function by making a locally quadratic approximation about some current model in the subspace of the model parameters. The procedure of minimization in the subspace of the model parameters led to a fast and stable inversion due to removing poor directions and using only those eigenvectors which correspond to the largest eigenvalues. We empirically determined an upper limit for the numbers of eigenvectors of the Hessian, calculated for a reference model, to be used without causing instability in the inversion when it can not be found from the eigenvalues plot. The plot of eigenvectors gives insight into the model perturbations that will occur when using different numbers of eigenvectors in the inversion and also about which set of

model parameters can be better resolved by the inversion when a limited number of eigenvectors are taken in the inversion.

We tested the method for solving the shape of the interfaces from the synthetic and real gravity data assuming two and three-layer models respectively. The inversion results show that the method is stable against the noise. Although this method estimates each model parameter as an average of all model parameters, this averaging is very localized. The localization depends on the number of eigenvectors used in the inversion. The tests showed the capability of the method even in detecting steep faults using a limited number of eigenvectors.

Although for the three-layer model case the problem is nonunique, choosing an initial model from other sources can result in a reliable solution.

We employed this method for inversion of gravity data assuming a two dimensional model; it can also be used for three dimensional inversion when the number of model parameters is quite large.

3.8 References

Burkhard, N. and Jackson, D.D. (1976) Application of stabilized linear inverse theory to gravity data. *Journal of geophysical research* **81,** 1513-1518.

Corbato, C.E. (1965) A least-squares procedure for gravity interpretation. *Geophysics* **30,** 228-233.

Jackson, D.D. (1972) Interpretation of inaccurate, insufficient and inconsistent data, *Geophys J.R.Astr.Soc.* **28,** 97-109.

Kennett, B.L.N. and Williamson, P.R. (1988) Subspace methods for large- scale nonlinear inversion, in N.J. Vlaar, G. Nolet, M.J.R. Wortel, S.A.P.L. Cloetingh and D. Reidel (eds.), *Mathematical Geophysics: a survey of recent developments in seismology and geodynamics, Dordrecht, pp. 139-154.*

Kunaratnam, K. (1972) An iterative method for the solution of a non-linear inverse problem in magnetic interpretation. *Geophysical Prospecting* **20,** 439-447

Menichetti, V. and Guilen A. (1983). Simultaneous interactive magnetic and gravity inversion, *Geophysical Prospecting* **31,** 929-944

Menke, W. (1989). Geophysical data analysis: *discrete inverse theory. Academic press Inc.*

Mickus, K.L. and Peeples, W.J. (1992) Inversion of gravity and magnetic data for the lower surface of a 2.5 dimensional sedimentary basin. *Geophysical Prospecting* **40,** 171-193.

Oldenburg, D.W., McGillivray, P.R. and Ellis, R.G. (1993). Generalized subspace methods for large-scale inverse problems. *Geophys.J.int.* **114,** 12-20.

Pedersen, L.B. (1977) Interpretation of potential field data-a generalized inverse approach. *Geophysical Prospecting* **25,** 199-230.

Sambridge, M.S. (1990) Non-linear arrival time inversion: constraining velocity anoma-
lies by seeking smooth models in 3-D. *Geophys.J.int.* **102,** 653-677.

Wiggins, R.A. (1972) The general linear inverse problem: Implications of surface waves
and free oscillations for earth structure, *Rev Geophysics and space physics* **10,**
251-285.

Chapter 4

Subspace method for inversion of 3D gravity data with seismic constraints

Abstract

In exploration for hydrocarbons, the use of gravity data in addition to a seismic survey can be advantageous. If the area investigated by both methods is partly overlapping, the seismic results can be used as constraints in the gravity interpretation, while the gravity data can be used to establish the depth of interfaces that are not well determined by the seismics. However, 3-D inversion of gravity data becomes cumbersome if both the number of model parameters and of data points is large. To overcome this problem a subspace method is introduced that yields a reliable solution for the inversion of large scale gravity data. The basis vectors for the subspace method are normalized data and model eigenvectors of the Jacobian matrix calculated for an initial model. Because of the reduced number of parameters used in the subspace method and because the calculation of the Hessian matrix is avoided, the method is fast and stable. The method was successfully applied to data for an area in The Netherlands where the seismic results did not give a decisive answer about the continuation of a potential hydrocarbon reservoir.

4.1 Introduction

Interpretation of geophysical data can often be assisted by inversion, which is usually formulated as a non-linear data-fitting problem. In other words, the objective of the inversion method is to obtain a model which is consistent with all available data.

The nonlinear problem can be reduced to a linear one by linearizing the model response function or forward problem about a reference or current model using Taylor series expansion ignoring second and higher order terms. This will lead to solving a linear system of equations or matrix inversion for model perturbations. This can be thought of as mapping between linear spaces of model vectors (perturbations) and data vectors.

Because the number of data and of model parameters are usually not the same, the solution of the linear system of equations or the matrix inversion can be approximated using a least-squares criterion which leads to the inversion of a square matrix. If the matrix inversion is well conditioned, the least-squares solution, i.e. the model perturbations, can be used for updating the current model. The process of matrix inversion and updating the model can be iterated until some norm of the residual between the observations and model responses or of the model perturbations is less than some preassigned threshold. Due to ill conditioning of the linearized system and to the presence of noise in the data, small changes in the data can lead to large changes in both the solution and in the number of iterations required. Thus matrix inversion generally requires some kind of regularization or damping in order to suppress unwanted oscillations in the model and generate physically plausible solutions.

A common way to damp a solution is using the Marquardt-Levenberg method. This method was introduced by Levenberg (1944) and later described in detail by Marquardt (1963). It is sometimes known as the method of damped least-squares; others refer to it as "ridge regression " (Inman 1975). This method prevents unbounded oscillations in the solution. This method has been used by Sain et al. (1994) and Pelton et al. (1978). Another approach to regularization is using singular value decomposition techniques which use only those eigenvectors which correspond to the largest eigenvalues and have most influence on the predicted data (Menichetti et al. 1983). These two regularization methods can be combined in one inversion procedure as described by Jupp et al. (1975), Pedersen (1977), Raiche et al. (1985) and Narasimha et al. (1994).

These methods work well and converge rapidly to a solution when the number of model parameters and the number of data are not large. When the number of data and of model parameters are large the matrix inversion is more ill-conditioned due to large dimensionality. The inverse process may need many iterations for convergence to a solution. In other words, for this situation convergence is very slow. To overcome this problem, the effective way is executing the matrix inversion in a subspace spanned by a limited number of vectors in the model space. The spanning vectors are called basis vectors. The success or failure of this method depends basically upon the selection and the number of basis vectors chosen for the subspace. This technique is well discussed and used by Kennett and Williamson (1988), Sambridge (1990), Oldenburg et al. (1993) and Unsworth et al. (1995).

In the present paper a subspace method is introduced that can handle a large scale 3-D inversion of the gravity data. This subspace technique is developed to solve a linear system, resulting from the linearization of the model response, in such a way that the calculation of the Hessian matrix (second partial derivatives matrix) is avoided. For this

subspace method the selected basis vectors are eigenvectors of the Jacobean matrix calculated only once for a reference or initial model. From these eigenvectors only a limited number corresponding to the largest singular values are selected as basis vectors. This causes the matrix inversion to be well conditioned and the inversion process to converge very fast to a solution with minimum variance.

4.2 Inversion scheme

Let the n observations of a data set be represented by the vector

$$\mathbf{g}_o = (g_{o1}, g_{o2}, \cdots, g_{on})^T .$$

The restricted earth model is determined by m parameters, which we write as the vector

$$\mathbf{x} = (x_1, x_2, \cdots, x_m)^T .$$

The model response function generates a set of model data for each choice of $\mathbf{x}$. This is denoted as a vector function by

$$\mathbf{g}(\mathbf{x}) = (g_1(\mathbf{x}), g_2(\mathbf{x}), \cdots, g_n(\mathbf{x}))^T$$

where $g_i(\mathbf{x})$ is the value predicted by the model, corresponding with observation g_{oi}.

The aim of the inverse problem is determination of $\mathbf{x}$ in such a way that $\mathbf{g}(\mathbf{x})$ matches $\mathbf{g}_o$. The Taylor-series expansion of the function $\mathbf{g}$ (sufficiently smooth) about a reference or initial model $\mathbf{x}$ allow us to construct simple approximations to the function in the neighbourhood of $\mathbf{x}$. Ignoring all but the linear term of the Taylor series gives

$$\mathbf{g}(\mathbf{x} + \delta\mathbf{x}) = \mathbf{g}(\mathbf{x}) + \mathbf{A} \ \delta\mathbf{x} \cdot \qquad (1)$$

The expression $\mathbf{g}(\mathbf{x}) + \mathbf{A} \ \delta\mathbf{x}$ defines a linear function of the m-vector $\delta\mathbf{x}$, the perturbation from $\mathbf{x}$, and will approximate $\mathbf{g}$ with an error of the order $\|\delta\mathbf{x}\|^2$. If the function $\mathbf{g}$ is linear with respect to $\mathbf{x}$ the error will be zero.
In the above equation $\mathbf{A}$ is the Jacobian or sensitivity or partial derivatives matrix which has elements such as

$$A_{ij} = \frac{\partial g_i}{\partial x_j} \qquad i = 1, 2, \cdots, n \qquad j = 1, 2, \cdots, m \cdot$$

Equation (1) can be simplified as

$$\delta\mathbf{g} = \mathbf{A} \ \delta\mathbf{x} \qquad (2)$$

where $\delta\mathbf{g} = \mathbf{g}(\mathbf{x} + \delta\mathbf{x}) - \mathbf{g}(\mathbf{x})$ is the residual data vector (in practice the difference between observations and model responses).

The solution of equation (2) gives the model perturbation $\delta\mathbf{x}$. This system can not be solved directly by inverting the matrix $\mathbf{A}$ since this matrix usually is not square. The

system can have an approximate solution in the following form

$$\delta x = A^{-g} \, \delta g \tag{3}$$

where A^{-g} is some pseudo or generalized inverse of matrix A.

When the number of data points or the number of model parameters becomes large, construction of the pseudo or generalized inversion meets with some difficulties. To overcome these difficulties the following expansion is introduced:
The data residual and model perturbation vectors can be expanded as follows

$$\delta g = U \, \beta \qquad\qquad \delta x = V \, \alpha \tag{4}$$

where β, α are expansion coefficients and U, V are matrices whose columns form orthonormal basis vectors for the data and model space respectively. The vectors U and V have dimensions $n \times p$ and $m \times p$ respectively (p is less than both n and m).
After replacing δg and δx by their equivalence from equation (4), equation (2) will get the following form

$$U \, \beta = A \, V \, \alpha \tag{5}$$

After premultiplying both sides of the above equation by U^T and knowing that $U^T U = I$ one finds

$$\alpha = (U^T A V)^{-1} \, \beta \cdot \tag{6}$$

Backprojecting into the original data and model space will lead to the final solution to the model perturbation

$$\delta x = V(U^T A V)^{-1} U^T \delta y \cdot \tag{7}$$

The square matrix $U^T A V$, the projected Jacobian, with dimension $p \times p$ can easily be inverted. After estimating model perturbation δx for a current iteration, say i , the current model x^i should be updated as follows

$$x^{i+1} = x^i + \delta x^i \cdot \tag{8}$$

The updated model should be used as the basis for further iterations. The iterations will be continued until significant reduction in the Root Mean Square (RMS) error between data and model response is no longer observed.

4.3 Basis vector selection

The Jacobian matrix is calculated for an initial or reference model and then the singular value decomposition technique is employed for decomposition of this matrix into data eigenvectors U, model eigenvector V and singular value Λ matrices. Subsequently p columns of the matrix U and also p columns of the matrix V associated with the largest

singular values, after normalization, are selected as basis vectors for the data and model space respectively. In this way the best directions which have the largest influence on the predicted data are selected for the inversion and in turn instabilities due to ill-conditioning and to data errors can be avoided. This stability is due to the fact that each model parameter in the subspace (p less than m and n) is well constrained by the data. Choosing significant eigenvectors as basis vectors will lead to a solution with minimum variance very fast. The choice for p (number of basis vectors) depends on the number and configuration of the data and the model parameters and also on the selected initial model.

It should be mentioned that the Jacobian matrix only one time and only in the first iteration will be decomposed into its eigenvectors and singular values. For the rest of the iterations the selected eigenvectors, from the first iteration, are taken as basis vectors for the inversion. This means that in equation (7) the matrices U and V are fixed for all iterations by their values obtained in the first iteration. However, the Jacobian A is updated during every iteration.

Selecting eigenvectors of the Jacobian matrix as basis vectors, has the advantage that the calculation of the Hessian or second partial derivatives matrix is avoided which is usually needed for subspace techniques or for gradient direction methods. This also reduces the calculation time.

4.4 Scaling and positivity constraints to the inversion

As we will see later, model eigenvector plots of three-layer model show that model parameters corresponding to the first layer will be better resolved than those of the second one from the inversion. This effect is partly due to the decreasing in resolving power of gravity data with depth and partly due to magnitude unbalancing between the model parameters associated with the first and second layer. This deficiency can be improved by making a balance between parameters corresponding to each layer through scaling of the Jacobian. To do so we scale the columns of the Jacobian matrix as suggested by Marquardt (1963) and worked out in detail by Smith and Shanno (1971). The scaled Jacobian will have the following form:

$$A_{scal} = D^{-1}A \qquad (9)$$

where D is a diagonal matrix whose *ith* element is equal to the root mean sum of squares value of the *ith* column of the unscaled Jacobian matrix A. The resulting model perturbation solution from the inversion in each iteration should be rescaled as follows:

$$\delta x = D^{-1} \delta x_{scal} \qquad (10)$$

Furthermore we introduce new model parameters by the transformation $x_i^{new} = \sqrt{x^i}$ to avoid negative results from the inversion. With this transformation each element of the new Jacobian matrix has the form $G_{ij}^{new} = 2.0\, G_{ij} x_j^{new}$. In all inversions, positivity

constraints will be used for the model parameters approximating the model.

4.5 Forward calculation

The gravity effect of a structure responsible for an anomaly can be calculated by dividing the volume of the anomaly into a limited number of three dimensional elementary rectangular prisms and then summing up the gravity effect of all the elementary prisms. The vertical component of the gravitational attraction g due to an arbitrary topographic mass of constant density ρ is give by

$$g = \gamma \rho \int \int \int_V \frac{z \, dz \, dy \, dx}{r^3} \tag{11}$$

where $r = (x^2 + y^2 + z^2)$ and γ is gravitational constant.
The simplified expression of the above equation for a vertical rectangular prism is given by Plouff (1976):

$$g = \gamma \rho \sum_{i=1}^{2} \sum_{j=1}^{2} \sum_{k=1}^{2} s \left[z_k \, atan \, \frac{x_i y_i}{z_k R_{ijk}} - x_i \ln(R_{ijk} + y_j) - y_j \ln(R_{ijk} + x_i) \right] \tag{12}$$

where $R_{ijk} = \sqrt{x_i^2 + y_j^2 + z_k^2}$ and $s = s_i s_j s_k$ with $s_1 = -1$ and $s_2 = +1$ and (x_1, x_2), (y_1, y_2) and (z_1, z_2) are the boundaries of the elementary rectangular prism in the x, y and z direction (for simplicity the observation point is taken at the origin)
The first partial derivative of the predicted data with respect to a lower or upper boundary (each element of the Jacobian matrix) can be calculated analytically in the following form

$$\frac{\partial g}{\partial z_k} = \gamma \rho \sum_{i=1}^{2} \sum_{j=1}^{2} \left[atan \, \frac{x_i y_j}{z_k R_{ijk}} - \frac{x_i y_j z_k (R_{ijk}^2 + z_k^2)}{R_{ijk}(z_k R_{ijk})^2 + (x_i y_j)^2)} - \frac{x_i z_k}{R_{ijk}(R_{ijk} + y_j)} \right.$$

$$\left. - \frac{y_j z_k}{R_{ijk}(R_{ijk} + x_i)} \right] \tag{13}$$

where $k = 1, 2$.

4.6 Numerical tests with synthetic data

Numerical tests for a small data set are presented in this section to illustrate the abilities and the limitations of the inversion scheme. The assumed model is a three layer-model
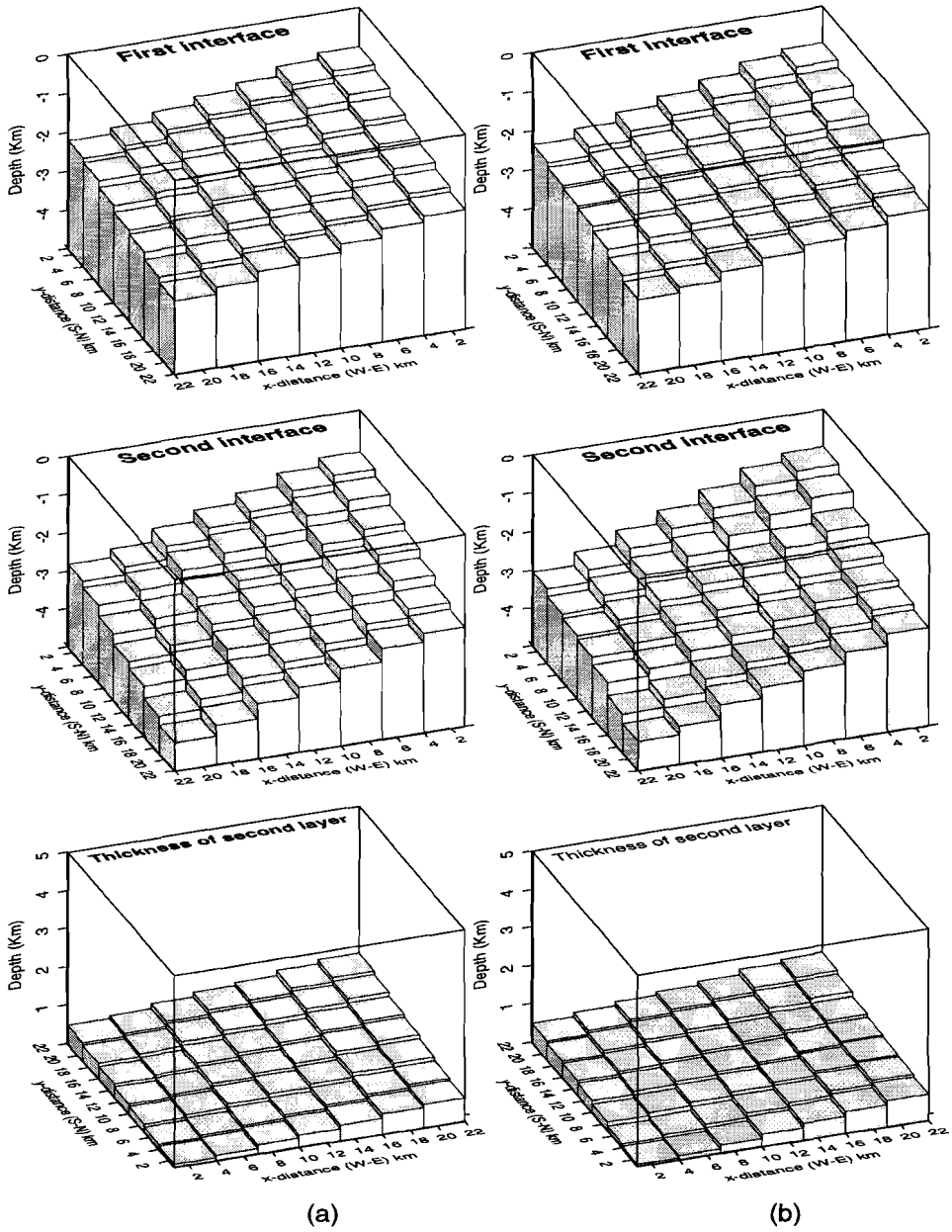
Figure 4.1: Model perspective plots a) true model , b) result of inversion of 49 synthetic noisy gravity data, using 10 eigenvectors.

which is approximated by several adjacent 3-D finite rectangular prisms whose edges are constrained to the north-south and east-west directions and all the prisms have the same horizontal dimensions. The third layer is a half-space. The region of the model is bounded from 1 to 21 km in both x (west-east) and y (south-north) direction. Each layer is approximated by 49 vertical rectangular prisms. Since in the real case there is an effect of the structures outside the measured area, this should also be considered for the synthetic case. To do this, outside the area an extra ring of 32 prisms up to a horizontal distance of 10 km is added to the prisms associated with each layer. After doing this 2×81 elementary rectangular prisms construct the model. The lower boundary of the prisms approximate the shape of each interface. Now our constructed model has roughly the same condition as we had in the real case. We generated the synthetic data from this model. In figure 4.1-a a perspective plot of the depth of the first and second interface and the thickness of the second layer from top to bottom are represented. The depth of the structure decreases from N-E to S-W. The thickness of the second layer varies from 1 to 0.2 km from N-E to S-W.

The assumed density contrasts for the first and second layer are -0.22 and -0.13 g/cm^3 respectively. The considered square rectangular grid for synthetic data is bounded from 0 to 23 km in both x and y direction. The total number of data in the regular grid is 49 (7×7) with a spacing of 3.83 km. We aim to invert the data (without noise and with noise) for solving the depth of the first interface (lower boundary of 81 prisms) and the thickness of the second layer (thickness of 81 prisms). In each layer the model parameters are numbered starting from the S-W in the following way: the first 9 numbers are in a row going from west to east (in the x direction), then 9 in a second row, which is one step further in the northern direction (the y direction) etcetera.

The number of model parameters (162) is more than the number of data (49), i.e. the inverse problem is underdetermined and hence nonunique. This nonuniqueness due to underdeterminancy can be overcome by using the subspace technique since the data are actually inverted for the new model parameters (which are combinations of the original model parameters) in the subspace of the original ones but the inherent nonuniqueness still exists even by introducing the density contrasts as known model parameters and even using the subspace technique. The nonuniqueness of the inverse problem can be reduced further by fixing some model parameters as constraints. One of the most important factors in all inversion schemes is the selection of a sufficiently accurate initial model. The more the selected starting model is close to the true one the more the chance exists that the minimum found is a global minimum. In some cases, if the selected initial model is too far from the true one the inversion process will diverge or the convergence will be poor. The considered initial model for this problem consists of a simple horizontal interface (bottom of the first layer) and a constant thickness (of the second layer) which have the values 2.0 and 0.5 km respectively.

After calculating the Jacobian matrix for the initial model we decompose it into its data and model eigenvectors and singular values matrices. The singular values and normalized model eigenvectors, ordered from top to bottom in order of decreasing corresponding singular values are plotted in figures 4.2-a and 4.2-b. Since the problem is
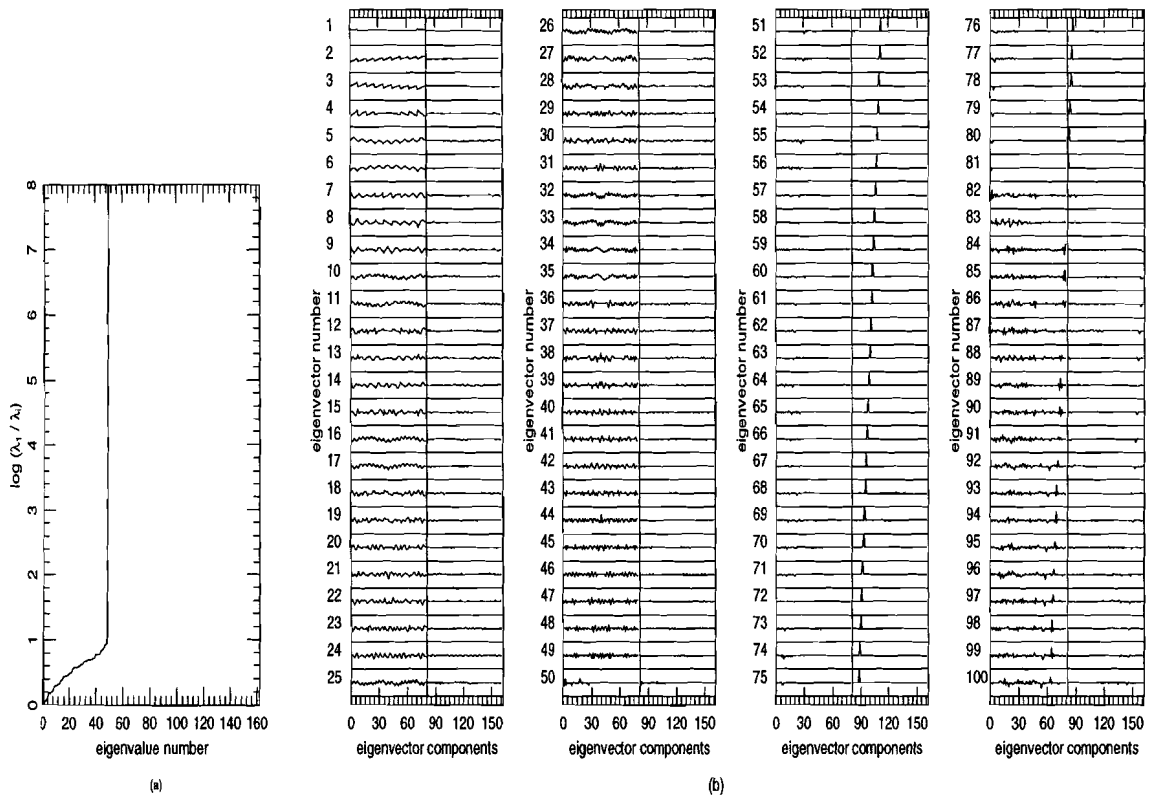
Figure4.2: Singular values and mdoel eigenvectors of the Jacobian matrix calculated for an initial horizontal interface at a depth 2 km (interface separating first and second layer) and a constant thickness of 0.5 km (thickness of second layer) and 49 synthetic measurements. a) largest singualar value divided by each eigenvalue plotted on a logarithmic scale with base 10. b) Normalized eigenvectors (vertical scale of each eigenvector box is from -1 to + 1).
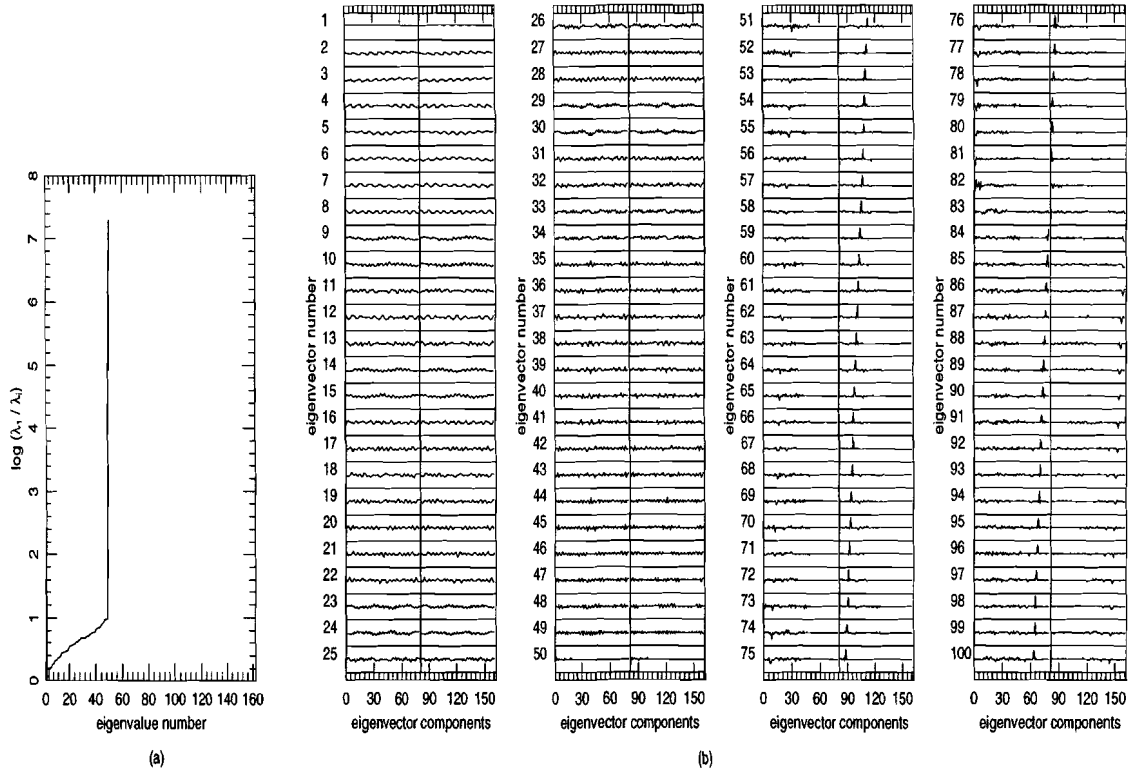
Figure 4.3: Singular values and model eigenvectors of the scaled-Jacobian matrix calculated for an initial horizontal interface at a depth of 2 km and a constant thickness of 0.5 km and 49 synthetic measruements. a) Largest singular value divided by each eigenvalue plotted on a logarithmic scale with base 10. b) Normalized eigenvectors (vertical scale of each eigenvector box is from -1 to + 1).

underdetermined 113 singular values are zero. In figure 4.2-a , $\log(\lambda_1/\lambda_i)$ approaches to infinity for $i > 49$ and because of space limitation from total 162 eigenvectors only 100 are plotted. Apart from the large jump due to zero singular values, few smaller jumps can be seen in the plot. These numbers can be considered as upper limits for the number of eigenvectors (basis vectors) to be used in the inversion. This consideration depends on the level of the noise in the data. In the model eigenvector plots we see that eigenvectors corresponding to the first layer (from 1 to 81) have larger components than those of the second one. This means, if these eigenvectors are taken as basis vectors in the inversion, the model parameters associated with the first layer will be better resolved than those of the second one. Most of the eigenvector plots corresponding to zero singular values (from 50 to 98) have a spiky shape, i.e. each of these only gives a large weight to the certain model parameter. These eigenvectors also show a small trade off between model parameters corresponding to the first and second layer in the form of positive and negatives spikes. If these are used as basis vectors in the inversion they make large model perturbations (especially in the model parameters associated with the second layer) without having any effect on the predicted data. These are sometimes called eigenvectors associated with irrelevant model parameters.

To see the effect of the inversion due to scaling of the columns of the Jacobian matrix as shown in equation (9) we replot the model eigenvectors of the scaled Jacobian matrix (figure 4.3). It can be seen that eigenvectors corresponding to the first and second layer (especially associated with the 81 largest eigenvalues) have the same amplitudes and those associated with the zero singular values have positive and negative amplitudes which have no effect on the data. Comparing figure 4.2-a with 4.3-a shows that the total condition number is also reduced by the scaling of the Jacobian matrix.

4.6.1 Results of the inversion

The result of the inversion for noise-free data, employing positivity constraints for the depth to the top and for the thickness of the second layer, after 3 iterations and using 22 eigenvectors, is a model that differs so little from the true model depicted in figure 4.1-a, that we will not show it in a new figure. Also the root mean square error (RMS) between predicted and true data is only 0.01 mGal.

To see the effect of the scaling, shown in equation (9), in the final results, we repeated the inversion process without scaling the Jacobian matrix. In this case we were not able to retrieve the true model as perfectly as when the Jacobian matrix was scaled. In this case the depth of the fist interface was better resolved than the thickness, while the normalized RMS error increased to 0.25 mGal (these results are not shown here). These facts show that the scaling can really improve the results of the inversion.

Next we added five percent Gaussian noise to the data. The RMS error for this level of noise was 1.04 mGal. We did an inversion using 22 eigenvectors. By comparing the RMS error of this inversion (0.70 mGal) with that of the true one (1.04 mGal) we
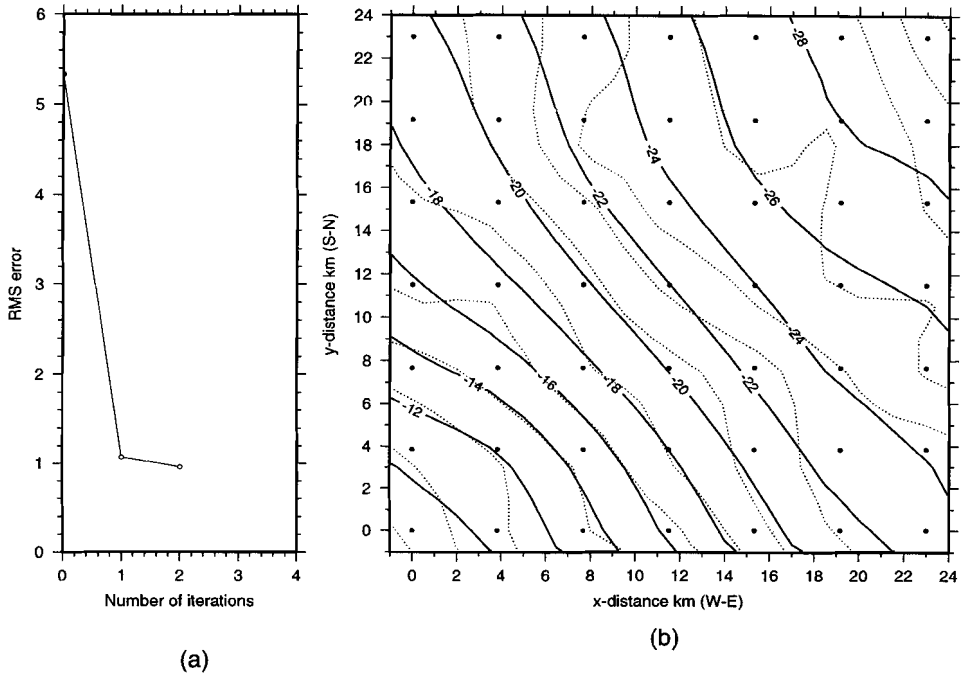
Figure 4.4: a) RMS error versus number of iterations. b) Counter plots of the 49 pre-dicted (bold-line) and original noisy data (dotted-line). Contour interval is 2 mGal.

saw that the noise was minimized and that in turn some artifacts were constructed in the model (the results are not shown here). Due to these fact, the results of this inversion can not be reliable. We also inverted the data using only 10 eigenvectors. The RMS error versus the number of iterations, using 10 eigenvectors, is plotted in figure 4.4-a. As can be seen the convergence is very fast. In figure 4.4-b the original data (dotted lines) together with the predicted data (bold lines) are shown as a contour map. It should be mentioned that irregularities in the contours of the original data (dotted-lines) are due to the effect of the noise which was added to the data generated from the synthetic model (figure 4.1-a). This plot also shows the stability of the inversion against the noise since the noise was not fitted . The interface and thickness perspective plots of this trial are also depicted in figure 4.1-b. For this case the RMS error (0.96 mGal) was very close to the true one (1.04 mGal). The resultant model from this trial (noisy data inversion) is almost the same as that of the noise-free one.

It should be mentioned that in the real case *a priori* information about the level of the noise of the measurements can help us to select the number of eigenvectors in such a way that the noise is not minimized. This number can be less than or equal to the upper limit which sometimes can be indicated by the singular values plot.

4.7 Numerical test with real data

In this example the reservoir of interest is a sandstone layer in the Bunter formation in an area in the southern part of The Netherlands. The three dimensional inversion scheme has been applied to estimate the depth of the top and the base of the Bunter which had not been resolved well by the seismic data. The selected area was 15×15 km^2. Along two SW-NE running lines gravity measurements had been performed earlier (figure 4.5). Of these data about 59 could be used in the present interpretation. In 1995 we performed an additional 237 gravity measurements. On an average the station separation is about 0.9 km for a total 296 gravity measurements. The elevations were determined by GPS measurements or from elevation maps, with an accuracy which is always better than 0.4 m. After applying the Free-air and Bouguer-correction (using a density of 2.05 g/cm^3) the final accuracy of the anomalies is 0.15 mGal. Contour lines as well as all anomaly values are shown in the map of figure 4.5-a.

4.7.1 Stripping the data

On the basis of the available seismic data and well information we will distinguish four geological units with increasing depth:
1. Tertiary and Quaternary (density 2.10 g/cm^3).
2. Upper Mesozoic (density 2.45 g/cm^3).
3. Bunter formation (density 2.54 g/cm^3).
4. Carboniferous (density 2.67 g/cm^3).
These units are shown in figure (4.6). Apart from a small area in the SW, the depth of the base of unit 1 (base Tertiary) is very well known from seismics. After extrapolation in the SW and extension beyond the 15×15 km^2 area at the same depth as at the borders of the area (to account for the effect of the structure beyond the area), we subtracted (stripped) the effect of the unit 1 from the data, using a density contrast of -0.57 g/cm^3 (with respect to the basement density). The result after stripping is shown as a stripped gravity map in figure 4.5-b. These stripped data will be used to locate the base of the Bunter and to determine its thickness.

4.7.2 The models

To parameterize the models to be used in the inversion, the area within the 15×15 km^2 was divided in 225 prisms of 1 km^2. Outside the area an extra ring of 64 prisms up to a horizontal distance of 10 km was added to reduce the side effects in the inversion. We inverted the data assuming a two-layer and a three-layer model. In the two-layer model the first layer is from the base Tertiary to the base of the Bunter and the second layer is
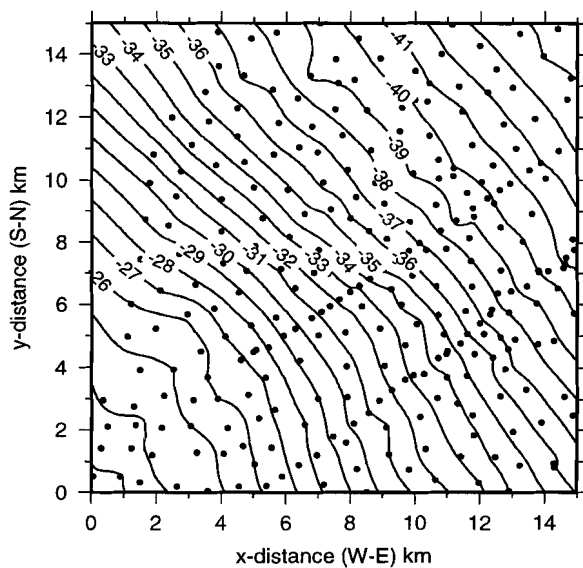
(a)
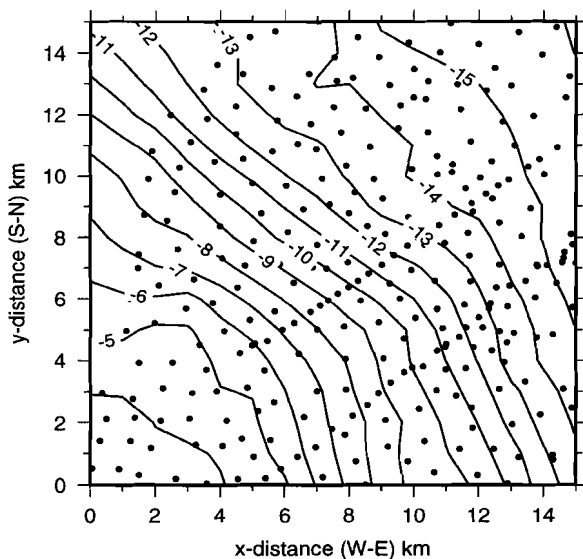
(b)

Figure 4.5: Contour plots of 296 measurements a) original data b) data after removing the Tertiary and Quaternary effects. The bold dots show the position of the stations. Contour interval is 1 mGal.
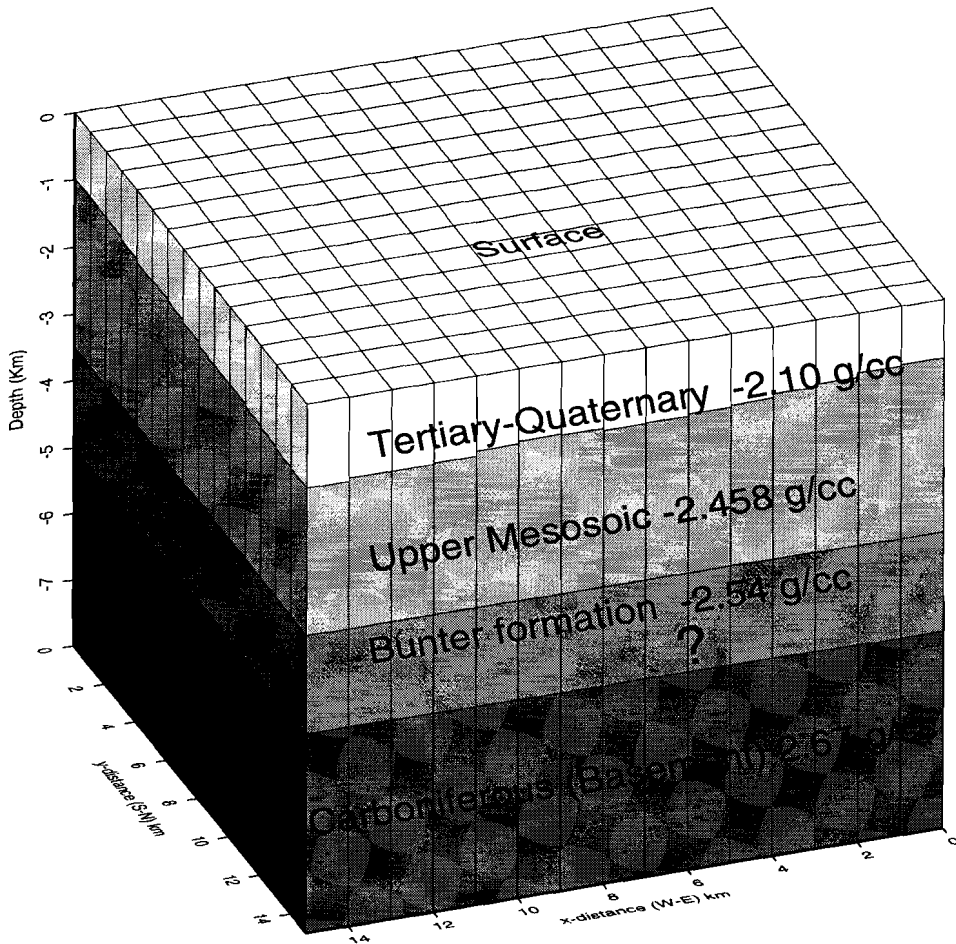
Figure 4.6: Geological section of the area on the basis of seismic and borehole information.

the Carboniferous as an infinite half-space. The average density contrast of the first layer with respect to the Carboniferous formation density ($2.67 \ g/cm^3$) was taken as $-0.196 \ g/cm^3$. In the three-layer model the first layer is from base Tertiary to top Bunter and the second layer from top Bunter to top Carboniferous. The first layer and the second layer have density contrasts -0.212 and $-0.130 \ g/cm^3$ (with respect to the Carboniferous density) respectively.

In both cases each layer is approximated by 289 vertical rectangular prisms. In the two-layer case the lower boundary depths of the 289 elementary prisms will be
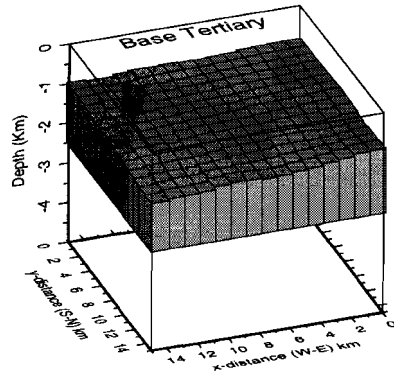
(a)
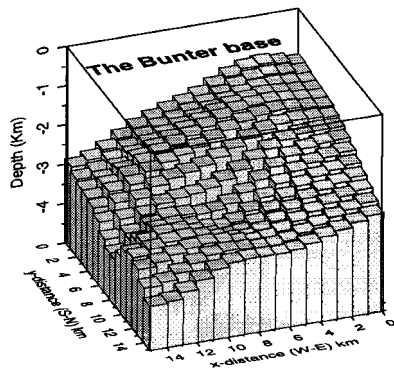
(b)
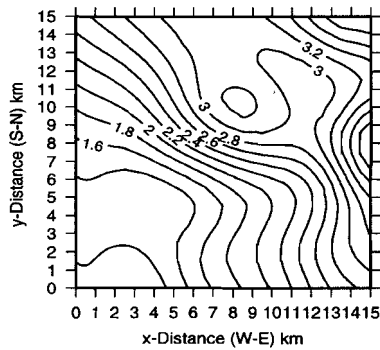
(c)

Figure 4.7: a) starting model b) base Bunter perspective c) contours of the base Bunter from two-layer inversion. The number of the stripped data and the number of eigenvectors used were 296 and 22 respectively.
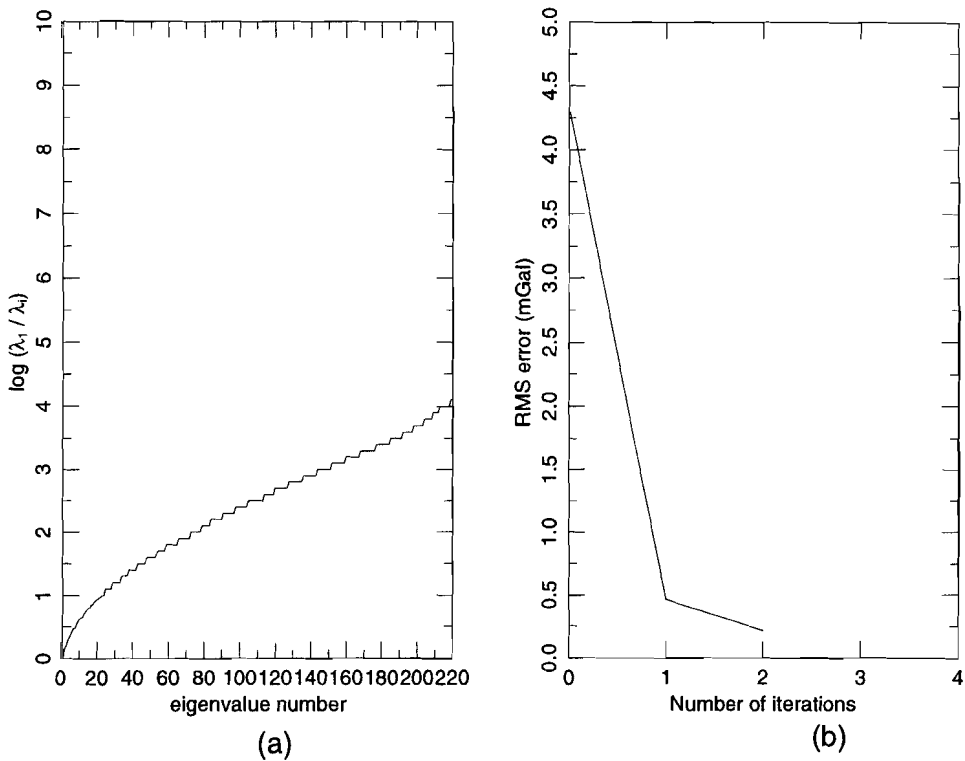
Figure 4.8: a. Singular values of the Jacobian matrix calculated for an initial horizontal base Bunter (two-layer model) at a depth of 2.5 km and 296 stripped data. Largest singular value λ_1 divided by λ_i plotted on a logarithmic scale with base 10. b. Reduction of RMS error in each iteration.

determined from the inversion. In the three-layer model case the depth of the Bunter base and the thickness of the Bunter formation will be determined by the 578 model parameters (without constraints). In the three-layer case the inversion can be conducted in two ways:

a. Without using any constraints for the parameters

b. Using available seismic information to constrain some of the model parameters defining the top Bunter.

4.7.3 Results of two-layer model inversion

The initial model used for the inversion is shown in figure 4.7-a. The first layer consists of the Bunter and the Upper Mesozoic, whose top is the base Tertiary (known from the

seismic results). The base of this layer is initialized at a constant depth of 2.5 km which is optimized by the inversion. The second layer is the Carboniferous basement.

The Jacobian matrix was calculated for this initial model and decomposed into its eigenvectors and singular values. The singular values are shown in figure 4.8-a. In the plot many small jumps are observable. The first small jump is associated with the singular value number 22. We took this number as an upper limit for the number of eigenvectors to be used in the inversion. Using this number of eigenvectors the inversion converged after only two iterations. The RMS error for this case was 0.21 mGal. Figure 4.8-b shows the speed of the convergence. After one iteration the RMS error is reduced about 90%.

The perspective and contour plots of the base Bunter are depicted in figures 4.7-b and 4.7-c. These plots show that the depth of the base Bunter decreases from N-E to S-W. We tried to reduce the RMS error by using 30 eigenvectors in the inversion. The RMS error was slightly reduced (to 0.196 mGal), but some artifacts were constructed into the model (the results of this trial are not shown here). This showed that the choice 22 for the number of eigenvectors from the singular values plot was reasonable.

Although the accuracy of the data is 0.15 mGal, we should also take into account the reduction error (reduction of the effect of the Tertiary from the data) and the effect of the structures outside this area which are not accurately considered by adding additional large blocks at the margins. Thus the RMS error of the data obtained from the inversion may be more than the true error of 0.15 mGal.

4.7.4 Results of three-layer model inversion

In the three layer-model the base and the thickness of the Bunter formation are determined from the inversion. We performed the inversion for two cases:

4.7.4.1 Inversion without constraints

The initial model for this case is shown in figure 4.9. The first layer is the Upper Mesozoic whose top layer is the base Tertiary (know from seismic) and its bottom is the top of the Bunter (initialized at a constant depth of 2.5 km), which will be adjusted by the inversion. The second layer is the Bunter whose thickness is initialized as 0.5 km and will be adjusted by the inversion. The Jacobian matrix was calculated for this initial model and then decomposed into its singular values and eigenvectors. The singular values are plotted in figure 4.10-a. The small jumps or oscillations start at the singular value number 22. This number can be considered as an upper limit for the number of eigenvectors which can be used in the inversion. To avoid negative results for the depths and thicknesses, positivity constraints are considered for the inversion as introduced before.
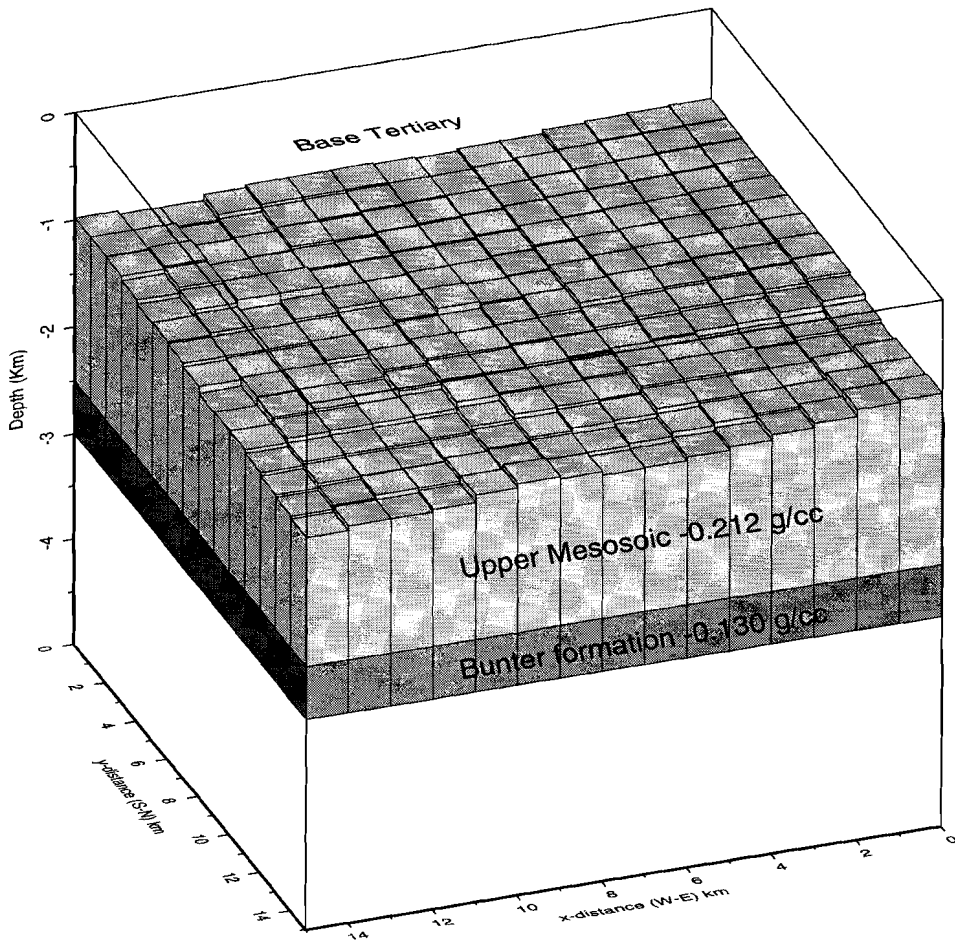
Figure 4.9: Starting model for three-layer inversion.

The inversion process after 4 iterations, using 22 eigenvectors as basis vectors, converged to a solution with RMS error 0.21 mGal. The RMS error versus number of iterations shows the rate of convergence for each iteration (figure 4.10-b). The perspective results for the top and base Bunter and also its thickness are shown in figures 4.11-a, b, c respectively. These interface depths are also contoured in figure 4.12-a, b,c. As we can see from the plots, the depth of the top and base Bunter and also its thickness decrease from N-E to S-W. If we compare the results of this inversion for the base Bunter (figures 4.11-b and 4.12-b) with those from the two-layer model (figure 4.7), the close agreement between these two results is observable. This demonstrates that the results of the inversion assuming a three-layer model can be reliable if an initial model
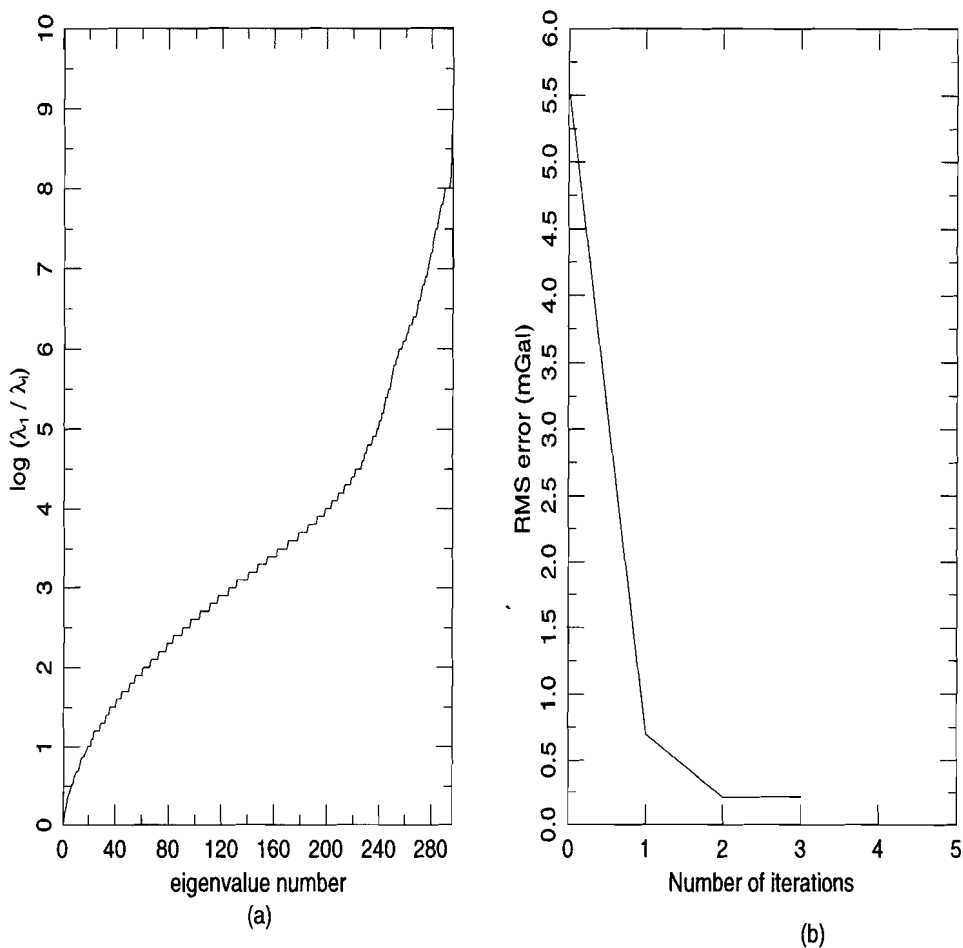
Figure 4.10: a. Largest singular value λ_1 of the Jacobian matrix (calculated for a three-layer model initialized by a horizontal top Bunter at a depth of 2.5 km and a constant thickness of the Bunter of 0.5 km and 296 measurements) divided by λ_i plotted on a logarithmic scale with base 10. b. Reduction of the RMS error in each iteration from inversion of 296 reduced measurements assuming a three-layer model.

is chosen based on seismic information or other sources.

4.7.4.2 Inversion with constraints

To reduce the effect of the nonuniqueness of the inversion we fixed 68 model parameters
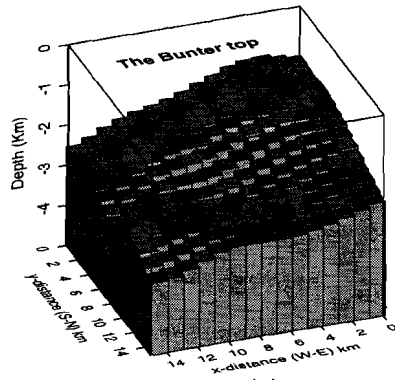
(a)
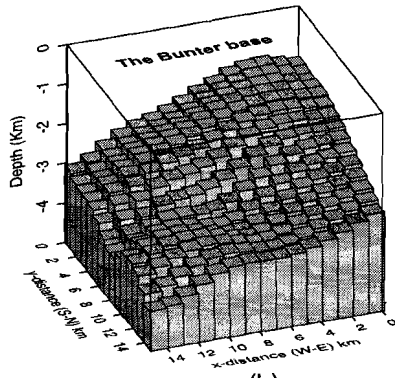
(b)
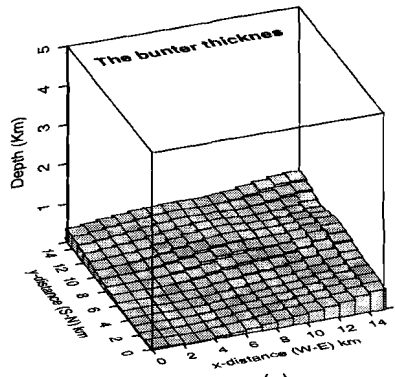
(c)

Figure 4.11: Perspective plot from inversion of 296 measurements assuming a three-layer model a) top Bunter b) base Bunter c) thickness of Bunter formation
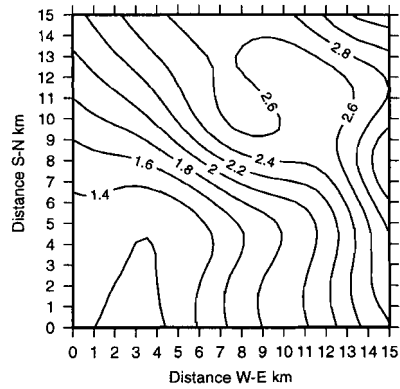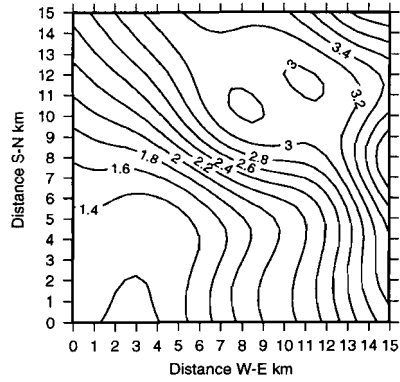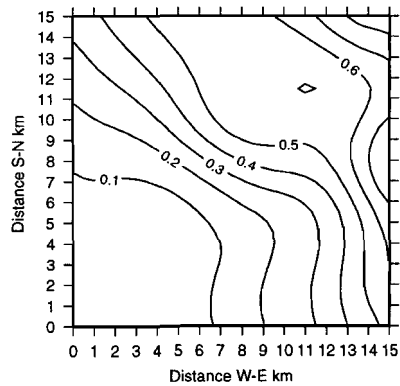
Figure 4.12: Contour map of depths from inversion of 296 measurements assuming a three-layer model a) top Bunter b) base Bunter c) thickness of Bunter.
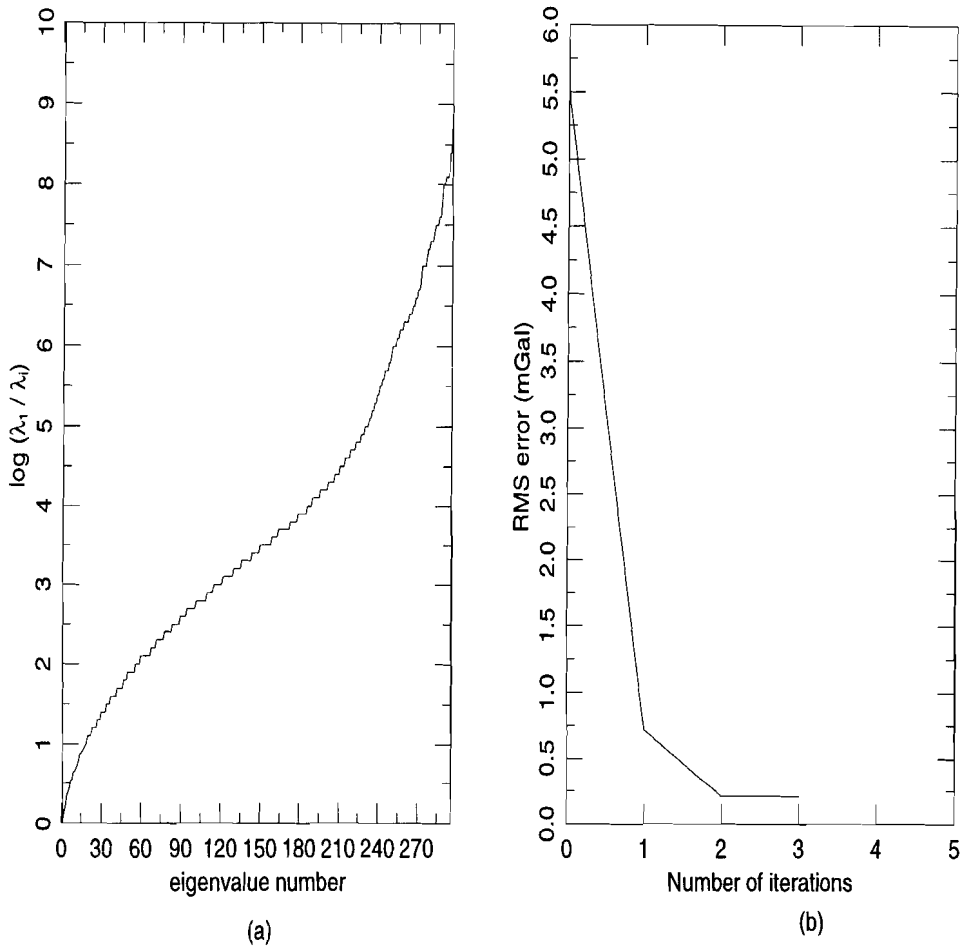
(a)   (b)

Figure 4.13: a. Largest singular value λ_1 of the Jacobian matrix (calculated for a three-layer model initialized by a horizontal top Bunter at a depth of 2.5 km and a constant Bunter thickness of 0.5 km and 296 measurements) divided by λ_i plotted on a logarithmic scale with base 10. b. Reduction of RMS error in each iteration from the inversion of 296 measurements (assuming a three-layer model) constrained by seismic information.

of the first layer, top Bunter, in the northern parts which are known from the seismic data. The initial Bunter top and its thickness are taken as 2.5 and 0.5 km respectively, the same as in the unconstrained inversion (figure 4.9). The singular values of the Jacobian matrix calculated for this initial model are plotted in figure 4.13-a. The small jumps or oscillations start again at singular value number 22. We inverted the data using
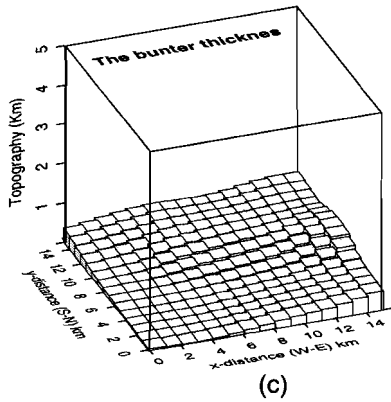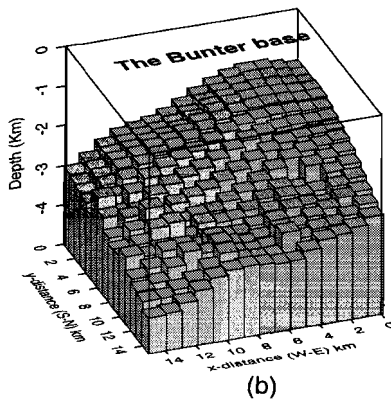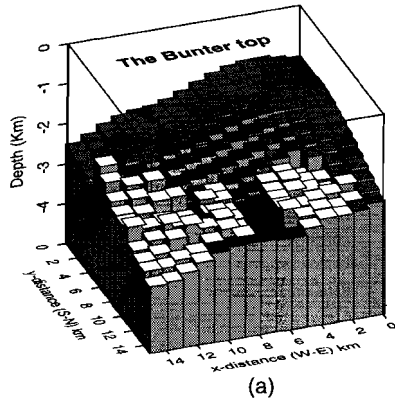
Figure 4.14: Perspective results of the constrained inversion using 296 measurements and assuming a three-layer model. a) top Bunter (whites are the depths which are known from the seismic) b) base Bunter c) thickness of Bunter formation.
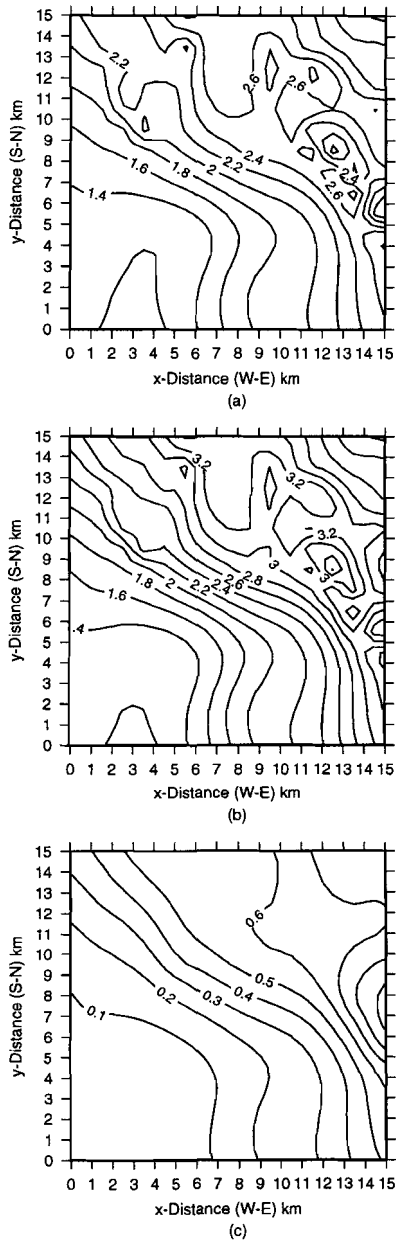
Figure 4.15: Contour map of depths from constrained inversion of 296 observations assuming a three-layer model a) top Bunter b) base Bunter c) thickness of Bunter formation
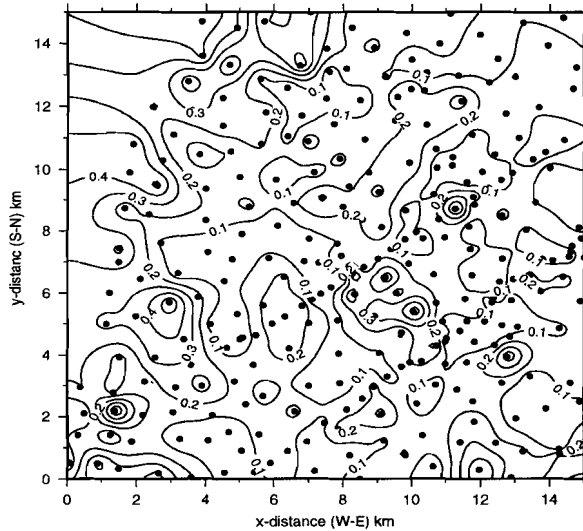
Figure 4.16: Contour map of misfit between 296 observed and predicted gravity data from constrained inversion assuming a three-layer model. The station positions are shown by bold dots.

22 eigenvectors to compare the results with those from the unconstrained case. The reduction of the RMS error in each iteration is again shown in figure 4.13-b. The plot shows that after 3 iterations the reduction in RMS error is negligible. The RMS error for this case was 0.21 mGal as before.

In figures 4.14-a,b,c and 4.15-a,b,c the perspective plot and the contoured depths of the top and base Bunter and its thickness are plotted. In the perspective figure of the top Bunter the depth of the white prisms are from the seismic information and were fixed in the inversion. The depth of top and base and also the thickness of the Bunter

again decrease from N-E to S-W, the same as in the unconstrained case. Comparing the results of the two inversions, unconstrained (figure 4.11 and 4.12) and constrained (figure 4.14 and 4.15), shows that the two models almost have the same configuration. The smaller details which are observable in the model of the constrained inversion are depths obtained from the seismics, which were fixed during the inversion. The residuals between the measured and predicted data from the model are also contoured in figure 4.16. In some stations this error is more than 0.3 mGal which is probably due to measurement errors. The thickness map of the Bunter (figures 4.12-c and 4.15-c) can be used for planning of future exploration activities in this area.

4.8 Conclusion

Although the introduced subspace method was used for a moderate scale 3D inversion, it can handle larger scale. In this subspace method calculation of the Hessian matrix (second partial derivatives matrix) is avoided which usually needs to be calculated for most subspace and gradient methods. Since the most important eigenvectors were selected as basis vectors, the inversion converged very fast to a solution with minimum variance. The scaling of the Jacobian matrix improved the results and the positivity constraint reduced the nonuniqueness of the inversion by confining the space of the search for the solution.

Comparison of the results of two and three-layer model inversions shows that the results of the three layer-model can also be reliable if a an initial model is selected using information from seismics or from other sources. The results of the three-layer model constrained inversion were, in general, the same as those of the unconstrained case. The thickness map of the Bunter can be used for planning future exploration activities. Because the potential hydrocarbon reservoir in this area is a sandstone layer in the Bunter formation.

4.9 References

Inman, J.R. 1975, Resistivity inversion with ridge regression, *Geophysics* **40**, 798-817.
Jupp, D.L.B. and Vozoff, K. 1975. Stable Iterative methods for the inversion of Geophysical data, *Geophys. J. R. astr. Soc.*, **42**, 957-976
Kennett, B.L.N. and Williamson, P.R. (1988) Subspace methods for large- scale nonlinear inversion, in N.J. Vlaar, G. Nolet, M.J.R. Wortel, S.A.P.L. Cloetingh and D. Reidel (eds.), *Mathematical Geophysics: a survey of recent developments in seismology and geodynamics, Dordrecht, pp. 139-154.*
Levenberg, K. 1944. A method for the solution of certain nonlinear problems in least-squares, *Quarterly of Applied Mathematics,* **2**, 164-168.
Marquardt, D.W. 1963. An algorithm for least-squares estimation of non- linear

Marquardt, D.W. 1963. An algorithm for least-squares estimation of non- linear parameters, *Journal of the Society of Industrial and Applied Mathematics* **11,** 431-441.

Narasimha Rao, B. Ramakrishna, P. and Markandeyulu, A. 1994. Some Oldenburg, D.W., McGillivray, P.R. and Ellis, R.G. (1993). Generalized subspace methods for large-scale inverse problems. *Geophys.J.int.* **114,** 12-20.

Pedersen, L.B. (1977) Interpretation of potential field data-a generalized inverse approach. *Geophysical Prospecting* **25,** 199-230.

Plouff D., 1976, Gravity and magnetic fields of polygonal prisms and application to magnetic terrain corrections. *Geophysics* **41,** 727-741.

Pelton W. H., Rijo L., and Swift C. M. 1978 Inversion of two-dimensional resistivity and induced-polarization data *Geophysics* **43,** 788-803.

Raiche A. P., Jupp D. L. B., Rutter H., and Vozoff K. 1985 The joint use of coincident loop transient electromagnetic and Schlumberger sounding to resolve layered structures *Geophysics* **50,** 1618-1627.

Sain, K. and Kaila K. L. (1994) Inversion of Wide-angle seismic reflection times with damped least-squares. *Geophysics* **59,** 1735-1744.

Sambridge, M.S. (1990) Non-linear arrival time inversion: constraining velocity anomalies by seeking smooth models in 3-D. *Geophys.J.int.* **102,** 653-677.

Smith, F.B. and Shanno, D.F. 1971. An improved Marquardt procedure for nonlinear regressions. *Technometrics* **13,** 63-75.

Unsworth M. and Oldenburg D. 1995 Subspace inversion of electromagnetic data: application to mid-ocean-ridge exploration. *Geophys.J.int.* **123,** 161-168.

Chapter 5

3D microgravity inversion for detecting cavities

Abstract

3D inversion of microgravity data was carried out to detect man made cavities which were expected to have a maximum width and height of 4 m and a depth of 6-10 m. The data is corrected for the topography by a triangular-element method. After applying all corrections, the regional trend is eliminated by fitting orthonormal polynomials to the data. Since it is expected that the cavities have small width (less than 4 m) the data region is parameterized by rectangular blocks with width 2 m. This leads to an underdetermined inverse problem. The residual data is inverted for the depth to the top of the cavities and for their height, with fixed density contrast between the cavities and the surrounding medium. The inversion is executed in the subspace of the data space to control the effect of the ill-conditionality and noise. In this way inversion is fast and stable against the noise. After one nonlinear inversion step (consisting of a linearized inversion) the results are not reliable (the cavities are scattered over the whole area) due to underdeterminancy. The inversion steps are then repeated a few times in such a way that the result of a previous inversion step is used as initial model for a next inversion step and model parameters corresponding to cavities with heights smaller than some threshold are fixed and their values set to a height equal to zero. This causes, in a current step, the number of model parameters to become smaller than that of the previous one and in turn the underdeterminancy of the problem is reduced. The inversion steps are continued until the minimum height of the cavities is equal to a preassigned value. This strategy is chosen since it is expected that the man made cavities are localized, connected and have a minimum height. The inversion results for synthetic data are excellent and those for real data from Sint Pietersberg near Maastricht are satisfactory.

5.1 Introduction

The modernization of buildings, the construction of new roads, railways and airports and other facilities create the necessity of detecting natural or man made cavities such as mines occurring at shallow depth. Microgravity is one of the most efficient geophysical methods which has been employed in engineering studies for detecting cavities. For instance, Arzi (1975) shows an example for verifying bedrock soundness at the foundation of a nuclear power plant and for delineating a zone of small cavities and tracing grout emplacement at the foundation of a large cooling tower.

A cave may be filled with air or water so that a density contrast exists between the cave and the surrounding material. This difference in density will give rise to lower gravity values which can be detected by a microgravity survey. The detection of caves from the surface by a microgravity survey depends on the volume of the caves in relation to their depth. This effect was discussed and illustrated for simple shapes by Colley (1962). As he has shown, small caves lying at large depths can not be detected from the surface since their gravity effect is negligible.

Microgravity surveys can also be employed for detecting buried gorges, shallow faults, contacts and other irregularities within bedrock of cavities or its buried surface, tracing of scour under structures, mapping the relative density of irregular formations such as coral reefs, certain volcanics, differentially weathered residues and glacial tills for excavation, planning of foundation design, locating underground workings, subsurface movements of fluids, interesting archaeological features, fine prospecting for minerals and various applications within mines.

A quantitative way of interpreting microgravity data is finding a model whose response fits the data best. This can be approached automatically by inverting the data to the parameters defining the model, employing a method which is able to handle the problem of nonuniqueness and ill-conditionality of the inverse problem.
In general the microgravity data can be inverted in three ways:
I- For both the position and the physical parameters if the density contrasts and position of the cavities are both unknown. Since for this case the inverse problem is strongly nonunique, a special strategy should be followed to reduce the effect of nonuniqueness.
II- For physical parameters (densities) while the position parameters are kept fixed during the inversion. This strategy has the advantage of linear inversion and the drawback of requiring many parameters to approximate the position of the cavities in 3D.
III- For position parameters only, while the density contrast is kept fixed. This strategy has the advantage that the position of the cavities can be quite well determined by a smaller number of model parameters if the density contrast is well known and if a sufficiently accurate initial model is selected.

For earlier interpretation of microgravity data inversion we can refer to the work of Neumann (1967) and Fajklewicz (1976). They determined the depth and height of isolated cavities by fitting simple models such as cylinders and prisms with the high precision gravity data.

A more complicated structure of cavities was studied using an inversion method by Camacho et al. (1994). Microgravity data collected in the flat bottom of the Lozoya Valley, about 500 m from the Lozoya Dam, 70 km to the north of Madrid (Spain) after corrections and removing the regional trend were modeled by least-squares predictions to separate several correlated signals. In this way the noise was also predicted and filtered from the data (by Camacho, 1994). The least-squares inversion led to the detection of a system of cavities and galleries.

We carried out a microgravity survey to locate man made cavities laying at a depth of 6 to 10 m from the surface. Knowledge of the location of these cavities is important in view of the danger of collapsing at places where new roads are planned. Since the cavities are filled with air, a considerable density contrast exists between the cavities and the surrounding rock. The magnitude of the gravity effect due to the cavities is a few tens of μGal. After all corrections, the irregular data were detrended using the orthonormal polynomial. In contrast to the work done by Camacho el al. (1994), we did not transform the data in a regular grid nor remove the effect of the noise from the data by the least-squares prediction method of Moritz (1980) since this technique did not lead to a reliable prediction in our case due to the limited number of data. Since the density contrast between the cavities and the surrounding medium is quite well known, we inverted the data for position parameters. We used a subspace technique for the inversion to control the effect of the noise and to have a fast convergence. The model was parameterized finely since it was expected that the cavities have dimensions between 2-4 metres. Due to this fine parameterization, the number of data points was much smaller than the number of model parameters, i.e. the inversion was underdetermined. To suppress the effect of underdeterminancy of the problem and to make the results of the inversion more localized several inversion steps were taken instead of one.

5.2 Inversion scheme

The model of the cavities consists of square rectangular prisms whose horizontal dimensions are the same and kept fixed in the inversion. Only the depth to their top and their height (vertical size) are allowed to be adjusted by the inversion. Since in our case the number of model parameters (depth to the top and the height of the elementary prisms) is much more than the number of data points, we used a minimum length criterion in the subspace technique as follows:

The inverse problem is nonlinear since the gravity model response function has a nonlinear dependency on the parameters describing the model. To take advantage of linear inversion methods the nonlinear model response function $\mathbf{g(m)}$ is expanded about some current model using Taylor series expansion ignoring terms of order two and higher

$$\mathbf{g(m + \delta m) = g(m) + G\delta m} \cdot \qquad (1)$$

The vectors $\mathbf{m}$ and $\mathbf{\delta m}$ are current model and model perturbation with dimension M,

and $\mathbf{G}$ is the first partial derivative or Jacobian matrix of the function $\mathbf{g(m)}$ with dimension $N \times M$ where N and M are the number of data points and of model parameters used in the inversion. In practice the effect of the model perturbation, $\mathbf{g(m + \delta m)} - \mathbf{g(m)}$, is taken to be equal to the data residual, $\boldsymbol{\delta}\mathbf{d} = \mathbf{d} - \mathbf{g(m)}$. With this assumption equation (1) can be reduced to

$$\boldsymbol{\delta}\mathbf{d} = \mathbf{G}\boldsymbol{\delta}\mathbf{m} \qquad (2)$$

Since the data does usually not have independent information we introduce a new data perturbation $\boldsymbol{\delta}\mathbf{d}^n$ in terms of the old one $\boldsymbol{\delta}\mathbf{d}$ and the matrix of the basis vectors $\mathbf{V}$ with dimension $N \times P$ (usually P is less than N) in the following form

$$\boldsymbol{\delta}\mathbf{d}^n = \mathbf{V}^T \boldsymbol{\delta}\mathbf{d} \cdot \qquad (3)$$

In this way each new data point is defined as a linear combination of all original data. This new definition for the data reduces the dimension of the data space. Using a judicious choice of the basis vectors defining the matrix $\mathbf{V}$ we want to allow only variations in the data that are due to significant model perturbations and to suppress variations in the data that are due to random noise and are not associated with significant model perturbations. In this way one can suppress the error propagation in the inversion. The success of this method depends of course on the choice of $\mathbf{V}$. We will return to this issue later.

The linear equation (2) for the new data perturbation $\boldsymbol{\delta}\mathbf{d}^n$ has the form

$$\boldsymbol{\delta}\mathbf{d}^n = \mathbf{V}^T \boldsymbol{\delta}\mathbf{d} = \mathbf{V}^T \mathbf{G}\boldsymbol{\delta}\mathbf{m} \qquad (4)$$

Since our linear inverse problem is underdetermined we used a minimum length criterion ($\boldsymbol{\delta}\mathbf{m}^T \boldsymbol{\delta}\mathbf{m} = Min$) in the following objective function

$$F(\boldsymbol{\delta}\mathbf{m}) = \boldsymbol{\delta}\mathbf{m}^T \boldsymbol{\delta}\mathbf{m} + \lambda(\mathbf{V}^T \boldsymbol{\delta}\mathbf{d} - \mathbf{V}^T \mathbf{G}\boldsymbol{\delta}\mathbf{m}) \qquad (5)$$

where λ is the Lagrange multipliers vector.

We minimize the above objective function in such a way that the equation $\mathbf{V}^T \boldsymbol{\delta}\mathbf{d} = \mathbf{V}^T \mathbf{G}\boldsymbol{\delta}\mathbf{m}$ is satisfied. To do this we set its partial derivatives with respect to the model perturbation $\boldsymbol{\delta}\mathbf{m}$ and the Lagrange multipliers λ to zero as

$$\frac{\partial F(\boldsymbol{\delta}\mathbf{m})}{\partial(\delta m_j)} = \delta m_j - \sum_{k=1}^{P} \sum_{i=1}^{N} \mathbf{G}_{ij} \mathbf{V}_{ik} \lambda_k = 0 \qquad (6)$$

$$\frac{\partial F(\boldsymbol{\delta}\mathbf{m})}{\partial \lambda_k} = \sum_{i=1}^{N} V_{ik} \delta d_i - \sum_{i=1}^{N} \sum_{j=1}^{M} V_{ik} G_{ij} \delta m_j = 0 \cdot \qquad (7)$$

The vector form of the above equations is

$$\boldsymbol{\delta}\mathbf{m} = \mathbf{G}^T \mathbf{V}\lambda \qquad \mathbf{V}^T \boldsymbol{\delta}\mathbf{d} = \mathbf{V}^T \mathbf{G}\boldsymbol{\delta}\mathbf{m} \cdot \qquad (8)$$

The two above equations can be solved for $\boldsymbol{\delta}\mathbf{m}$ and λ. Doing this will result in the following equation for the model perturbation

$$\delta\mathbf{m} = \mathbf{G}^T\mathbf{V}(\mathbf{V}^T\mathbf{GG}^T\mathbf{V})^{-1}\mathbf{V}^T\delta\mathbf{d} \cdot \qquad (9)$$

The square matrix $(\mathbf{V}^T\mathbf{GG}^T\mathbf{V})^{-1}$ with small dimension $P \times P$ can easily be inverted.

To prevent negative results in the inversion we introduce positivity constraints by the transformation $m_j^{new} = \sqrt{m_j}$. With this transformation each element of the new Jacobian matrix has the form $G_{ij}^{new} = 2.0\ G_{ij}m_j$. Notice that this constraint will reduce the effect of the nonuniqueness of the inverse problem because negative model parameters are not allowed anyway. To suppress instability in the inversion we combine the Marquardt method (Marquardt 1963) with our method by adding a constant value to each diagonal element of the matrix $\mathbf{GG}^T$, calculated at each iteration for the current model. The diagonal elements of the matrix $\mathbf{GG}^T$ will be modified as

$$[\mathbf{GG}^T]_{jj} \Rightarrow [\mathbf{GG}^T]_{jj}(1 + \alpha) \cdot$$

The constant α is initialized at the first iteration and is reduced during the iterative inversion. In the final iteration this parameter will be set to zero. In all the inversions which will be discussed in the following, we set α equal to 0.01. After calculating the model perturbation $\delta\mathbf{m}$ the current model will be updated and the updated model is used as the basis for further linear inversion. The iterations will be continued until convergence is achieved.

5.3 Choice of basis vectors

We choose basis vectors in such a way that they can easily be calculated and that they contain information of both the model and data space. Since the inverse problem is underdetermined, we take advantage of the smaller dimensionality of the data space for the basis vector calculations. We choose eigenvectors of the square and symmetric matrix $\mathbf{GG}^T$, calculated by the singular value decomposition routine for an initial model, as basis vectors. These eigenvectors can easily be calculated since the square matrix $\mathbf{GG}^T$ has dimension $N \times N$ (the square of the data space dimension). This matrix has properties of both the data and the model parameters since it is constructed from the Jacobian matrix. From these data space eigenvectors, only those are chosen as basis vectors which have the largest effect on the predicted data. In this way we only allow for those variations in the data that are strongly influenced by changes in the model parameters. It should be stressed that the basis vectors $\mathbf{V}$ are calculated only one time for the first initial model and kept fixed for all iterations.

5.4 Forward calculation

The gravity anomaly due to cavities can be calculated by dividing the volume of the

cavities into a limited number of three dimensional elementary rectangular prisms and then summing up the gravity effect of all the elementary prisms. The vertical component of the gravitational attraction g due to an arbitrary topographic mass of constant density ρ is given by

$$g = \gamma \rho \int \int \int_V \frac{z \, dz \, dy \, dx}{r^3} \tag{10}$$

where $r = (x^2 + y^2 + z^2)$ and γ is gravitational constant. The simplified expression of the above equation for a vertical rectangular prism is given by Plouff (1976) as follows

$$g = \gamma \rho \sum_{i=1}^{2} \sum_{j=1}^{2} \sum_{k=1}^{2} s \left[z_k atan \frac{x_i y_i}{z_k R_{ijk}} - x_i \ln(R_{ijk} + y_j) - y_j \ln(R_{ijk} + x_i) \right] \tag{11}$$

where $R_{ijk} = \sqrt{x_i^2 + y_j^2 + z_k^2}$ and $s = s_i s_j s_k$ with $s_1 = -1$ and $s_2 = +1$ and (x_1, x_2), (y_1, y_2) and (z_1, z_2) are the boundaries of the elementary rectangular prism in the x, y and z direction (for simplicity the observation point is taken in the origin).

The first partial derivatives of the predicted data with respect to a lower or upper boundary of each prism (each element of the Jacobian matrix) can be calculated analytically in the following form

$$\frac{\partial g}{\partial z_k} = \gamma \rho \sum_{i=1}^{2} \sum_{j=1}^{2} \left[atan \frac{x_i y_j}{z_k R_{ijk}} - \frac{x_i y_j z_k (R_{ijk}^2 + z_k^2)}{R_{ijk}(z_k R_{ijk})^2 + (x_i y_j)^2)} - \frac{x_i z_k}{R_{ijk}(R_{ijk} + y_j)} \right.$$

$$\left. - \frac{y_j z_k}{R_{ijk}(R_{ijk} + x_i)} \right] \tag{12}$$

where $k = 1, 2$.

5.5 Example with synthetic data

We tested the inversion scheme with synthetic data to find out the limitations of the inversion scheme. The true model consists of five isolated cavities represented by five rectangular prisms whose top boundaries are at depths 3, 7, 8, 9 and 12 m and all have the same height of 3 m. The perspective plot of the position and height of the cavities is shown in figure 5.1-a. We assumed a density contrast of 2.2 g/cm^3 for the model and calculated its effect for 64 measurement points in a regular grid form with a spacing of 14.29 m. The locations of the data points shown in figure 5.2 by the bold dots. The response of the model is also contoured in this figure. The maximum anomaly, 80 μGal, can be seen roughly at position (55,45), where the shallowest cavity (at 3 m depth) is lying.
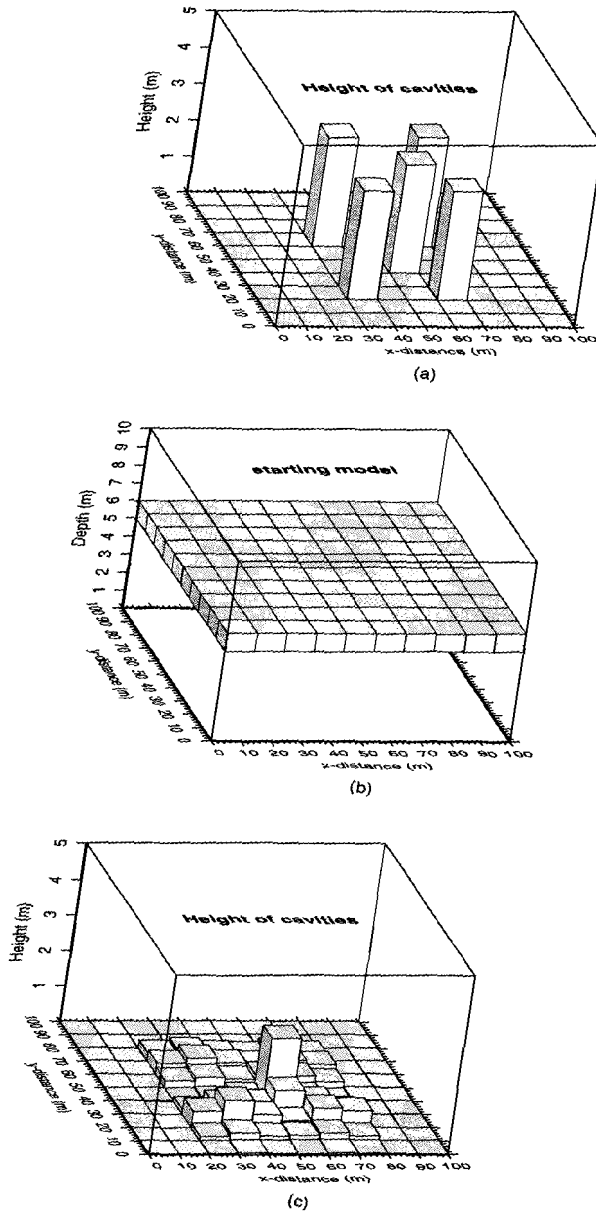
Figure 5.1: a) Perspective plot of the height of the cavities of the true synthetic model. b) Starting model. c) Perspective plot of the height of the model cavities after the first inversion step.

The chosen starting model consists of 100 prisms whose top boundaries are taken at a depth of 5 m and all have a height of 1 m and a width of 10 m (figure 5.1-b). The eigenvectors calculated for this initial model are taken as basis vectors for all the iterations. The condition number for the starting model was rather small (28) which indicates that the problem is well conditioned.

We inverted the noise free data taking all the basis vectors or eigenvectors in the inversion. The results of the inversion after 7 iterations with a root mean square error between the original and predicted data (RMS error) of $7.8 \times 10^{-9} \mu$Gal are shown in figure 5.1-c. Although the fit was very good (with a fast convergence) the localized cavities are not reconstructed well due to the underdeterminancy of the problem. Also, the minimum length solution discourages this type of solution. In fact, each model parameter (depth to the top boundary and the height of each prism) is as a linear combination of neighbouring model parameters. The reconstructed model therefore does not reflect the localized nature of the true distribution of the cavities. In order to obtain a model that reflects the localized character of the cavities, we set to zero the values of model parameters (depths and heights) corresponding to prisms whose height were less than 0.1 m (current minimum height criterion) and used these modified results as initial model for the next inversion (next step). The rational for this step is that, in many applications, one knows *a priori* that the cavities have a certain minimum height, for example because they are tunnels made by man. In the next step we also froze those model parameters at zero whose values were less than 0.1 m. After doing this the total number of model parameters for the next inversion was reduced from 200 to 78. The eigenvectors were again calculated for this new initial model and used as basis vectors for the second inversion step.

After doing the second inversion step to make the results more localized , the values of the model parameters corresponding to the prisms whose height were less than 0.2 m (current minimum height criterion) were set to zero and the modified results used as initial model for the third inversion step. In the third step model parameters with zero values were kept fixed in the inversion as before. In the third step the data inverted for an even smaller number of model parameters (56).

The inversion steps were continued in such a way that in each step 0.1 m was added to the previous minimum height criterion (taken as new minimum height criterion) and also the values of the model parameters (estimated from previous inversion step) corresponding to the prisms whose height were less than the new minimum criterion height were set to zero. Then the inversion step was executed with the previous modified results as initial model and some fixed model parameters (those whose values were zero).

We stopped the inversion steps when the minimum height criterion was 0.8 m. The result of the last inversion step (depth to the top boundary and the height of the cavities) was almost the same as the true model (figure 5.1-a). Since it is indistinguishable from the model shown in figure 5.1-a, the reconstructed model is not shown. These results were obtained after 8 inversion steps.
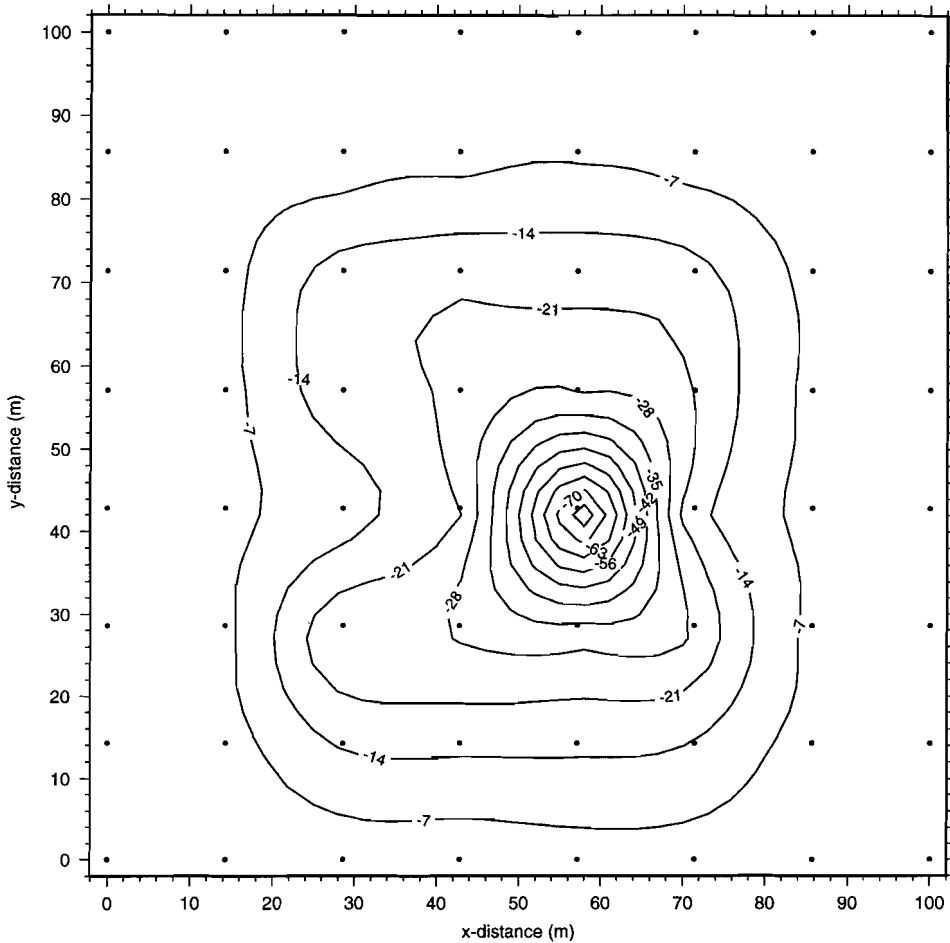
Figure 5.2: Contour plot of the 64 data, generated from the synthetic model with 5% noise.

In all nonlinear inversion steps the number of eigenvectors or basis vectors was chosen in such a way that the condition number for the first iteration of all nonlinear inversion steps was less than 500 (upper limit for the condition number). In the first nonlinear inversion step all eigenvectors were used in the inversion since the condition number of the first iteration was 28 (less than 500). In the next nonlinear inversion and further the condition number of the first iteration was increased since some of the model parameters were fixed and their values set to zero. Because of this fact an upper limit of 500 was considered to handle potential instabilities in the second and further nonlinear inversion steps.

(a)

(b)
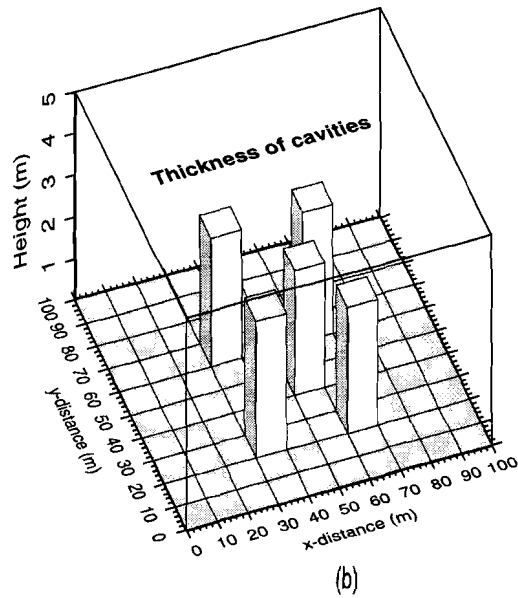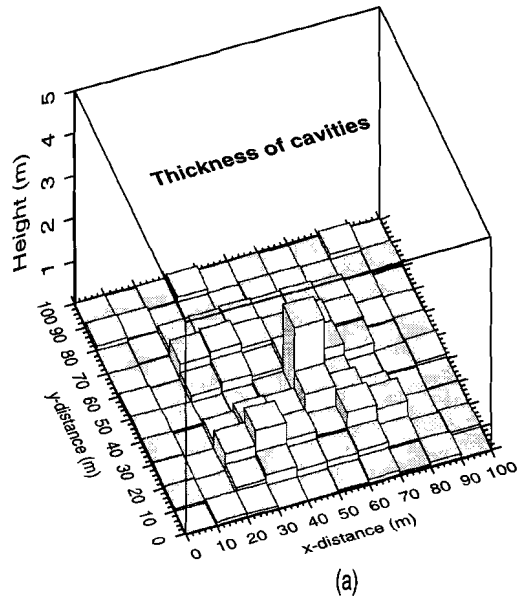
Figure 5.3: Height perspective of the cavities after a) one inversion step b) eight inversion steps using synthetic data with 5% noise.

We also tried inversion without any regularization by using all eigenvectors in the inversion and by setting $\alpha = 0$. The results were not reliable (they are not shown here) due to the construction of the artifacts in the model. The RMS error of this trial was about 10 μGal which indicates that the fit was also poor.

To test the efficiency of the method against noise we added five percent Gaussian noise to the data (RMS error of 0.79 μGal) and run the algorithm for 8 inversion steps as before. For this case the upper limit for the condition number was reduced to 100 in order to take into account the effect of the noise in the data and avoid constructing artifacts into the model. The RMS error after the final inversion step was the same as the true one (0.74 against 0.79 μGal). This proves that the noise was not minimized.

A perspective plot of the position and height of the cavities after the first and the last inversion step are shown in figure 5.3-a and 5.3-b. We can see that the cavities after the first inversion step are not localized (is almost the same as that of the noise-free data case shown in figure 5.1-c), while after the last step they are quite localized and detected in the right positions. The height and the depth to the top boundary of all the cavities are estimated very well (the discrepancy between estimated values and true ones is less than 0.5 m).

From the synthetic tests we can conclude that taking several inversion steps (instead of one step) and freezing some model parameters in each step leads to a localized solution. This scheme can handle quite well the problem of nonuniqueness due to underdeterminancy and can be used for detecting isolated structures such as cavities.

5.6 Example with real data

In 1995 a microgravity survey was carried out on the Sint Pietersberg near Maastricht in the south of The Netherlands. The cavities in this area are the remainder of ancient mining of marl as building material. These cavities have a height of 1-4 m and are connected. A gravimeter with an precision better than 3 μGal was used. The total number of measurements in this area was 99. The microgravimetry survey covered an area of about 100×20 m^2. The measurements were performed on an irregular grid. The data spacing is variable from about 4 to 10 m. The height and the position of the measurements are determined by levelling and GPS surveys with an accuracy of few millimeters. In total the accuracy of the data was about 5 μGal.

Corrections were made for instrument height and for tidal effects using the Cartwright et al. (1971 and 1973) harmonic development and assuming an elastic earth. The tidal waves were scaled using the synthetic data set of Timmen et al. (1994).

For terrain correction the height of about 20000 points to a horizontal distance of about 1000 m from the area under investigation were determined by digitization of a map on the scale 1 : 10000, with a contour interval of 2.5 m. This map was digitized roughly every 4 m. The heights of the digitized points are contoured in figure 5.4. The
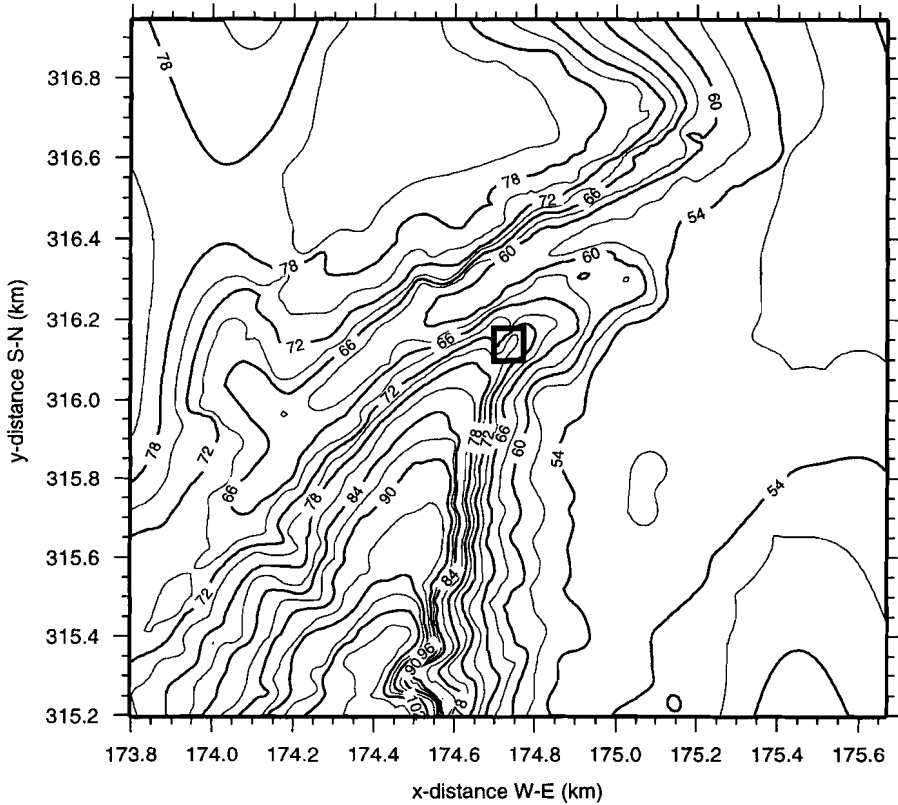
Figure 5.4: Contour plot of the topography surrounding the area under investigation. Contour interval is 3 m. The flat square on the plot shows the area where the microgravity survey was performed.

area under investigation is shown by a square on the contour map. From the contour map it can be seen that the topography of the terrain, surrounding the area under investigation, is variable, especially in the N-W where there is a steep slope. We could not remove the effect of this slope from the data perfectly since the resolution of the contours of the topographic map used for the digitization was not high. The digitized points (nodes) were triangulated by the optimum triangulation routine (Wessel et al. 1995). The terrain correction for each gravity station was automatically computed using the triangular-element method (Okaba 1979, Zhou 1990) for about 40000 triangles constructed from the nodes.

    The anomaly map after these corrections, together with the positions of the measurements (bold dots), is shown in figure 5.5. It shows a distinct NE-SW regional
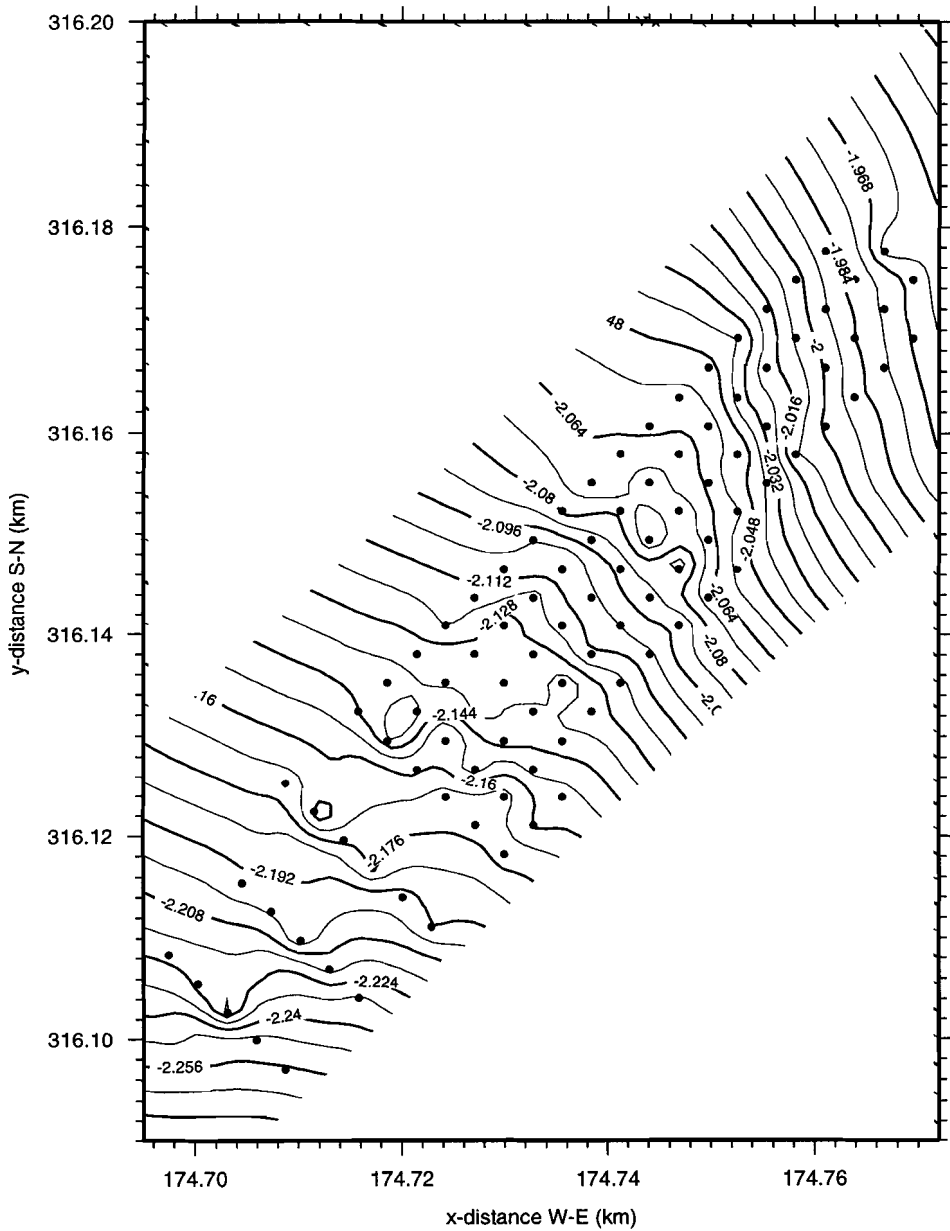
Figure 5.5: Contours of the Bouguer anomaly. Bold dots show the position of the measurements. Contour interval is 0.008 mGal.
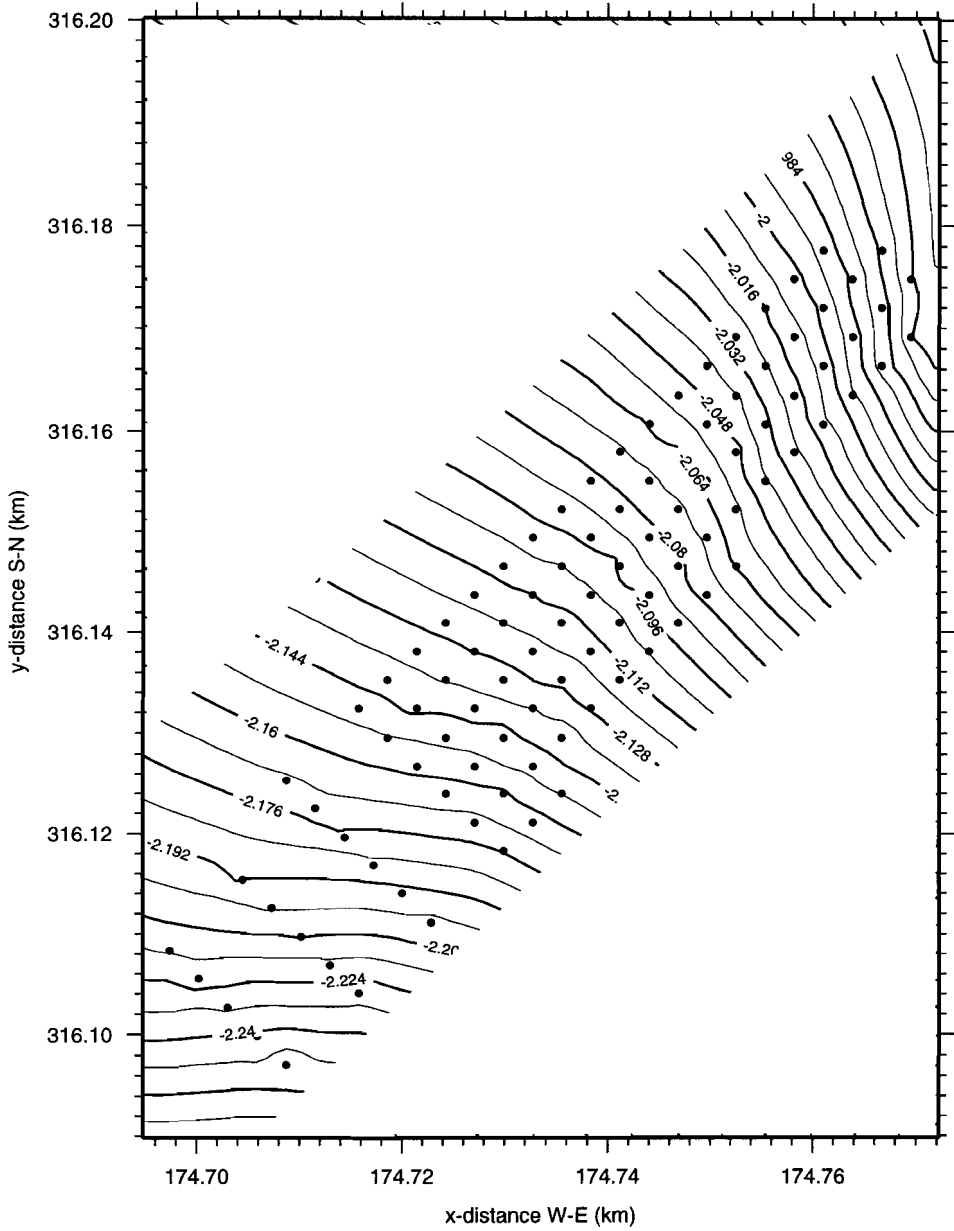
Figure 5.6: Model data as a result of fitting 3rd-degree orthonormal polynomials to the data. Contour interval: 0.008 mGal.

trend which is probably due to the deeper geological structure of the region. To enhance the local anomaly (short wavelength), the long-wave effect or the regional trend was removed from the data. For eliminating this the data were modelled by two-dimensional orthonormal trend surfaces as follows:

$$d_i = \sum_{j=0}^{k} P_j f_j(x_i, y_i) \qquad i = 1, \cdots, n \qquad (13)$$

where $f_j(x_i, y_i)$ are orthonormal polynomials in two dimensions, which can be obtained using the Gram-Schmidt method (Thomas 1996), k is the number of polynomials, n the number of data points. x_i and y_i are the data coordinates and P_j are coefficients of the orthonormal polynomials. The above linear system of equations can be solved for the coefficients P_j using a least-squares criterion. When the coefficients P_j are computed the regional trend can be predicted by equation (13) and eliminated from the data.

The advantages of using orthonormal polynomials over conventional polynomials is that the equations for evaluating trend coefficients are not ill-conditioned, since the basis functions are uncorrelated, and the convergence power of this method is greater than when the conventional polynomials are used (Sarma et al. 1990).

We fitted a 3rd-order orthonormal polynomial trend surface to the data. We also tested higher order orthonormal polynomial trend surfaces for the data fitting but improvement in the fit was not significant. The predicted trend and the residual (detrended) anomaly are contoured in figure 5.6 and 5.7. Negative anomalies observable in the residual plots are mainly due to the cavities. The most negative anomaly (about -17 μGal) can be seen in the middle part.

5.6.1 Inversion results of the real microgravity data

For the inversion we only used that part of the data with spacing 4 m, which shows the most negative anomalies. These data, after 45 degree rotation in the clockwise direction and after shifting, are contoured in figure 5.8. The data are rotated to facilitate model parameterization for the inversion. Here it can be seen that these data cover an area of $56 \times 20 \ m^2$. The number of data used for the inversion was 66 whose positions are shown with the bold circles in figure 5.8. In the plot some negative anomalies are observable. The most negative anomaly can be seen at about 46 m in the x direction and is elongated in the y direction. This anomaly is most likely due to the major cavities.

The area within $56 \times 20 \ m^2$ was modeled by 26×8 prisms. To account for the effect of the structure beyond the area and to reduce the side effects in the inversion an extra ring of 68 prisms up to a horizontal distance of 20 m was added.
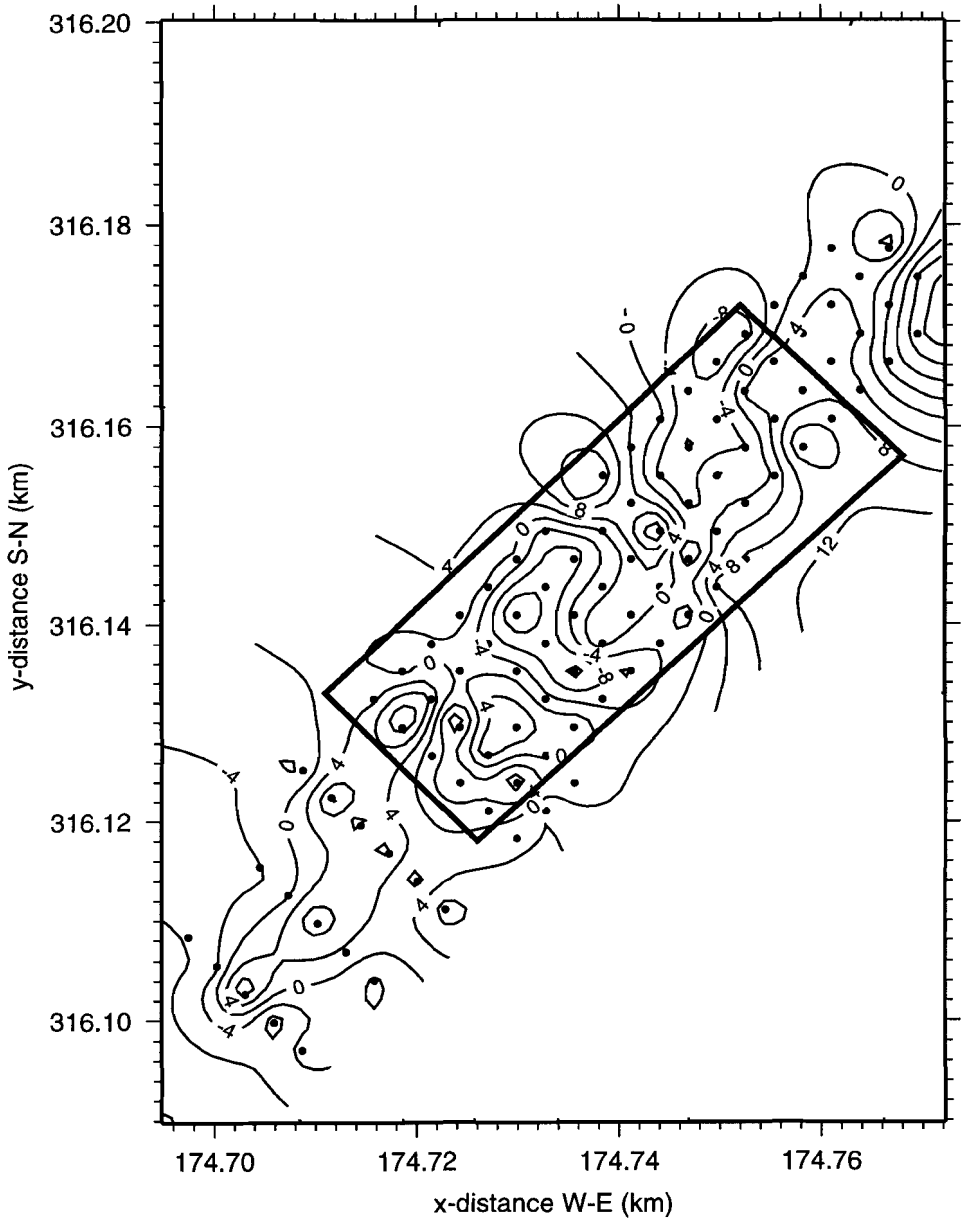
Figure 5.7: Local anomaly, obtained as residual of the orthonormal polynomial fit. Contour interval: 4 μGal. The flat square on the plot shows the area of the data which is used in the inversion.
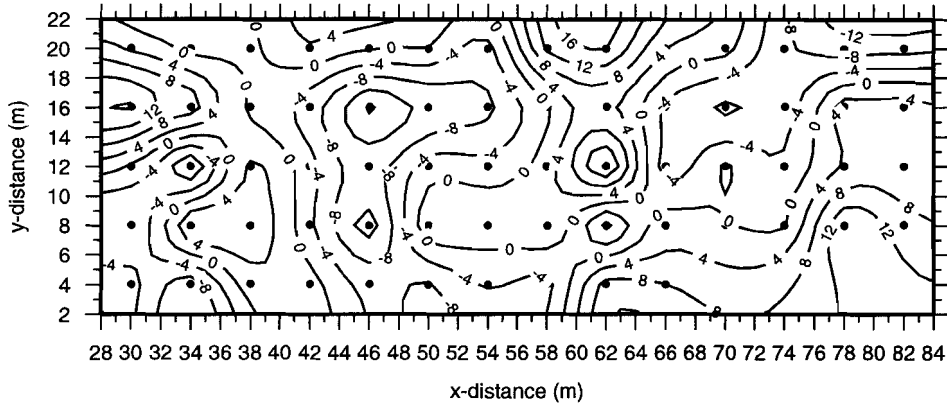
Figure 5.8: Contour plot of 66 measurements used for the inversion. Contour interval: 4 µGal.

In this way the total number of model parameters used for the inversion was $2 \times (28 \times 10)$, half of these corresponding to the depth to the top of the cavities and the rest to the height.

The inversion was started with the model shown in figure 5.9-a. The eigenvectors were calculated for this initial model and used as basis vectors for all iterations of the first inversion step. An upper limit of 100 was chosen for the condition number as a criterion for selecting the number of eigenvectors for the inversion. This upper limit was the same for all inversion steps. We also used positivity constraints for both the depth to the top and the height of the prisms.

The results of the first inversion step are presented in figure 5.9-b. It can be seen that the model parameters approximating the height of the cavities are not estimated in a localized way due to underdeterminancy of the inverse problem. To have a localized model we repeated nonlinear steps several times as we did in the synthetic case. We stopped the inversion process when detected cavities had a minimum height of 0.8 m. This criterion was chosen to stop the inversion process since it is expected that the real man made cavities have a minimum height of about 1 m.

The inversion results of the last step are shown in figure 5.10. The RMS error of the final inversion step was 4.86 μGal which seems to be reasonable given the accuracy of of about 5 μGal. The height of the detected cavities varies from 1 to about 4 m. A gallery is detected between position 44-48 in the x direction which is elongated along the y direction (figure 5.10).

A perspective plot of the depth to the top of the cavities is represented in figure 5.10-b (notice that the positive direction is upward). It can be seen that the estimated depths of the gallery varies from 6 to 10 m.
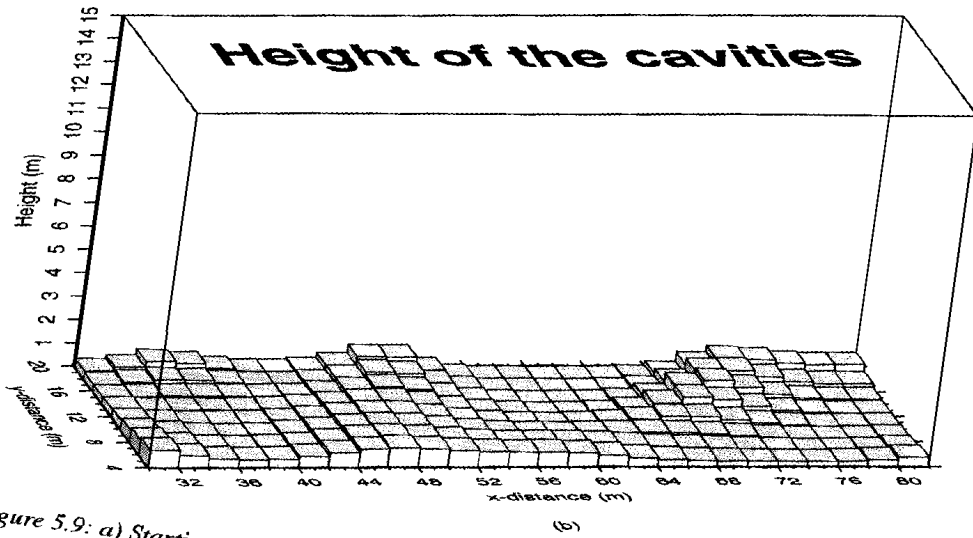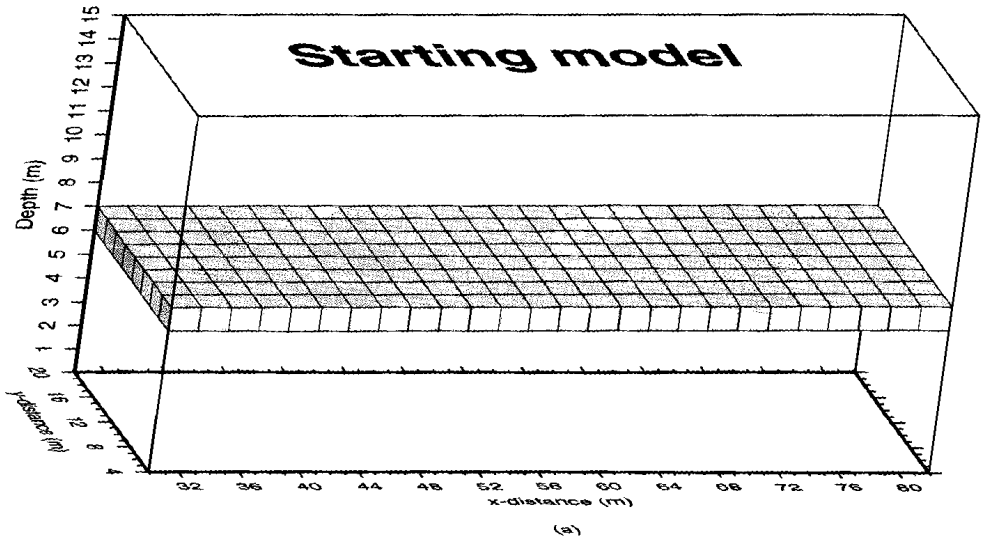
(a)

(b)

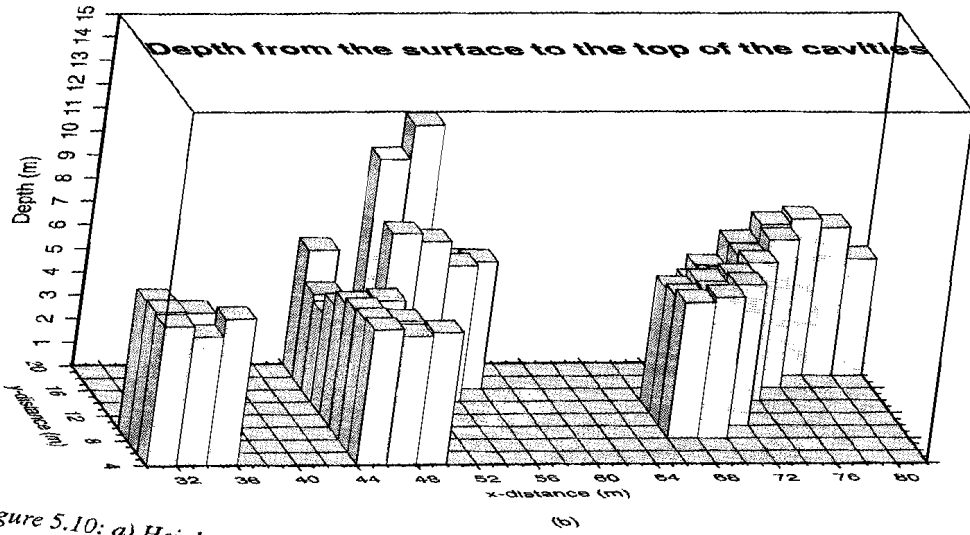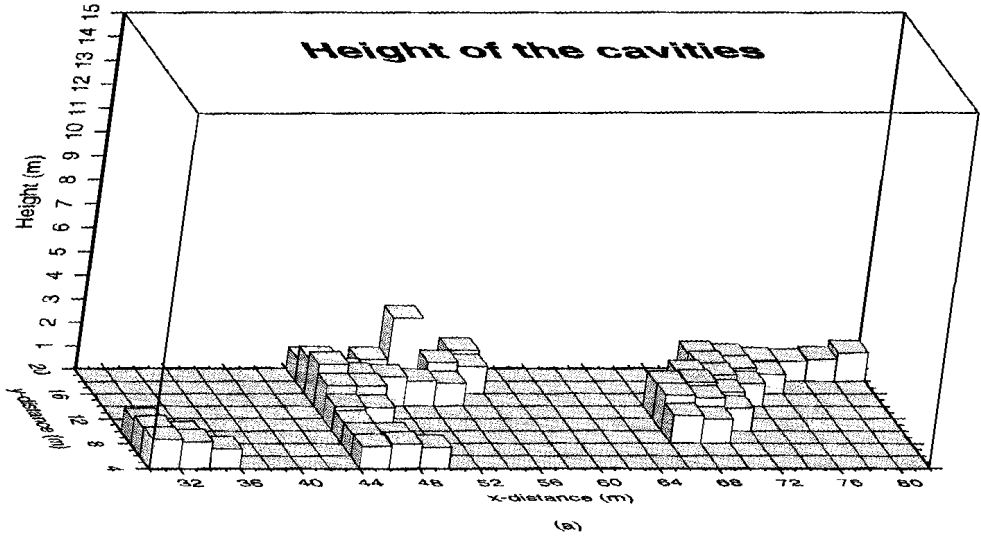Figure 5.9: a) Starting model. b) Height of the cavities after first inversion step.

Figure 5.10: a) Height of the cavities after 8 inversion steps. b) Depth of cavities after 8 inversion steps.

The position and depth of most of the cavities in this area are known and indicated on a map from 1977, prepared by Provinciale Waterstaat Limburg. The position of the gallery detected by the inversion, between position 44-48 m in the x direction, is in good agreement with that from the map. The true height and depth of the gallery, indicated in the map, varies between 1.8-3 and 6-10 m (below the datum 75.508 m) respectively. Although the height and the depths in some parts of the gallery are underestimated (due to underdeterminancy) they are in an acceptable range and almost at the right positions. The existence of the cavities depicted in the upper right corner (figure 5.10-a) are also proven by the map except that they are slightly shifted.

For the cavities shown in the lower left corner (figure 5.10-a) there are no indication on the map. However this does not mean that the result of the inversion is wrong. It is very well possible that not all cavities in this area are known and that therefore they are not indicated on the map.

5.7 Conclusion

3D inversion of micro gravity data with a finely parameterized model and an inadequate number of data led to an underdetermined inverse problem. The solution of the inversion was not localized and reliable since each model parameter was estimated as a linear combination of all model parameters due to underdeterminancy.

The results of the inversion were improved by doing a few inversion steps rather than one step, in such a way that the results of a previous inversion step were taken as the initial model for a new inversion step. After each step, model parameters corresponding to the cavities with height less than some threshold value were fixed and their values set to zero and the remaining free parameters were optimized by the new inversion step. The inversion steps were continued until the minimum height of the cavities, whose parameters were free to be adjusted, was equal to a preassigned value. In this way the underdeterminancy of the problem was reduced by reducing the number of model parameters in each step. The capability of this strategy was shown with synthetic and real microgravity data. The results of the inversion for both cases were localized and reliable after several inversion steps contrary to the results of only one step.

Inversion of real microgravity data led to detecting cavities whose positions, depths and heights were almost estimated the same as those of the true ones. Each inversion step was fast and stable due to using only those eigenvectors as basis vectors, which have the largest effect on the predicted data. In this way the effect of the noise in the inversion was minimized.

The disadvantage of using several inversion steps rather than one step is the increasing calculation time, which will be paid off by a more reliable solution.

5.8 References

Arzi A.A. 1975. Microgravimetry for engineering applications. *Geophysical Prospecting* **23**, 408-425.

Camacho A.G., Vieira R., Montesinos F.G. and Cuellar V. 1994. A gravimetric 3D Global inversion for cavity detection. *Geophysical Prospecting* **42**, 113-130.

Cartwright D.E. and Tayler R.J. 1971. New computations of the tide-generating potential. *Geophy.J.Roy.Astron.Soc.* **23**, 45-73.

Cartwright D.E. and Edden A.C. 1973. Corrected tables of tidal harmonics. *Geophy.J.Roy.Astron.Soc.* **33**, 253-264.

Colley G.C. 1963. The detection of caves by gravity measurements. *Geophysical Prospecting* **11**, 1-9.

Fajklewicz Z.J. 1976. Gravity vertical gradient measurements for the detection of small geologic and anthropogenic forms. *Geophysics* **41**, 1016-1030.

Marquardt, D.W. 1963. An algorithm for least-squares estimation of non- linear parameters, *Journal of the Society of Industrial and Applied Mathematics* **11**, 431-441.

Neumann R. 1976. La gravimetrie de haute precision, application aux recherches de cavities. *Geophysical Prospecting* **15**, 116-134.

Okabe M. 1979. Analytical expressions for gravity anomalies due to homogeneous polyhedral bodies and translations into magnetic anomalies. *Geophysics* **44**, 730-741.

Sarma D.D. and Selvaraj 1990. Two-dimensional orthonormal trend surfaces for prospecting. *Computers and Geosciences* **16**, 897-909.

Timmen L. and Wenzel H.G. 1994. Worldwide synthetic gravity tide parameters available on internet. *Bulletin d'Information BGI* **75**, 32-40.

Thomas G. B. 1969. *Calculus and analytical geometry (4th ed.).* Addison-Wesley Publ. Co., Reading, Massachusetts, 818 p.

Wessel P. and Smith W. H. F. 1995. The Generic Mapping Tools (GMT) version 3.0. *Technical Reference & Cookbook, SOEST/NOAA.*

Zhou X., Zhong B. and Li X. 1990. Gravimetric terrain correction by triangular-element method. *Geophysics* **55**, 232-238.

Summary

This thesis deals with the inversion of potential field data. Theoretical aspects and applications in gravimetry and magnetometry are treated. Inverse theory provides mathematical techniques to obtain useful information about the earth based on measurements (data). These techniques estimate numerically parameters which have some properties of the earth. These properties are called model parameters and are related to data by a theory or model. The object of all inversion methods is to obtain a model which is consistent with all available data and is physically plausible.

Performing this task a number of problems occur, such as:
- Inherent nonuniqueness of the inverse problem; for the inversion of potential field data there are many solutions or models which all equally fit the data.
- Nonuniqueness due to underdeterminancy; when the number of data is smaller than the number of model parameters the solution of the inversion is not unique.
- Ill-conditionality of the inverse problem; this effect is due to uncertainty in the data, insufficient parameterization and large dimensionality of the data and model parameters which cause unwanted oscillations in the solution or instability in the inversion.
These problems lead to finding a solution which is unreliable and/or also increase the time and memory of the computer required for the calculations.

The purpose of this work was to reduce these problems which are involved in an inversion. In this thesis the chapters are constructed in such a way that they can be studied independently. In the following a summary of each chapter is given:

In *chapter 1*, a general introduction about the theoretical and practical aspects of the geophysical inversion is given and literature about gravity and magnetic data inversion is reviewed.

In *chapter 2* a combination of linear and non-linear 3-D inversion is developed to determine the position and magnetization vector of buried iron objects producing a magnetic anomaly. The borehole data are inverted by assuming a two and a three-dipole model. Since the anomaly is due to a number of small objects, a stripping procedure is employed for finding them. Thus the inversion process for detecting all the objects is executed in several steps. In each step of the non-linear inversion process, an objective function is calculated at a number of fixed positions. For each of these fixed positions, the best fitting values for the magnetic moments of the dipoles are determined by linear inversion. These best values are used for the calculation of the objective function of the non-linear inversion. The solution of the linear inversion is obtained by the weighted least-squares criterion. To take into account the effect of all data in the inversion, more weight is given to data far from the object and less to data close to it. The resultant

linear system of equations is solved using the singular value decomposition technique which can handle potential singularity in the inversion by filtering small eigenvalues. The nonlinear objective function is the absolute norm of the data misfit (l_1-norm). An l_1-norm criterion is used rather than an l_2-norm or least-squares criterion since the former can handle data which represent more than one anomaly and contain some inaccurate or out-of range points (outliers). The objective function is minimized using the simplex (polytope) algorithm. This algorithm is used for optimization of the initial position of the dipoles. Since the problem is highly nonlinear, the objective function is not smooth, and the model contains high spatial frequencies. The reliability of the results from synthetic and real tests prove that the method can reduce the effect of nonuniqueness of the inverse problem when both physical and shape parameters are unknown. This method was successfully applied to detect unexploded bombs left from the second world war at Schiphol Airport in The Netherlands.

In *chapter 3*, a subspace technique is introduced to solve an ill-conditioned inverse problem due to the rather large number of data and model parameters. In order to realize a fast convergence of the inverse process to a solution with minimum variance, the basis vectors chosen for the subspace method are a limited number of eigenvectors of the Hessian matrix (second partial derivatives), namely those which have the largest influence on the predicted data. The eigenvectors of the Hessian are calculated only once in the first iteration and a limited number of them is used for all iterations. An upper limit for the numbers of eigenvectors of the Hessian to be used without causing instability in the inversion is found empirically when it can not be found from the eigenvalue plot. This method was employed to solve the shape of interfaces, separating geological units, using gravity data from the Roervalley graben in the southern part of the Netherlands, assuming a two-dimensional model. The inversion results show that the method is stable against noise and also the steep faults can be delineated properly. The reliability of the depth of the interfaces found by the inversion in most of locations are proven by other sources.

In *chapter 4*, a 3D inversion is developed which minimizes an objective function in the subspace of the data and model space. The spanning vectors of the subspace are the data and model eigenvectors of the Jacobian or first partial derivatives matrix calculated for an initial model. From these eigenvectors a limited number which have the largest effect in the predicted data are chosen as basis vectors. This selection avoids the calculation of the Hessian which is needed for most of the gradient or subspace methods. Since the matrix inversion is executed in the subspace of the data and model space the matrix inversion will be fast and stable against the noise. This subspace can handle ill-conditionality of an inverse problem which is due to the large number of data and of model parameters. It should be mentioned that this inversion scheme is sufficient for the case when the objective function is a smooth function of model parameters. The data are inverted for parameters defining a two or three-layer model in three dimensions, constructed by a limited number of square rectangular prisms. Only the depth to the top and the thickness of the prisms (vertical dimensions) are optimized by the inversion and the horizontal dimensions and density contrast are kept fixed.

This method was first tested with synthetic gravity data assuming a three-layer model to show the limitations. The method was also successfully applied for the inversion of gravity data assuming a two and three-layer model for an area in The Netherlands where the seismic results did not give a decisive answer about the continuation of a potential hydrocarbon reservoir. To reduce the effect of nonuniqueness of the inversion some parts of the model in the three-layer case are constrained using seismic results. Comparison of the results of two and three-layer model inversion shows that the results of a three layer-model can also be reliable if an adequate initial model is selected using seismic information or other sources of information. The results of the three-layer model constrained inversion, in general, were the same as those of the unconstrained case.

In *chapter 5,* a strategy is introduced to handle a 3-D microgravity data inversion for detecting cavities with a maximum dimension of 4 m and a depth to the top of 6-10 m. To detect these cavities with small dimensions , from the surface, most of the measurements are performed with a spacing of 4 m. The data used were from a survey at Sint Pietersberg near Maastricht. Since a considerable density contrast exists between the cavities and the surrounding rock and the density contrast is well known, the residual data is inverted only for position parameters. To outline the shape of the cavities rather accurately by the inversion a model is constructed of a large number of square rectangular prisms. In the inversion, horizontal dimensions of the prisms (all are 2 m) are kept fixed and only the depth to their top and their thickness are adjusted by the inversion. With this parameterization the number of data points is much smaller than the number of model parameters, i.e the inverse problem is highly underdetermined. The nonlinear inversion is linearized and solved by a subspace method iteratively. To minimize the effect of the noise in the inversion a limited number of data eigenvectors of the square and symmetric matrix GG^T (G is the Jacobian matrix calculated for an initial model) is used as basis vectors for all iterations. After one nonlinear inversion step (consisting of a few iterations of linear inversion) the results are not reliable (the cavities are scattered over the whole area). Therefore the inversion steps are repeated a few times in such a way that the result of a previous inversion step is used as an initial model for a next inversion step and model parameters corresponding to cavities with thicknesses smaller than some threshold are fixed and their values set to zero. The inversion steps are continued until the minimum thickness of the cavities is equal to a preassigned value. The results both the synthetic data and the real data show the capability of this method in handling an underdetermined inverse problem with a reliable and localized solution consisting of isolated structures.

Summarizing it can be said that the methods described in this thesis are able to reduce some of the problems that occur in the inversion of potential field data.

Samenvatting

Dit proefschrift gaat over de inversie van potentiaalveld gegevens.Theoretische aspecten en toepassingen in de gravimetrie en de magnetometrie worden behandeld. De inversie theorie verschaft wiskundige technieken om uit meetgegevens nuttige informatie over de opbouw van de aarde af te leiden. De aarde wordt beschreven met een model, dat wordt vastgelegd door middel van de getalswaarde van een aantal variabele modelpa- rameters die het model karakteriseren. Voor zo'n model waarvan de parameters bekend zijn kan theoretisch berekend worden watvoor meetgegevens dit model zou opleveren. Het doel van elke inversie methode is om een model (dat wil zeggen de getalswaarde van de modelparameters) te vinden dat consistent is met alle beschikbare meetgegevens en dat fysisch acceptabel is.

Bij het uitvoeren van die taak stuit men op een aantal problemen, zoals:
- Inherente meerduidigheid van het inversie probleem: bij de inversie van potentiaalveld gegevens bestaan er vele verschillende oplossingen (modellen) welke alle even goed met de meetgegevens overeenstemmen.
- meerduidigheid als gevolg van onderbepaaldheid: wanneer het aantal modelparameters kleiner is dan het aantal meetgegevens bestaat er geen unieke oplossing.
- slechte gedefinieerdheid van het inverse probleem: dit effect treedt op in het geval van onnauwkeurige meetgegevens, ontoereikende parameterisatie en bij zeer grote aan- tallen parameters en/of meetgegevens; het gevolg is dat er ongewenste oscillaties in de oplossing en instabiliteiten in de inversie ontstaan.
Al deze problemen leiden ertoe dat een onbetrouwbare oplossing wordt gevonden of dat de benodigde rekentijd of geheugenruimte van de computer ongewenst groot wordt.

Het doel van het in dit proefscrift beschreven onderzoek is om deze problemen die zich bij de inversie kunnen voordoen te overwinnen. De verschillende hoofd- stukken, die elk voor zich afzonderlijk gelezen kunnen worden, zijn als volgt samen te vatten:

Hoofdstuk 1 geeft een algemene inleiding in de theoretische en practische aspecten van de geofysische inversie.

In *hoofdstuk 2* wordt een combinatie van lineaire en niet-lineaire 3-dimensionale inversie ontwikkeld voor het localiseren van ijzeren objecten op basis van magnetische metingen. Magnetische metingen in boorgaten worden geïnverteerd, waarbij het gemagnetiseerde ijzeren object benaderd wordt door een model bestaande uit twee of drie magnetische dipolen. Aangezien het anomale magneetveld veroorzaakt wordt door een groot aantal kleine objecten, wordt een "afstrip" methode gebruikt om elk afzonder- lijk object te vinden.

De inversie wordt uitgevoerd in een aantal stappen. In iedere stap wordt voor een set van 2 of 3 dipolen op een aantal posities door middel van lineaire inversie bepaald welke grootte en richting de magnetische dipoolmomenten moeten hebben om de beste overeenstemming met de meetgegevens op te leveren. Vervolgens wordt in de volgende stap hetzelfde gedaan met de dipolen op andere posities. Het vinden van die posities die uiteindelijk de beste overeenstemming met de meetresultaten geven is een niet-lineair inversie proces.

De oplossing van de lineaire inversie in elke stap (om de best passende magnetische momenten te vinden) wordt verkregen met een kleinste-kwadraten criterium. Teneinde alle meetgegevens even sterk in de inversie te betrekken wordt meer gewicht gegeven aan de meetresultaten in veraf gelegen boorgaten en minder aan die in dichtbij gelegen boorgaten. Het verkregen systeem van lineaire vergelijkingen wordt opgelost met de "singular value decomposition" techniek, die door het uitfilteren van kleine eigen-waardes niet gevoelig is voor mogelijke singulariteiten in de inversie.

Als objectfunctie, die in de achtereenvolgende stappen van de niet-lineaire inversie wordt geminimaliseerd, wordt de absolute norm van de data misfit ($l1$-norm) genomen. De objectfunctie wordt geminimaliseerd door het simplex (of wel polytope) algoritme te gebruiken. De resultaten verkregen bij testen met synthetische zowel als echte meet-gegevens tonen aan dat het effect van de meerduidigheid van de inversie onderdrukt kan worden. Deze methode is op Schiphol met succes toegepast bij de opsporing van onont-plofte bommen uit de tweede wereldoorlog.

In *hoofdstuk 3* wordt een zogenaamde "subspace techniek" geïntroduceerdd voor het oplossen van een slecht gedefinieerd inversieprobleem, als gevolg van het tamelijk grote aantal meetgegevens en modelparameters. Teneinde een snelle convergentie van het inversieproces te realiseren worden de basisvectoren die gekozen worden voor de subspace methode beperkt tot een gering aantal van de eigenvectoren van de Hessian-matrix, namelijk diegene die de grootste invloed op de voorspelde meetgegevens hebben.

Deze methode is toegepast op zwaartekrachtsgegevens uit Limburg. Uitgaande van een twee-dimensionaal model konden de posities worden bepaald van enkele grensvlakken tussen geologische formaties. De inversie bleek stabiel te zijn ondanks het hoge ruis-niveau van de meetgegevens. Steile breuken konden zeer precies gelocaliseerd worden. De resultaten van de inversie stemmen overeen met geologische gegevens uit andere bronnen.

In *hoofdstuk 4* wordt een 3-dimensionale inversie techniek ontwikkeld die een objectfunctie minimaliseert in een subspace van meetgegevens en modelparameters. Als basisvectoren voor de subspace worden de eigenvectoren van de Jacobian genomen, berekend voor een startmodel. Weer wordt een beperkt aantal van deze eigenvectoren gebruikt in de inversie. De anders noodzakelijke berekening van de Hessian-matrix wordt hiermee vermeden.

De inversie in deze subspace van data en modelparameters is snel en zeer stabiel tegen-over ruis, ondanks het grote aantal meetgegevens en modelparameters. Deze inversie methode is bruikbaar als de objectfunctie een glad verloop heeft als functie van de

modelparameters.

De methode is toegepast op synthetische en echte zwaartekrachtsgegevens, waarbij het model bestond uit drie lagen in drie dimensies. De echte data waren afkomstig van een gebied in Nederland, waar seismische gegevens geen duidelijkheid gaven over het verloop van een potentiële gashoudende formatie. De beschikbare seismische informatie werd gebruikt als een beperkende randvoorwaarde in de inversie van de zwaartekrachtsgegevens. De resultaten waren veelbelovend.

In *hoofdstuk 5* wordt een strategie ontwikkeld om micro-gravimetrische metingen te inverteren voor het detecteren van holtes in de ondergrond met afmetingen van ongeveer 4 m en op een diepte vana 6-10 m. De gebruikte meetgegevens waren afkomstig van een locatie op de St. Pietersberg nabij Maastricht. Het model ter beschrijving van de ondergrond bestaat uit een groot aantal rechthoekige prisma's van verschillende hoogte. De posities van de onder- en bovenkanten van de prisma's vormen de vrije modelparameters. Het aantal meetgegevens is in dit geval veel kleiner dan het aantal parameters, hetgeen betekent dat het inverse probleem in hoge mate onderbepaald is.

Weer wordt het in principe niet-lineaire probleem gelineaiseerd en iteratief opgelost met een subspace methode. Teneinde het effect van de ruis te minimaliseren wordt een beperkt aantal van de eigenvectoren van de matrix $\mathbf{GG}^T$ ($\mathbf{G}$ is de Jacobian matrix berekend voor een startmodel) gebruikt als basisvectoren in alle iteraties. Na één niet-lineaire inversie stap (bestaande uit een aantal lineaire iteraties) blijken de resultaten niet acceptabel te zijn (de holtes liggen verspreid over de hele ruimte). Daarom wordt een nieuwe inversie stap ondernomen, waarin het resultaat van de vorige stap als startmodel gebruikt wordt, waarbij echter de modelparameters van die holtes (prisma's) met een hoogte kleiner dan een bepaalde drempelwaarde op een hoogte nul worden gefixeerd. Vervolgens wordt in iedere nieuwe inversie stap deze drempelwaarde verhoogd totdat de minimaal te verwachten hoogte bereikt is. Deze procedure werkt goed wanneer bekend is dat de holtes altijd een minimale hoogte hebben, zoals in dit geval op de St. Pietersberg waar we met door de mens uitgehakte holtes te maken hebben.

Samenvattend kan worden gesteld dat de methodes die in dit proefschrift worden beschreven een groot aantal van de problemen die zich voordoen bij de inversie van potentiaalveld gegevens kan overwinnen.

بنام خدا

خلاصهٔ پایان نامه

وارون سازی داده های میدان پتانسیل
تئوری و کاربردها در اندازه گیریهای گرانی و مغناطیسی

در این پایان نامه وارون سازی داده های پتانسیل مورد بحث و بررسی قرار می‌گیرد. جنبه های تئوری بسط داده شده عملاً در وارون سازی اندازه گیریهای گرانی و مغناطیسی بکار گرفته شده است. تئوری وارون سازی روشهای ریاضی را فراهم می‌سازد که این روشها می‌توانند براساس اندازه گیریها (داده ها) اطلاعات مفیدی دربارهٔ زمین ارائه نمایند. این روشها بطور عددی پارامترهایی را برآورد می‌کنند که بعضی از خواص زمین را دارا می‌باشد. این خواص پارامترهای مُدل نامیده می‌شوند و توسط یک تئوری یا مدل به داده ها مربوط می‌شوند. هدف تمام روشهای وارون سازی بدست آوردن یک مُدل می‌باشد که با تمام داده های موجود سازگار باشد و از نظر فیزیکی نیز معقول باشد. برای انجام این کار با مشکلاتی مواجه می‌شویم که در زیر بدانها اشاره می‌شود:

الف- چند جوابی بودن ذاتی مسئله وارون سازی: وارون سازی داده های میدان پتانسیل شامل تعداد زیادی راه حل یا مُدل می‌باشد که همگی بطور یکسان با داده ها برازش پیدا می‌کند.

ب- چند جوابی بودن مسئله وارون سازی ناشی از فرّو تعیّن شدگی:

124

وقتی تـعداد داده ها كمتر از تـعداد پارامترهای مُدل باشد وارون سازی داده ها تعداد بیشماری جواب خواهد داشت.

ج- بد شرایـطی مسئله وارون سـازی: این اثـر ناشـی از خطاهای اندازه گیری، ناکافی بودن پارامترهای مدل و تعداد زیاد داده ها و پارامترهای مُدل می‌باشد كه سبب نوسانهای ناخواسته در مُدل و ناپایداری پروسه وارون سازی می‌شود. این مشكلات منجر به یافتن یك جواب، غیرقابل اطمینان شده و هـمچنین زمان محاسبه و حافظه كامپیوتر را افزایش می‌دهند.

هدف از تحقیقات گردآوری شده در این پایان نامه كاهش این مشكلات می‌باشد كه معمولا" یك مسئله وارون سازی مواجه به آنها می‌باشد.

<u>فصل اول- در این فصل یك خلاصه كلی درباره مسئله وارون سازی</u> داده شده است و مقالات نوشته شده درباره وارون سازی داده های گرانی و مغناطیسی مرور گردیده است.

<u>فصل دوم- در این فصل یك تركیبی از وارون سازی خطی و غیر خطی</u> بسط داده شده است كه برای تعیین بردارهای موقعیت و گشتاور مغناطیسی اجسام آهنی مدفون، مسئول برای نابهنجاری مغناطیسی اندازه گیری شده بكار برده شده است. اندازه گیریهای انجام گرفته شده در چاههای آزمایشی با فرض مدلهایی مركب از دو دو-قطبی و سه دو-قطبی وارون سازی شده اند. از آنجایی كه نابهنجاریها ناشی از یك تعداد اجسام كوچك می‌باشند یك روش برهنه سازی برای پیدا كردن آنها بكار گرفته شده است. بنابراین كل

پروژه٬ وارون سازی برای یافتن تمام اجسام مدفون شامل چندین مرحله می‌باشد که در هر مرحله یک جسم پیدا می‌شود. در هر مرحله٬ وارون سازی غیرخطی(تابع مقصود (تابعی که می‌خواهد کمینه شود) برای یک تعداد موقعیت ثابت شده (برای اجسام) محاسبه می‌گردد برای هریک از این موقعیتهای ثابت بهترین مقادیر برازش داده شده برای گشتاور مغناطیسی دو قطبی‌ها با روش وارون سازی خطی تعیین می‌گردد. این بهترین مقادیر برای محاسبه تابع مقصود در نظر گرفته شده برای وارون سازی غیرخطی بکار برده می‌شوند. راه حل وارون سازی خطی با ذابطه٬ کمترین مربعات وزن داده شده بدست می‌آید. برای اینکه اثر تمام داده ها در وارون سازی در نظر گرفته شــود بیشترین وزن به داده های دور از جسم مدفون و کمتـرین به داده های نزدیک به آن داده شده است. سیستم معادلات خطی حاصل با بکار بردن روش تجزیه مقدار منفرد حل می‌گردد این روش می‌تواند اثر منفردی در وارون سازی را با هدف مقادیر ویژه کوچک از بین ببرد. تابع مقصود غیرخطی اندازه مطلق نُرم داده های برازش داده نشده می‌باشد. یک مقدار مطلق نُرم بجای نُرم کمترین مربعات بکار گرفته شده است زیرا اولی می‌تواند به یک راه حل قابل اطمینان تری منجر شود وقتی داده ها شامل بیشتر از یک نابهنجاری بوده و شامل تعدادی داده غیر دقیق و خارج از رنج باشند. تابع مقصود غیرخطی با روش سیمپلکس (simplex) یا پُلی‌تاپ (polytope) کمینه می‌شود. این روش برای بهینه سازی موقعیتهای اولیه فرض شده برای دو قطبی‌ها بکار گرفته می‌شود. از آنجایی که مسئله وارون سازی بطور بالایی غیرخطی می‌باشد تابع مقصود هموار نمی‌باشد و مُدل شامل فرکانس های مکانی بالایی می‌باشد. قابل اطمینان بودن نتایج حاصل از وارون سازی داده های مصنوعی و واقعی نشان می‌دهد که این روش وارون سازی می‌تواند اثر چند جوابی داشتن مسئله را به

126

مقدار زیادی کاهش دهد مانند هر دوی پارامترهای فیزیکی و شکل نامعین
میباشند. این روش بطور موفقیت آمیزی برای پیدا کردن محل بمبهای
منفجر نشده باقی مانده از جنگ جهانی دوم در فرودگاه اسخیپ هلّ
(schiphol) هلّند بکار برده شده است.

<u>فصل سوم</u>- در این فصل یک روش زیر فضایی (subspace) معرفی
شده تا یک مسئله وارون سازی بد شرایط داده شده ناشی از تعداد نسبتاً
زیاد داده ها و پارامترهای مُدل را حل نماید. برای زیر فضا یک تعداد
معدودی از بردارهای مقادیر ویژهٔ ماتریس مشتقات جزئی مرتبه دوم تابع
مقصود (Hessian) که بیشترین اثر را در داده های پیش بینی شده دارند به
عنوان بردارهای پایه در نظر گرفته میشوند. پروسهٔ وارون سازی شامل
چندین تکرار میباشد. بردارهای مقادیر ویژه تنها یک مرتبه در تکرار اول
برای مدل اولیه فرض شده و محاسبه میگردند و برای تکرارهای بعدی این
بردارها ثابت میباشند. یک حد بالا برای تعداد بردارهای مقادیر ویژه، بدون
ساختن ناپایداری در پروسهٔ وارون سازی، بطور تجربی تعیین میگردد،
وقتی این حد نمی‌تواند از روی منحنی مقادیر ویژه مشخص شود. این روش
برای تعیین شکل سطح مشترک لایه ها در ناحیه ای در هلند با وارون سازی
داده های گرانی بکار گرفته شده است.مدل فرض شده برای وارون سازی دو
بُعدی بوده است. نتایج وارون سازی نشان می‌دهند که این روش مقاوم در
مقابل نوفه میباشد و حتی شکستگی‌ها با شیب تند نیز می‌توانند مشخص
شوند. قابل اطمینان بودن عمق سطح مشترک لایه های برآورد شده (با
وارون سازی داده ها) در بیشتر مکانها بوسیلهٔ منابع دیگر تأیید گردیده
است.

فصل چهارم- در این فصل یك روش وارون سازی سه بعدی كه یك تابع مقصود را در زیر فضای داده ها كمینه می‌سازد بسط داده شده است. بردارهای پوششی زیر فضا، بردارهای ویژه داده ها و مُدل ماتریس مشتقات مرتبه اوّل تابع مقصود می‌باشند. از این بردارهای مقادیر ویژه یك تعداد محدود كه بیشترین اثر را در داده های پیش بینی شده دارند به عنوان بردارهای پایه انتخاب می‌شوند. در این روش به ماتریس مشتقات جزئی مرتبهٔ دوم نیاز نمی‌باشد در حالی كه برای بیشتر روشهای زیر فضایی یا گرادیانی باید این ماتریس محاسبه شود. بخاطر آنكه وارون سازی در زیر فضای داده ها و مدل انجام می‌گیرد آن سریع و پایدار در برابر نوفه خواهد بود.این روش زیر فضایی، یك مسئله وارون سازی با شرایط بد را (ناشی از تعداد زیاد داده ها و پارامترهای مدل) براحتی می‌تواند حل نماید. این روش وارون سازی برای حالتی مناسب می‌باشد كه تابع مقصود هموار باشد. داده ها برای تعیین پارامترهایی كه یك مدل دو یا سه لایه ای را تقریب می‌كنند وارون سازی می‌شوند. هر لایه مركب از تعدادی منشور راست گوشه می‌باشد. تنها عمق و ضخامت منشورها (ابعاد قائم) بوسیلهٔ وارون سازی بهینه می‌شوند و ابعاد افقی و جرم مخصوص ثابت نگاه داشته می‌شوند. برای اینكه محدودیتها مشخص شوند ابتدا این روش با داده های گرانی مصنوعی، با فرض یك مدل سه لایه ای آزمایش شده است. این روش همچنین برای وارون سازی داده های گرانی، بافرض یك مدل دو و سه لایه ای، در ناحیه ای از هلند جایی كه نتایج لرزه ای نتوانسته اند جواب قطعی برای ارائه یك لایه ای مركب از هیدروكربن بدهند بكار برده شده است. برای آنكه اثر چند جوابی وارون سازی داده ها كاهش داده شود قسمتی از مُدل (بااستفاده از داده های لرزه ای) در حین پروسه وارون سازی ثابت نگاه داشته می‌شود. مقایسه نتایج حاصل از مدل دو لایه ای و

سه لایه ای نشان می‌دهد که نتایج مدل سه لایه ای می‌تواند قابل اطمینان باشد اگر یک مدل اولیّه مناسب با استفاده از اطلاعات لرزه ای یا منابع دیگر انتخاب گردد. بطور کلی نتایج مدل سه لایه ای مقیّد شده و غیر مقیّد شبیه به یکدیگر بوده است.

فصل پنجم- در این فصل یک استراتژی وارون سازی انتخاب گردیده است که می‌تواند داده های مایکروگرانی را برای کشف حفره های زیرزمینی با حداکثر بُعد ۴ متر و عمق ۱۰-۶ متر وارون سازد. برای آنکه این حفره ها کشف شوند فاصله بین اندازه گیریها ۴ متر انتخاب گردیده است. اندازه گیری‌ها در نزدیکی شهر ماستریخ (Maastricht) در هلند انجام گرفته اند برای آنکه تباین جرم حجمی بین حفره ها و سنگهای اطراف نسبتا" قابل توجه و شناخته شده می‌باشد تنها داده ها برای ضخامت حفره ها و ارتفاع آنها تا سطح زمین، وارون سازی شده اند.

برای آنکه شکل حفره ها نسبتا" دقیق مشخص شوند مدل از تعداد زیادی منشور راست گوشه ساخته شده است. در وارون سازی داده ها ابعاد افقی منشورها (تماما" ۲ متر) ثابت نگه داشته می‌شوند و تنها عمق و ضخامت منشورها بهینه می‌شوند. با این انتخاب پارامترسازی تعداد داده ها خیلی کمتر از تعداد پارامترهای مُدل می‌شود یعنی مسئله وارون سازی فرّو تعیین شده می‌باشد. مسئله وارون سازی غیرخطی باستفاده از بسط تیلور خطی شده و بطور تکراری با روش زیرفضایی حل می‌گردد. برای به حداقل رساندن اثر نوفه در وارون سازی، تعدادی محدود از بردارهای ویژه ماتریس GG^T (G ماتریس مشتقات جزئی مرتبه اول می‌باشد که برای یک مُدل اولیه فرض شده محاسبه شده است)به عنوان بردارهای پایه برای تمام تکرارهای

وارون سازی در نظر گرفته می‌شوند. بعد از یک مرحله' وارون سازی غیرخطی (شامل یک تعداد از وارون سازیهای خطی) نتایج قابل اطمینان نخواهند بود (حفره ها در تمام ناحیه پخش می‌شوند) بنابراین مراحل وارون سازی غیرخطی چندین مرتبه تکرار می‌شوند بطریقی که نتایج مرحله وارون سازی قبلی به عنوان مُدل اولیه برای وارون سازی بعدی در نظر گرفته می‌شود و پارامترهای مُدل مربوط به حفره ها با ضخامت های کمتر از یک مقدار آستانه ای ثابت نگاه داشته شده و مقادیرشان مساوی صفر قرار داده می‌شود. مراحل وارون سازی تا جایی ادامه پیدا می‌کنند که ضخامت حفره ها بیشتر از یک مقدار آستانه ای شوند. نتایج وارون سازی داده های مصنوعی و واقعی توانایی این متد را در حل یک مسئله وارون سازی فَرو معیّن برای کشف ساختارهای ایزوله شده (محلی) نشان می‌دهد.

Acknowledgment

131

Curriculum vitae

Mahmoud Mirzaei was born on April 1st, 1957 in Komein a town located in the central province of Iran. After receiving the High School Diploma in mathematics, he entered the Training Teacher University of Arak in Iran in 1975 to study physics. In September 1978, he obtained his bachleror's degree in this field. Soon after, he was employed by the Ministrey of Education and Training as a physics teacher of High School. After a few months, he was accepted in the Institute of Geophysics of the University of Tehran as a graduate student in the field of geophysics. After one year study the university was closed due to the cultural revolution. Then he continued his job as a teacher for another five years. In 1985 after the re-opening of the Institute he continued his study. He obtained his M.S degree in 1988. Soon after, he was employed as a junior lecturer, first in the Institute of Geophysics of Tehran university and then in the Training Teacher University of Arak. In 1989, through an examination he was awarded a scholarship from the Ministrey of Culture and Higher Education of Iran to complete his study in geophysics with a PhD. He started his PhD study in April 1991 at the Geophysics Department of Utrecht University.